

Diss. ETH No. 17922

Interannual-to-Decadal Variability of the Stratosphere during the 20th Century:

Analyses with a Chemistry-Climate Model

A dissertation submitted to
ETH Zurich

for the degree of
DOCTOR OF SCIENCES

presented by

Andreas Marc Fischer

Dipl. Umwelt-Natw. ETH Zurich
born on 22 October 1979
citizen of Steinhausen (ZG) and Menznau (LU)

accepted on the recommendation of

Prof. Dr. Stefan Brönnimann, examiner
Dr. Eugene Rozanov, co-examiner

Zurich 2008

The cover displays a simulation of the Arctic polar vortex in March 1926 (geopotential height field at 100 millibar) as well as time series of an index measuring the strength of the vortex.

Abstract

The stratosphere exhibits chemical and dynamical variability on different time-scales, ranging from day-to-day variability to interannual and decadal variability. Through propagation of planetary waves the stratosphere is tightly coupled to the troposphere. Variability originating from the troposphere can affect dynamics and composition in the stratosphere and vice versa. Interannual-to-decadal variability in the stratosphere has a number of common sources such as variations in solar irradiance, volcanic eruptions, El Niño-Southern Oscillation (ENSO) and the quasi-biennial oscillation (QBO).

This thesis is aiming at improving our still limited understanding of interannual-to-decadal variability in the stratosphere using a coupled chemistry-climate model (CCM). Previous modeling and observational studies have focused on the past few decades, which is often a too short time period for studying stratospheric low-frequency variability. It is also the time period when the stratosphere was strongly perturbed with concentrations of greenhouse gases and ozone depleting substances (ODS) and hence less suitable for analyzing natural variability. A better knowledge of natural variability is highly relevant with respect to assessments of current and future climate change as well as ozone recovery.

Nowadays, with the emergence of reconstructed upper-level fields, CCM simulations can be extended much further back. Here, I present results of two types of model simulations using the CCM SOCOL: the model was applied (A) in transient mode to simulate the whole twentieth century with nine ensemble members and (B) in time-slice mode to simulate the anomalous warm ENSO event from 1940-1942 and the anomalous cold event from 1975-1976 using twenty ensemble members.

First, an extensive validation has been performed comparing the output of the transient runs (A) to statistically reconstructed indices, historical re-evaluated total ozone series, ozonesondes as well as satellite and reanalysis datasets. The performance of the runs was also assessed in process-oriented view, looking at ozone trends and the relationship between upward propagating wave energy and polar temperature and ozone, respectively. Overall, it could be concluded that the model is in reasonable agreement with observational data, simulating realistically the main processes within the stratosphere.

Second, forced and internal variability of the subtropical jet, the polar vortex and the stratospheric wave driving were analyzed. It could be shown that the spread of ensemble variability is strongly dependent on the analyzed parameter and region. While the strength of the subtropical jet exhibits a small ensemble spread with interannual fluctuations being ENSO related and hence predictable, year-to-year variations in the strength of the polar vortex are dominated to a large degree by internal variability. A large ensemble spread is

also found for trend estimates of the wave driving, but statistical significance is mostly absent precluding reliable conclusions. The transient runs were further assessed by looking at frequency, seasonality, and intensity of major warmings (MWs). It could be shown that MWs evolve less frequent in the model compared to the reanalysis data, but in a climatological view, seasonality and intensity displayed large similarities with observational data.

A multiple linear regression model was applied to the ensemble mean simulation of the transient simulation (A) in order to extract the main drivers of stratospheric variability in the northern hemispheric winter. It was found that the QBO at 30 hPa and solar variability are both important contributors for zonal wind variability in the high-latitude stratosphere. Both processes lead to an acceleration of the polar vortex during its positive phases. Furthermore, the response to stratospheric aerosols - injected by volcanoes into the stratosphere - is characterized by an increased meridional temperature gradient and accelerated zonal winds at the high latitudes. On the contrary, warm ENSO events and low-frequency variability of sea surface temperatures in the North Atlantic tend to decelerate the zonal flow.

A main focus of this thesis was the role of ENSO on the high-latitude stratosphere. The time-slice runs (B) of SOCOL were compared to two other CCMs. The stratospheric boreal winter climate difference between warm and cold ENSO event revealed in all models an increased wave-mean flow interaction, accelerating the residual mean circulation and weakening the polar vortex. As a consequence ozone is transported from the equatorial stratosphere towards the Arctic stratosphere, where temperatures are anomalously warm. Comparing the response of the models to the response of reconstructed geopotential height and temperature fields, a good match was found over the tropics and the Pacific North American sector but less so over the North Atlantic European region with respect to the wave structure which could be an effect of the low horizontal grid resolution of all three models. A rather high ensemble spread is seen over mid- to high latitudes in two of the analyzed models, suggesting that a sufficiently large set of ensemble member simulations must be carried out, to detect and attribute ENSO signals in long-term transient simulations.

Zusammenfassung

Die Chemie und Dynamik der Stratosphäre variieren auf verschiedenen Zeitskalen. Diese Variabilität spannt ein zeitliches Spektrum von täglichen, über interannuelle bis zu dekadalen Veränderungen auf. Durch planetare Wellenausbreitung ist die Stratosphäre eng mit der Troposphäre gekoppelt. Variabilität, ausgehend von der Troposphäre, kann die Dynamik und die chemische Zusammensetzung der Stratosphäre verändern. Umgekehrt gilt diese Beziehung ebenfalls. Interannuelle bis dekadale Variabilität in der Stratosphäre haben folgende gemeinsame Ursachen: die Variation der Sonnenstrahlung, vulkanische Eruptionen, El Niño-Southern Oszillation (ENSO) und die quasi-biennial (-zweijährige) Oszillation (QBO).

Die vorliegende Arbeit hat zum Ziel, unser bis heute begrenztes Verständnis der interannuellen bis dekadalen Variabilität in der Stratosphäre zu verbessern. Dies wird mit Hilfe eines Klima-Chemie Modells (CCM) untersucht. Frühere Modell- und Beobachtungsstudien fokussierten die Analyse vorwiegend auf die drei bis fünf vergangenen Jahrzehnte. Diese Zeitperiode ist aber oft zu kurz, um niederfrequente stratosphärische Schwankungen zu untersuchen. Zudem haben die hohen Treibhausgaskonzentrationen und Ozon zerstörende Substanzen während den letzten paar Jahrzehnte die Stratosphäre stark beeinflusst, womit diese Zeitperiode weniger geeignet ist, um natürliche Variabilität zu analysieren. Ein tieferes Verständnis über die natürliche Variabilität ist entscheidend, um den Klimawandel und die Ozonentwicklung in Gegenwart und Zukunft besser beurteilen zu können.

Mit dem Aufkommen von rekonstruierten Höhenfeldern können CCMs heutzutage das Klima weiter zurück in die Vergangenheit simulieren. Hier präsentiere ich Resultate zweier Typen von Modellsimulationen mit dem CCM SOCOL: das Modell wurde benützt, um (A) das ganze 20. Jahrhundert mit neun transienten Modellläufen (Ensemble Members) zu simulieren und (B) um Zeitscheiben-Experimente eines aussergewöhnlich warmen (1940-1942) und eines kalten (1975-1976) ENSO Ereignisses mit 20 Ensemble Members durchzuführen.

Zuerst wurden die transienten Läufe (A) mit statistisch rekonstruierten Indices, re-evaluierten Total Ozon Reihen, Ozonsonden, sowie Satelliten- und Reanalyse-Daten validiert. Die prozess-orientierte Validierung beinhaltete die Analyse von Ozontrends und die Beziehung zwischen aufwärts propagierender Wellenenergie und polarem Ozon bzw. Temperatur. Im Grossen und Ganzen konnte gefolgert werden, dass das Modell in vernünftiger Weise mit den Beobachtungsdaten übereinstimmt und die Hauptprozesse der Stratosphäre realistisch wiedergibt.

Danach wurden extern und intern beeinflusste Variabilitäten des Subtropenjets, des Polarwirbels und der stratosphärischen Wellenaktivität analysiert. Es konnte gezeigt werden, dass die Spannweite der verschiedenen Modellrealisationen stark von den analysierten Variablen und Regionen abhängt. Während die Stärke des Subtropenjets eine relativ kleine Ensemble-Spannweite aufweist, ist die Jahr-zu-Jahr Variabilität in der Stärke des Polarwirbels zu einem grossen Teil durch interne Variabilität dominiert. Interannuelle Fluktuationen in der Stärke des Subtropenjets werden durch ENSO ausgelöst und sind deshalb vorhersagbar. Eine grosse interne Variabilität wurde in Trendabschätzungen der Wellenaktivität gefunden. Jedoch fehlt hier oft statistische Signifikanz, was verlässliche Schlussfolgerungen verunmöglicht. Die transienten Läufe wurden weiter auf Häufigkeit, Saisonalität und Stärke von Haupt-Warmperioden über der Arktischen Stratosphäre (Englisch: major warmings, MWs) untersucht. Es konnte dabei gezeigt werden, dass MWs im Modell weniger häufig auftreten als in Reanalyse-Daten. Jedoch stimmen Saisonalität und Intensität der modellierten MWs in Klimatologien gut mit Beobachtungsdaten überein.

Ein multiples lineares Regressionsmodell wurde auf die gemittelte transiente Simulation (A) angewandt. Ziel dieser Analyse war es, die wichtigsten Einflussfaktoren auf die stratosphärische Variabilität im nordhemisphärischen Winter zu eruieren. Die QBO auf 30 hPa, die Variabilität der Sonne und ENSO sind die Haupteinflussfaktoren für die Variabilität von Zonalwind in den hohen Breiten. Die QBO und die Sonnenvariabilität führen in ihrer positiven Phase beide zu einer Beschleunigung der Zonalwinde in den hohen Breiten, während warme ENSO Ereignisse mit einer Abschwächung des Polarwirbels assoziiert sind. Stratosphärische Aerosole zeigen eine Verstärkung des meridionalen Temperaturgradienten und führen dadurch zu einer Intensivierung des Polarwirbels. Ähnlich wie ENSO tragen niederfrequente Schwankungen in der nordatlantischen Meeresoberflächentemperatur in ihrer positiven Phase zu einer Abschwächung des Polarwirbels bei.

Ein Hauptfokus dieser Arbeit war der Einfluss von ENSO auf die nördliche Stratosphäre. Die Zeitscheiben-Experimente (B) wurden mit entsprechenden Simulationen von zwei weiteren CCMs verglichen. Die Differenz vom warmen und kalten ENSO Zustand zeigt im stratosphärischen borealen Winterklima in allen Modellen erhöhte Interaktion von Wellen mit dem Zonalwind, was zu einer Beschleunigung der Residualzirkulation und zu einer Abschwächung des Polarwirbels beiträgt. Dadurch wird Ozon vermehrt von der tropischen Stratosphäre zu den nördlichen Breiten transportiert, wo die Temperatur anomal warm ist. Verglichen mit dem Signal in rekonstruierten Feldern der geopotentiellen Höhe und Temperatur zeigte sich über den Tropen und dem Pazifisch Nordamerikanischen Sektor eine gute Übereinstimmung, im Gegensatz zum Nordatlantischen Europäischen Sektor, wo die Wellenstruktur weniger gut reproduziert wurde. Dies könnte im Zusammenhang mit der eher groben horizontalen Gitterauflösung stehen. In zwei Modellen wurde eine relativ hohe Ensemble-Spannweite gefunden, was nahe legt, dass für transiente Simulationen eine grosse Anzahl von Modellrealisationen nötig ist, um ENSO Signale zu extrahieren.

Table of Content

Abstract	i
Zusammenfassung	iii
1 Introduction	1
1.1 Motivation	1
1.2 Objectives and Outline	5
2 Experimental Setup and Validation	7
2.1 Model Description	7
2.1.1 SOCOL version 1.1	7
2.1.2 SOCOL version 2.0	8
2.2 Computational setup of model simulations	9
2.3 Validation of 20th century climate variability.....	13
3 Low-frequency Variability in the Stratosphere	17
Abstract.....	17
3.1 Introduction	18
3.2 Descriptions of new model version, boundary conditions and observational data for comparison.....	19
3.2.1 Model Description	20
3.2.2 Boundary Conditions.....	21
3.2.3 Experimental Design	25
3.2.4 Comparison to observational data	25
3.3 Results	26
3.3.1 Analysis of Ozone	26
3.3.2 Analysis of Dynamics.....	37
3.3.3 Summary and Discussion	51
3.4 Conclusion and Outlook	52
3.5 Acknowledgments	53
4 Stratospheric Response to ENSO	55
Abstract.....	55
4.1 Introduction	55
4.2 Methods	56

4.3	Results	57
4.4	Conclusion.....	63
4.5	Acknowledgments	64
4.6	Online Supplementary Material	65
4.6.1	Model Spread	65
4.6.2	Eliassen Palm Flux	66
4.6.3	Model Descriptions	66
5	The Main Drivers of Stratospheric Variability	69
5.1	Introduction	69
5.2	Data and Methods.....	69
5.3	Results	72
5.3.1	Summary and Discussion	79
6	Conclusions and Outlook	81
6.1	Conclusions	81
6.2	Outlook.....	83
	Appendix A	87
	Abstract	87
A.1	Introduction	88
A.2	Observational data and model description	90
A.3	Results	92
A.3.1	The troposphere.....	92
A.3.2	Stratospheric dynamics and chemistry	95
A.4	Discussion	109
A.5	Conclusions	112
A.6	Acknowledgements	112
	References	113
	Acknowledgments	127
	Curriculum Vitae	129

1 Introduction

“... the finest of all [particles], mixed with a quantity of vapour, remained a long time floating in the upper air-currents, and, propelled by the wind, have made a journey round the world. The vapour was condensed to water, and froze in the cold currents; the refraction through the innumerable ice crystals caused the beautiful dark red globe which was observed the last months in so many places in Asia, Africa, Europe, and America; while the ash particles partly obscured the sunlight, or gave the sun blue and green tints as its rise and setting ... the steam cloud ... during the much more violent explosions on August 26 and 27 may very well have reached 15 to 20 kilometres.”

[R. D. M. Verbeek, Nature, 1884]

1.1 Motivation

This statement after the volcanic eruption of Krakatoa in 1883 by the Dutch geologist Rogier Verbeek emerging in a Nature article (Verbeek, 1884) is probably one of the first, mentioning the importance of upper air circulation in communicating climate anomalies over vast regions of the Earth. It also suggests upper air particles being responsible for producing intense red sunsets as observed worldwide after major volcanic eruptions, which inspired a number of famous artists in their work (Zerefos, *et al.*, 2007). Although it later turned out that the upper air particles mainly consist of sulphate particles instead of ice crystals (Robock, 2000), it is remarkable how intensively this topic was discussed at that time: a special committee of the Royal Society was created investigating the causes and effects of the eruption. Papers, comments, hypotheses and independent observations were collected from all over the world and put together (Symons, 1888). One interesting atmospheric analysis from today's perspective revealed that the ash cloud after the eruption was circling around the globe from east to west within about two weeks, which became famous as the “Krakatoa easterlies” (Hastenrath, 2007; Schaller, *et al.*, 2008).

Nowadays we can interpret these upper air observations as one among several manifestations of variability in the stratosphere. A great deal of knowledge about volcanic impacts on the stratosphere could be gained from the eruption of Mt. Pinatubo more than 100 years after the Krakatoa event (Robock, 2000) and the “Krakatoa easterlies” could later be explained as an easterly phase of the Quasi-Biennial Oscillation (QBO) (Baldwin, *et al.*, 2001). Natural stratospheric variability, observable in dynamics as well as composition, is occurring on different temporal and spatial scales (Solomon, 1999). In addition to volcanic eruptions and the QBO, variability of the sun's irradiance and temperatures at the ocean's

surface can be regarded as the main natural drivers of stratospheric interannual-to-decadal variability. An in-depth knowledge about this kind of variability is essential with regard to the key role the stratosphere plays in the atmospheric system. The stratosphere is the region of the atmosphere where harmful incoming shortwave radiation is absorbed and hence blocked by ozone, preventing ecological damage at the Earth's surface. It is also the layer which is tightly linked to the troposphere and hence climate at the ground via effects from both sides: tropospheric climate variability affects stratospheric composition and dynamics even on long time scales (e.g., *Randel, et al.*, 2002) whereas stratospheric interannual-to-decadal variability can lead to anomalous climate signals at the ground (e.g., *Shindell, et al.*, 2001). Much of our scientific knowledge about the stratosphere has emerged over the past decades in the context of stratospheric ozone depletion (*Solomon*, 1999). The discovery of the Antarctic ozone hole (*Farman, et al.*, 1985) has triggered enormous scientific efforts and studies all over the world in order to identify the mechanisms behind these phenomena. With globally binding regulations about the release of ozone depleting substances (ODS) (Montreal Protocol and subsequent Amendments), important milestones could also be set on the international political stage. Nowadays, stratospheric abundances of ozone depleting gases show a downward trend from their peak values of the late 1990s (*WMO*, 2006). As a consequence, stratospheric ozone is expected to increase in future and to return to pre-1980 values in the second half of the 21st century. However, detection and attribution of ozone recovery as well as exact projections of ozone returning to pre-1980 levels is complicated by overlaying natural variability and increasing amounts of greenhouse gases (GHGs), which directly and/or indirectly affect the ozone layer.

This thesis is contributing to this discussion by looking at stratospheric interannual-to-decadal variability in the past. A number of observational and scientific studies have addressed the relationship between individual drivers and stratospheric climate. Knowledge mainly arose from statistical extraction using multiple linear regression analysis (e.g., *Brunner, et al.*, 2006b; *Crooks and Gray*, 2005), empirical orthogonal function (EOF) analysis (e.g., *Kodera*, 1995), composite and case studies (e.g., *Brönnimann, et al.*, 2004; *Sassi, et al.*, 2004), and idealized model experiments (e.g., *Langematz, et al.*, 2003; *Rozanov, et al.*, 2005). A prominent role in causes and effects of interannual-to-decadal stratospheric variability play propagating planetary scale waves. Large-scale planetary waves in winter can penetrate deep into the stratosphere, where they break, dissipate and thereby decelerate the zonal flow and induce a residual meridional circulation from the tropics towards the winter hemisphere (*Holton, et al.*, 1995). An anomalous increase of upward propagating waves (e.g. as a consequence of tropospheric variability) causes a slowdown of the wintertime polar vortex and a rise of polar temperatures and ozone with a certain time lag (*Hadjinicolaou, et al.*, 2002; *Newman, et al.*, 2001; *Randel, et al.*, 2002). On a daily time scale this can also lead to a complete breakdown of the polar vortex with temperatures rising by up to 40°C, also known as major warmings (MWs) (*Limpasuvan, et al.*, 2004). The strength of the zonal flow affects the propagation characteristics for subsequent waves, which break at a lower level, leading

to a downward propagation. Furthermore, changes in the meridional stratospheric temperature and ozone distribution can also directly impose disturbances on the stratospheric zonal flow. Strong perturbations in the stratosphere may even affect weather at the ground a few weeks later (*Baldwin and Dunkerton, 2001*). Baldwin et al. (2003) showed that an adequate representation of the stratosphere in numerical extended-range weather forecast models might be important for simulating additional predictive skill from stratospheric memory effects. Through the effect of planetary waves, the circulation of the stratosphere is closely coupled to the troposphere. Variability in sea surface temperatures (SSTs) in the equatorial Pacific, known as the El Niño-Southern Oscillation (ENSO), is the most prominent mode of interannual-to-decadal climate variability, also affecting the stratosphere in the extra tropics. Anomalous upward propagating wave activity during wintertime is related to warm ENSO events leaving an imprint at polar latitudes in the winter hemisphere with a weakened polar vortex and warmer stratospheric temperatures (*Garcia-Herrera, et al., 2006; Manzini, et al., 2006; Sassi, et al., 2004; Van Loon and Labitzke, 1987*). It also affects stratospheric ozone as shown in an analysis of an unusually strong ENSO event (*Brönnimann, et al., 2004*). Variability of dynamics and composition in the northern extratropical stratosphere is also strongly linked to the phase of the QBO. The QBO modulates polar wind speeds by altering the wave guide for propagating planetary waves (*Baldwin, et al., 2001*). Westerly (easterly) wind regimes over the equatorial stratosphere are associated with a strengthening (weakening) of the polar vortex (*Holton and Tan, 1980*). However, this is further modulated by the 11 year solar cycle with a reversal of the “Holton-Tan effect” when solar activity is in its positive phase (*Labitzke, 1987; Labitzke, et al., 2006*). Solar variability directly affects chemical processes and, during maximum conditions, increases differential meridional heating in the winter stratosphere (e.g., *Egorova, et al., 2005b*). The signal first appears as an intensification of the polar night jet in the upper stratosphere in early winter. Kodera and Kuroda (2002) have proposed downward propagation of planetary waves to be responsible for communicating the signal of increased zonal winds to the polar lower stratosphere and possibly to the troposphere. Downward propagation from the stratosphere has also been suggested to explain observed tropospheric climate anomalies after major volcanic eruptions (*Robock, 2000*). Similar to solar heating, the injection of particles to the stratosphere leads to an intensification of the meridional temperature gradient and a strengthening of the polar vortex during wintertime. This may be amplified by positive feedbacks from the troposphere via reduced upward propagating wave activity (*Stenchikov, et al., 2002*). These recent studies underscore the need for a detailed understanding of stratospheric variability on long time scales, not only in the view of ozone depletion but also for assessing current and future climate change.

In this thesis investigations of interannual-to-decadal stratospheric variability are made with simulations of the coupled chemistry-climate model (CCM) SOCOL (*Egorova, et al., 2005a; Schraner, et al., 2008*). CCMs are global models incorporating the relevant dynamical, radiative and chemical processes in the atmosphere (*Eyring, et al., 2006*). Since they are coupled, they allow various feedbacks of dynamics on chemical processes and

vice versa, which makes them indispensable tools for understanding past changes and predicting the future evolution of the stratosphere. Through their high vertical resolution and a model top, usually located well in the mesosphere, the models are specifically designed for the application of middle atmosphere studies. Intercomparisons and assessments of a large number of CCMs with respect to key stratospheric processes have been addressed in Austin et al. (2003) and Eyring et al. (2006). Within the SPARC (Stratospheric Processes And their Role in Climate) Chemistry-Climate Model Validation Activity (CCMVal) (Eyring, *et al.*, 2005) these models are used to simulate the recent past (back to 1960) and to project stratospheric ozone development across the 21st century.

However, to study natural interannual-to-decadal variability in the stratosphere, the last four decades of the 20th century are a less suitable period due to strong anthropogenic perturbations through emissions of GHG and ODS. Moreover, to capture the full natural variability of the stratosphere, long simulation periods are needed. It is interesting to note that large anomalies in stratospheric drivers occurred already in the first half of the 20th century (e.g. strong ENSO event in 1940-1942 (Brönnimann, *et al.*, 2004), volcanic eruption of St. Maria in 1902 and a high-latitude eruption of Mt. Katmai in 1912 (Oman, *et al.*, 2005; Oman, *et al.*, 2006)). It is therefore of great relevance to simulate the whole 20th century with a CCM. The major hindrance up to now has been the absence of upper-level fields to validate model results as well as missing information on forcing parameters. This has nowadays been relieved by the emergence of statistical reconstructions giving valuable information on the past upper air circulation (Brönnimann, *et al.*, 2007; Brönnimann, *et al.*, 2006a; Brönnimann and Luterbacher, 2004; Griesser, *et al.*, 2008).

Based on this background we have applied the CCM SOCOL for two different kinds of simulations: (a) We applied SOCOL for the first ever CCM simulation over the whole 20th century (1901-1999). This was accomplished in transient mode using the most relevant forcing parameters (i.e. SSTs, sea ice, stratospheric aerosol properties, QBO, solar irradiance changes, anthropogenic emissions, and land surface properties). (b) Time slice experiments were performed simulating the strong ENSO event from 1940-1942. Results were contrasted to simulations of an unusually weak ENSO event from 1975-1976. The same simulations were additionally performed by two other research groups with different CCMs (D. Shindell, NASA-GISS, New York and M. Bourqui, McGill University, Montreal) to allow a model intercomparison of the stratospheric response to strong ENSO events. All simulations, (a) and (b), were performed using a reasonable large set of ensemble members (nine members for experiment (a) and twenty members for experiment (b)) to account for internal variability in the stratosphere. This is another point making these simulations unique, since to date no long-term transient CCM simulations were performed with more than three ensemble members (Austin, *et al.*, 2007; Dameris, *et al.*, 2005; Garcia, *et al.*, 2007; Shindell, *et al.*, 1998; Tegtmeier and Shepherd, 2007).

1.2 Objectives and Outline

The previous section has embedded the topic of the thesis into a broader context of stratospheric research. The results of the simulations outlined above will provide useful insights in processes and feedback mechanisms in the stratosphere and largely contribute to our still limited knowledge of interannual-to-decadal variability in stratospheric climate, ozone and its relation to climate at the ground. Special emphasis will be devoted to the role of SSTs on the high-latitude stratosphere.

The main objectives which will be addressed in this thesis are:

- **to perform transient ensemble simulations of the 20th century with a state-of-the art CCM.** This entails compiling all relevant boundary conditions, setting up the computational resources for the simulations and validating the model results with the focus on interannual-to-decadal variability.
- **to better understand the effect of ENSO on the northern high-latitude stratosphere.** This analysis is accomplished in a model intercomparison using three CCMs and complemented by investigations of the 100 year transient runs.
- **to investigate internal and forced interannual-to-decadal variability of stratospheric circulation and ozone in a CCM.** A special focus is set on the northern polar stratosphere, its causes for internal variability and the role of external drivers.

The thesis is sub-divided into four sections with the following content:

Chapter 2 gives an overview of the model versions used within this thesis and details the computational setup of the model runs. It also highlights the main results of a model intercomparison within the Climate of the 20th Century Project (C20C) focusing on the performance of the SOCOL model.

Chapter 3 (*Fischer, et al.*, 2008a) presents results of the 100 year transient simulations with the CCM SOCOL. The compilations of boundary conditions are extensively detailed. A validation of the model's performance in the stratosphere is described which encompasses the development of total ozone (TOZ), zonal wind, zonal temperature and zonal ozone over the century as well as process-oriented analyses. The chapter further explores the region of the northern polar stratosphere which displays a high internal variability.

Chapter 4 (*Fischer, et al.*, 2008b) examines the stratospheric winter climate response to ENSO in three CCMs using a large set of ensemble members. Results of time-slice simulations of an unusual warm ENSO event from 1940-1942 and an unusual cold ENSO event from 1975-1976 are compared. Modeled differences of the two events show remarkable similarities among the models such as decelerated zonal flow at polar latitudes, strengthened residual mean circulation, as a result of intensified wave-mean flow interaction, and an enhanced equator-to-pole transport of stratospheric ozone.

Chapter 5 explores the main drivers of stratospheric interannual-to-decadal variability in the Northern Hemisphere winter. Results of a multiple linear regression analysis are presented for zonal temperature, zonal wind and ozone. The large time period covered by the simulations allows investigating the stratospheric influence of low-frequency SST variability in the North Atlantic and Pacific Basin.

Chapter 6 summarizes the work presented and gives an outlook on subsequent projects.

Appendix A (*Brönnimann, et al., 2006b*) presents a related analysis similar to Chapter 4. The climatic response to the ENSO cycle 1986-1989 is investigated using the CCM SOCOL. This study additionally explores the climatic anomalies in the troposphere. For this project I contributed to the analysis by producing the figures in collaboration with Brigitte Müller (third co-author).

2 Experimental Setup and Validation

2.1 Model Description

The CCM SOCOL (modeling tool for studies of **SO**lar **C**limate **O**zone **L**inks) has been developed at the Physical and Meteorological Observatory / World Radiation Center (PMDO/WRC) in Davos in collaboration with ETH Zurich and MPI Hamburg (*Egorova, et al.*, 2005a). Over recent years SOCOL has gone through major model development and testing. This led to several model versions which are described in *Schraner et al.* (2008) and *Schraner* (2008).

Here, we highlight the two versions used within this thesis (named according to *Schraner et al.* (2008)). SOCOL version 1.1 was applied for the ENSO runs (see Chapter 4 and Appendix A). The 100 year transient simulations (Chapter 3 and 5) were performed with the improved version of SOCOL (version 2.0).

2.1.1 SOCOL version 1.1

The CCM SOCOL is a combination of a modified version of the MA-ECHAM4 GCM (Middle Atmosphere version of the European Center/Hamburg Model 4 General Circulation Model) (*Manzini and McFarlane*, 1998) and a modified version of the UIUC (University of Illinois at Urbana-Champaign) atmospheric chemistry-transport model MEZON described in detail by *Rozanov et al.* (2001; 1999) and *Egorova et al.* (2001; 2003). The GCM and CTM components of SOCOL are coupled via the three-dimensional fields of wind, temperature, ozone, water vapor, methane, nitrous oxide, and chlorofluorocarbons (CFCs).

MA-ECHAM4 is a spectral model with T30 horizontal truncation resulting in a grid spacing of about 3.75° . In the vertical direction the model has 39 levels in a hybrid sigma-pressure coordinate system spanning the model atmosphere from the surface to 0.01 hPa. A semi-implicit time stepping scheme with weak filter is used with a time step of 15 min for dynamical processes and physical process parameterizations. Full radiative transfer calculations are performed every 2 hours, but heating and cooling rates are interpolated every 15 min. With respect to the standard MA-ECHAM4, the gravity wave source spectrum of the Doppler spread parameterization has been modified according to *Manzini et al.* (1997).

The chemical-transport part MEZON (**M**odel for the **E**valuation of **o**Z**O**Ne trends) simulates 41 chemical species from the oxygen, hydrogen, nitrogen, carbon, chlorine and bromine groups, which are determined by 118 gas-phase reactions, 33 photolysis reactions

and 16 heterogeneous reactions on/in sulphate aerosol (binary and ternary solutions) and polar stratospheric cloud (PSC) particles. The scheme for photolysis rate calculations spans the spectral region 120–750 nm divided into 73 spectral intervals and specifically includes the Lyman- α line and the Schumann–Runge continuum. The chemical solver is based on the implicit iterative Newton-Raphson scheme. The reaction coefficients are taken from *Sander et al.* (2000) and the photolysis rates are calculated at every time step using a look-up-table approach (*Rozanov, et al.*, 1999). The transport of all considered species is performed with the hybrid numerical advection scheme of *Zubov et al.* (1999).

Several validations of the original MEZON and SOCOL version have been performed (*Egorova, et al.*, 2005a; *Egorova, et al.*, 2003; *Rozanov, et al.*, 1999). However, the model intercomparison by *Eyring et al.* (2006) revealed serious problems of the model in simulating the stratospheric chlorine content and water vapor.

2.1.2 SOCOL version 2.0

The latest SOCOL version is a follow-up on version 1.1. Several attempts were undertaken to tackle the shortcomings of the model (*Schraner, et al.*, 2008). In the new model version halogen chemistry is treated more comprehensively: for chemical reactions, ODS are not anymore grouped into three families as in version 1.1 but treated separately. 13 new photolytic, 14 O(¹D)-based and 8 OH-based oxidation reactions were added to the model. In order to avoid artificial accumulations as detected in chlorine peaks at the edge of the southern polar vortex, the transport scheme was extended to include also the very short lived species. In total, the number of transported species has been increased by 19 substances.

The most prominent flaw in SOCOL was much too low total chlorine concentrations at the southern high latitudes at 50 hPa during winter/early spring (*Eyring, et al.*, 2006). It could be shown that this behavior is directly linked to the mass fixer applied after each horizontal transport step, which can lead to artificial mass accumulation and loss in certain geographical regions. To overcome this problem, a family-based mass fixing procedure was introduced for nitrogen, chlorine and bromine species. For ozone, where this concept could not be applied, we instead restricted mass fixing to 40°S – 40°N. In this way we accounted for unjustified corrections at high latitudes resulting from transport errors in the tropics and sub-tropics. Furthermore, a new cirrus parameterization in the tropical tropopause region was introduced to consider cloud formation in the tropics and sub-tropics above 100 hPa.

Overall, the new version of SOCOL has significantly improved, most notably seen in climatologies of chlorine and water vapor. For a more detailed description of the modifications and latest validations we refer to *Schraner et al.* (2008) and *Schraner* (2008).

2.2 Computational setup of model simulations

The code of the CCM SOCOL is written in the standard programming languages of Fortran 77 (CTM MEZON) and Fortran 90 (GCM ECHAM4). Calculations are based on the numerical software libraries Basic Linear Algebra Subprograms (BLAS) and Linear Algebra PACKage (LAPACK). A third library linked to the model code supports the format of the Network Common Data Form (netCDF) - a state-of-the-art binary data format developed to facilitate the exchange of scientific data. SOCOL is currently not designed for use in parallel mode but rather runs as a single-processing job. Core of the work flow during a model run is a namelist allowing to set parameters and switches to control the run. Various data formats, from ASCII to netCDF and binary, are used as input files. The raw output (i.e. before post-processing) comes as GRIdded Binary (GRIB) for ECHAM4 and ordinary binaries for MEZON. According to our settings, the model is running for one month and needs to be re-executed for continuation using the latest information (restart files) of the previous run.

The maintenance of individual ENSO simulations (see Chapter 4) over more than one model-year was established by means of shell scripts. These scripts took care of providing the boundary data corresponding to the current model-month as well as managing re-submission with the appropriate files. The ensemble simulations were run on individual Linux computers at the Institute for Atmospheric and Climate Science (IAC) using a Lahey/Fujitsu Fortran compiler. Post-processing of the output was only little automatized and applied to each ensemble simulation separately.

Given the high computational costs and enormous data amounts in case of 100 year transient simulations with a total of ten realizations (see Chapter 3), a similar proceeding as in the ENSO runs could not be pursued. Instead, we switched to the Linux cluster Hreidar maintained by the High Performance Computing group at ETH Zurich. This was especially beneficial with respect to data flow handling but also with respect to the better performance of the model on this system by switching to an Intel Fortran compiler. Hreidar is a Beowulf class computing cluster. It consists of 196 dual-CPU compute nodes, two login nodes and three file servers. Each compute node has two AMD (Advanced Micro Devices, Inc.) Opteron processors, 4 GB memory and about 100 GB disk storage. The interconnect is a mix of 1 GB and 100 MB Ethernet. The queuing system used on Hreidar is the PBS Pro version of the Portable Batch System. The queues that put the jobs into the appropriate complex are determined automatically based on the requested number of nodes and the time limit. Since the infrastructure is a 64-bit system, some adjustments in the model code of SOCOL were necessary.

The two file servers (HOME and WORK) are global file systems establishing the connection between the internal and the external world (i.e. files coming from the outside have first to be saved in the global area before being used on the computing node and vice versa). HOME is meant for casual work, testing and submission of the job, whereas the WORK server is employed for data being used (actively or passively) during a calculation

on the compute node. However, for efficiency reasons, it is recommended to distribute input data to a local scratch disk residing on the node (i.e. not shared between the nodes) beforehand and re-distribute output files after the calculation to WORK. Since disk space on the WORK server was limited to 100 GB for the whole project, this part could only be utilized as a temporary file storage system, given the massive computation with SOCOL. Instead, we made use of the Archive file server of the Swiss National Supercomputing Centre (CSCS) located in Manno. This system was considered as long-term data storage for files which were not actively used anymore. Data needed for further calculations or visualizations were stored on a file server at IAC. Figure 2.1 gives an overview of the archive and file servers as well as the computing node, involved in the 100 year transient simulations.

The computation of these simulations run over eight to nine months (late January 2007 until October 2007) and produced a data amount of around 11.5 TB (9 TB of data stored at CSCS and 2.5 TB at IAC). This involved data flow of more than 130'000 individual files consisting of raw output files, restart files, post-processed netCDF files and a large number of netCDF files created in the aftermath of the core run on the cluster. A suite of elaborated shell-scripts was necessary to automatize, maintain and control the simulations.

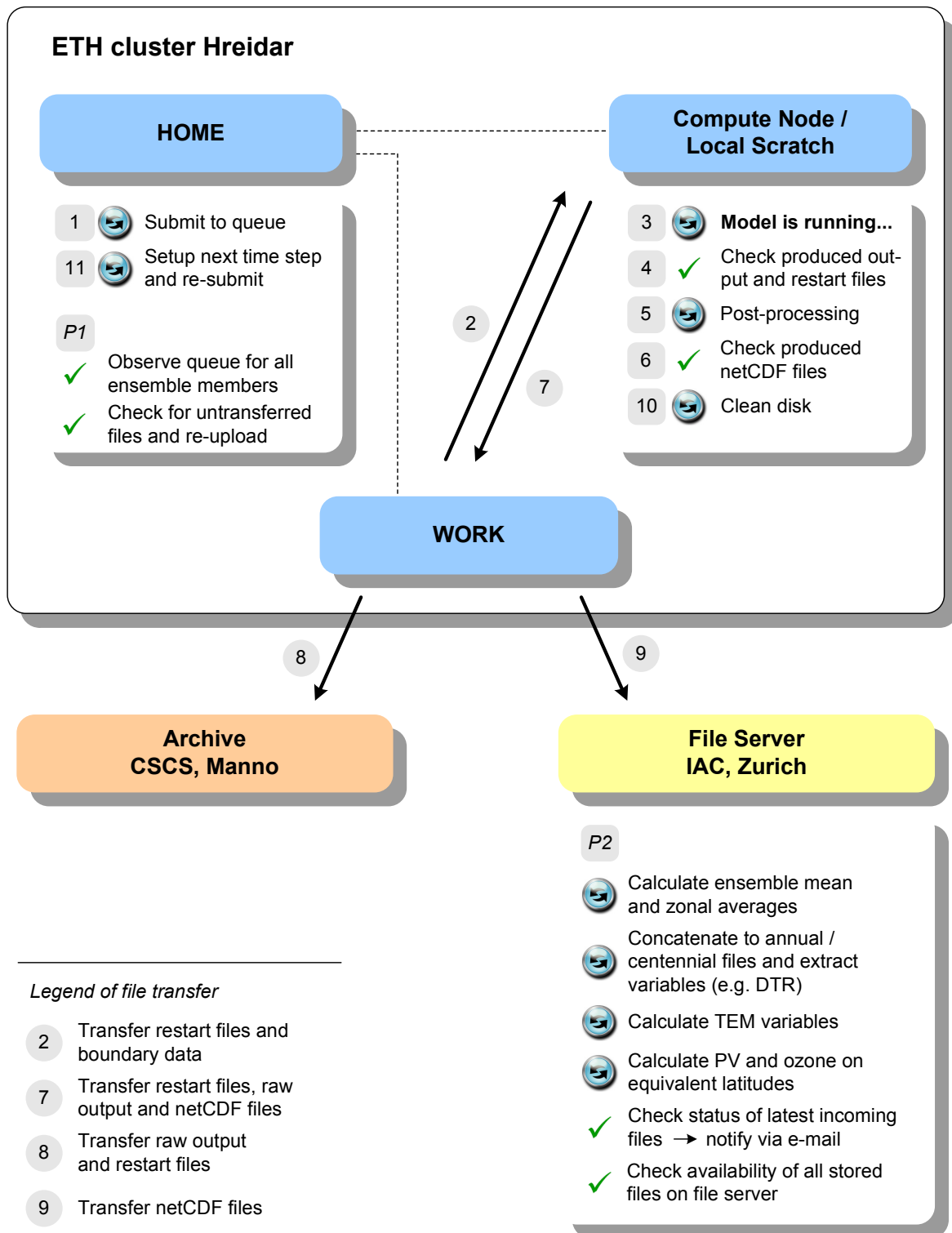


Figure 2.1 Schematic representation of the involved processes during the computation of the 100 year transient simulations. Single arrows denote data transfer, encircled double arrows represent processes on the different systems and check marks symbolize routines used to control progress. For the different enumerated steps, see text.

In the following an overview of the involved processes in the course of one ensemble member simulation is given (see Figure 2.1):

- 1) The job submission file is submitted to the queue at each model-month. A wall clock time limit is specified to terminate a job after some time in case a process hangs.
- 2) Input data and restart files of the current month are remotely copied (using rcp) to the local scratch of the compute node.
- 3) The model is running on the computing node. Standard error and output is stored as a text file on WORK server.
- 4) The availability of the output and restart files is checked. In case of failure the job stops and an e-mail- and SMS-notification is sent out.
- 5) The raw output is post-processed to monthly netCDF files using Fortran and C. For a small number of variables the output is additionally converted to 12-hourly netCDF files.
- 6) The availability of the netCDF files is checked. In case of failure the job stops and an e-mail- and SMS-notification is sent out.
- 7) Restart files, raw output and netCDF files have to be stored again on WORK before sending them to the outside world (see above).
- 8) Raw output and restart files are copied to CSCS using secure copy. A passwordless connection between Hreidar and CSCS was established offline. If the connection is broken, the run is continued and an e-mail-notification is sent.
- 9) NetCDF files are sent to the file server at IAC using secure copy. A passwordless connection between Hreidar and IAC was established offline. If the connection is broken, the run is continued and an e-mail-notification is sent.
- 10) The local scratch on the computing node must be cleaned before re-submission.
- 11) Month and year of the next time step is re-defined and exported as global variable. The script is re-submitted to the queue.

By means of cronjobs, a number of processes on Hreidar and IAC were periodically running during the full eight-month-computation:

- P1) One script regularly checked the queue to see if all ensemble member simulations are still running. If this is not the case, a notification was sent out. Since disk space on the WORK server was strongly limited and produced files could potentially reside (due to transfer connection failures, see step 8 and 9), another script checked the availability of these files and uploaded them independently to the file servers of CSCS and IAC.

P2) Several Perl-scripts were written to handle the flow of incoming data at IAC. Ensemble mean and (in case of chemistry) zonal mean calculations were accomplished using netCDF operators (NCO). For a more convenient handling, a large set of files were concatenated to annual and centennial files. Some variables (e.g. daily temperature ranges, DTR) were extracted from the standard netCDF files and stored in separate files. Moreover, using IDL in batch mode standard calculations (Transformed Eulerian Mean variables, potential vorticity and ozone on equivalent latitudes) were performed using netCDF files in 12-hourly resolution. Two scripts controlled the data flow at IAC: one script observed the latest incoming files from Hreidar and periodically sent out a status report. Another script checked for potentially missing files on the file server.

2.3 Validation of 20th century climate variability

The reproduction of prominent 20th century climate variability in the 100 year transient runs of SOCOL (version 2.0) was assessed within the CLIVAR C20C experiments (Folland, *et al.*, 2002, <http://grads.iges.org/c20c>). To test models against actual 20th century events, the model intercomparison, described in Scaife *et al.* (2008), only included models which completely specified the ocean state. By prescribing SSTs and sea ice extent, and by including various natural and anthropogenic forcings, both, the immediate atmospheric effects and the feedbacks from the ocean in a manner consistent with observed 20th century changes are considered (see also Sexton, *et al.*, 2001). In the following, the main results of Scaife *et al.* (2008) with respect to the performance of SOCOL (red in Figure 2.2 - Figure 2.4) against observations (black) and other GCMs (grey) are summarized:

Figure 2.2 (a) displays ensemble mean time series of global mean land surface air temperatures against observations. Increases in land surface temperature since the middle of the 20th century are mostly reproduced in all models showing around 0.7 K increase in temperature. The observed increase lies within the range of ensemble means and is therefore potentially predictable and forced (see Figure 1 in Scaife, *et al.*, 2008 for methodology). Most of the observed year-to-year fluctuations in land surface temperature, partly reflecting ENSO events and volcanic eruptions, are captured by the models. While in some models the amplitude of these fluctuations is considerably smaller than in observations, SOCOL shows a good match to the observed time series. This also holds for temperature trends over the last three decades of the 20th century (Figure 2.3 (a)), which is in SOCOL only slightly overestimated.

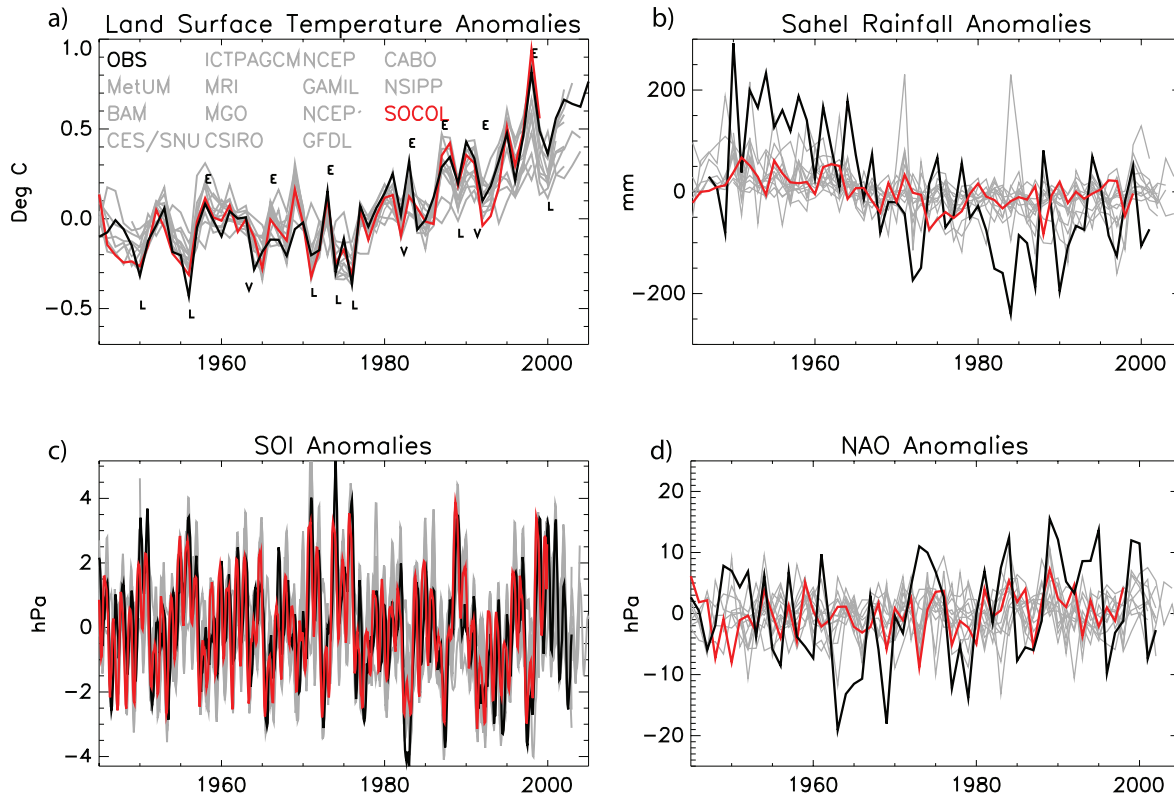


Figure 2.2 Time series of ensemble mean model simulations (grey) of: (a) Global mean land surface temperatures with large El Niño (E), La Niña (L) and volcanic eruptions (V) marked, (b) Sahel rainfall averaged over 12.5°N-17.5°N and 15°W-37.5°E and June-September, (c) Southern Oscillation index (5 month running mean of mean sea level pressure (PMSL) difference between nearest gridpoints to Darwin and Tahiti) and (d) Winter North Atlantic Oscillation index (DJF mean of PMSL difference between nearest gridpoints to Iceland and the Azores) from 1945 to 2005. Observations are highlighted in black and SOCOL in red.

The reproduction of observed Sahel rainfall anomalies and in particular the Sahel drought between 1950 and 1980 is shown in Figure 2.2 (b) and Figure 2.3 (b) and (d). Most models, including SOCOL, do not capture the observed year-to-year changes which is suggested to be only weakly driven by SST feedback or climate forcings. The observed negative trends over 1950 to 1980 are strongly underestimated in all models and only one single ensemble member reaches the observed long-term change. Interestingly, two models which show the largest changes in rainfall, have land surface changes via parameterized vegetation-climate interaction or specified changes incorporated. When switching off this interaction in one of the models (see closed circles for CABO model in Figure 2.3 (d)) the agreement got worse. However, vegetation interaction is sensitive to model details, since other models (e.g. SOCOL) show relatively weak trends despite prescribed vegetation changes.

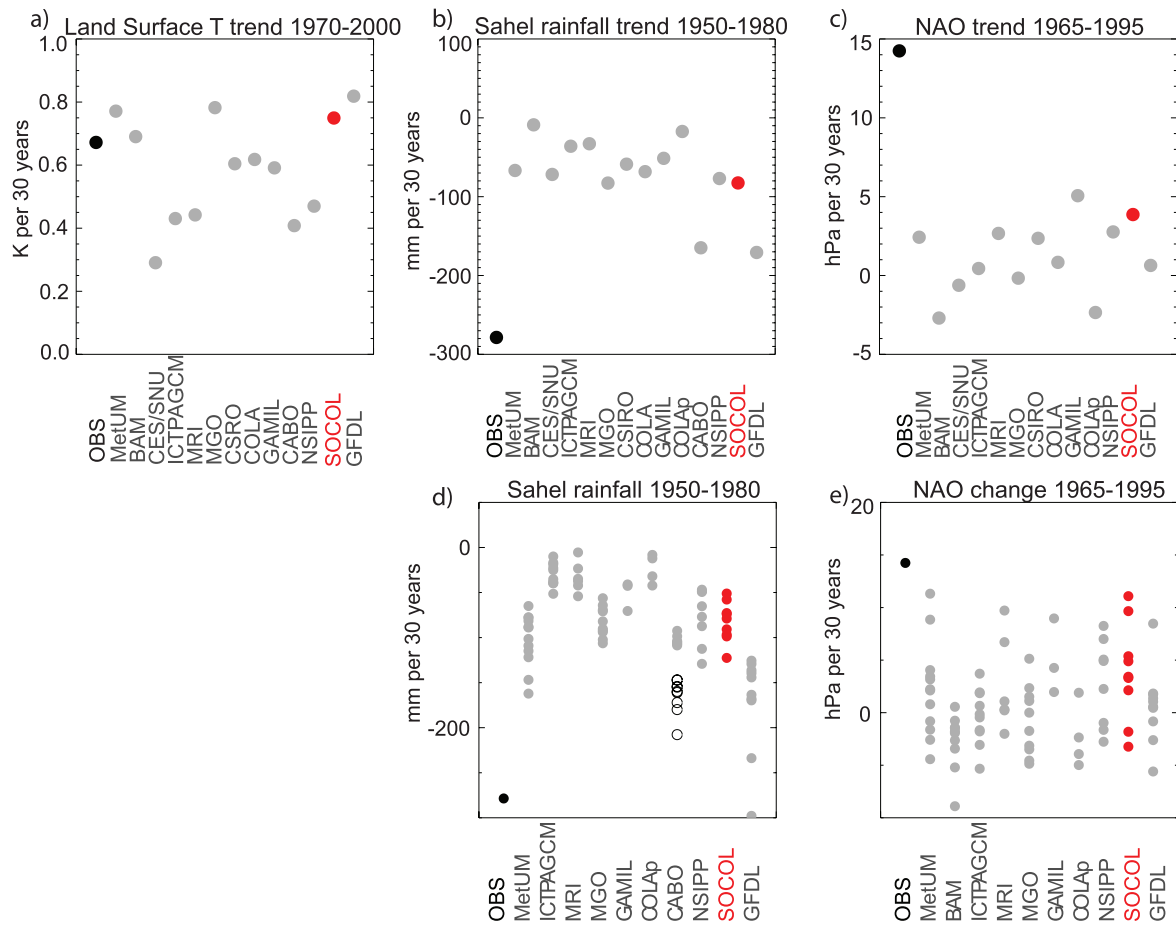


Figure 2.3 Above: Linear trend (in unit change per 30 years) for ensemble means of global mean land surface temperature from 1970 to 2000 (a), Sahel rainfall from 1950 to 1980 (b) and North Atlantic Oscillation index from 1965 to 1995 (c). Below (d and e): the same as (b and c) but for all ensemble member simulations. Observations are shown in black, SOCOL in red and all other model simulations in grey.

All the models simulate a strong ocean-atmosphere coupling in the tropical Pacific and the basic characteristics of the observed interannual variation in the Southern Oscillation index (SOI) (Figure 2.2 (c)). However, the models vary greatly with respect to the strength of the response. Modelled and observed regression coefficients between SOI and NINO3 SST were examined (Figure 2.4 (a)), where SOCOL displays a near perfect match with observations. It was suggested that the reason for very weak responses in some of the models is related to simplified representations of atmospheric physical processes in the models. Interestingly, the relationship of SOI and ENSO gives evidence of saturation in the surface pressure response during the strongest El Niño events (Figure 2.4 (b)). This is presumably due to a full shift in the convection cell out to the central tropical Pacific and a corresponding complete breakdown of the Walker circulation during very strong El Niño events.

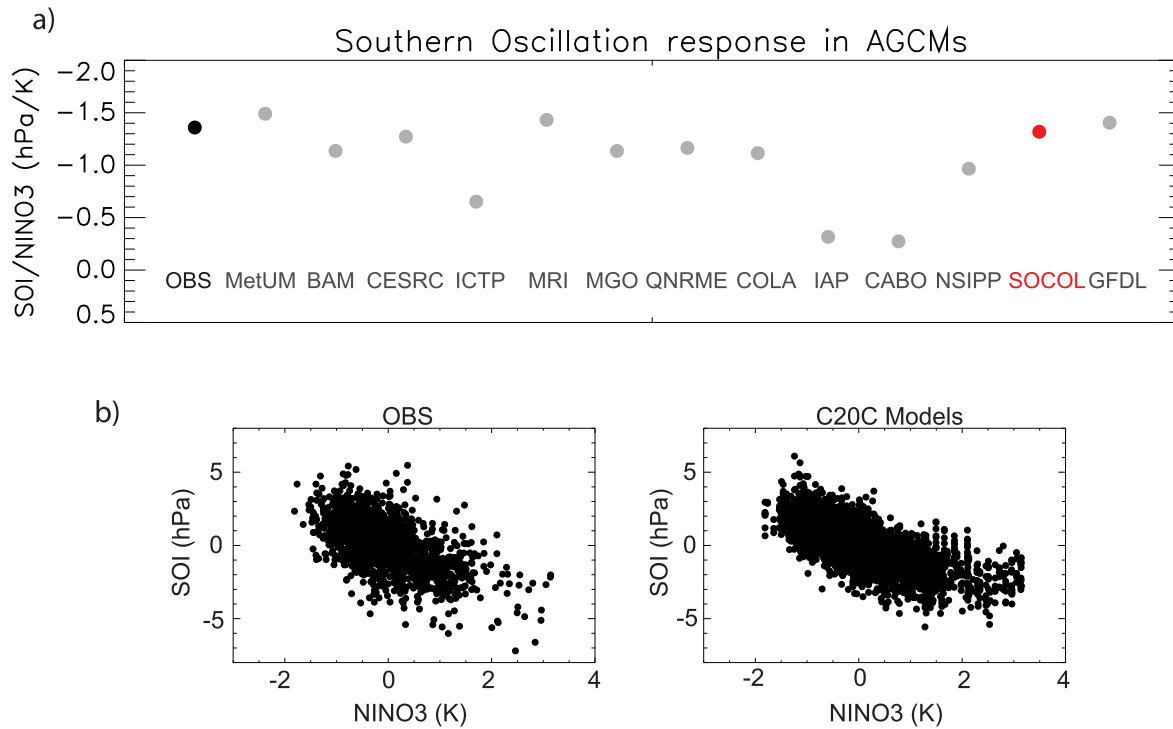


Figure 2.4 (a) Regression coefficients (in hPa/K) between SOI and NINO3 plotted for monthly deseasonalized data. (b) Scatter plots of monthly, deseasonalized SOI vs. NINO3.

Despite the prescription of observed SST and radiative forcings, there is only very weak correspondence between the ensemble mean evolution of the NAO and the observed index (Figure 2.2 (d)). On the decadal scale, the observed index rose over the 1965-1995 period followed by a subsequent decrease. In agreement with earlier modeling studies (*Hoerling, et al., 2004*) ensemble mean simulations strongly underestimate this change showing only a weak positive trend. The poor reproduction of the NAO increase can also not be further explained by the spread of ensemble members (Figure 2.3 (c) and (e)). Hence, a missing process or forcing might be responsible for the discrepancy. It is interesting to note that SOCOL simulates the second largest NAO trend in the ensemble mean suggesting that the interaction with the stratosphere could play an important role, since it is the only participating model with a detailed representation of stratospheric processes (including full interactive chemistry).

3 Low-frequency Variability in the Stratosphere

Interannual-to-Decadal Variability of the Stratosphere during the 20th Century: Ensemble Simulations with a Chemistry-Climate Model

A. M. Fischer¹, M. Schraner¹, E. Rozanov^{1,2}, P. Kenzelmann¹, C. Schnadt Poberaj¹, D. Brunner³, A. Lustenberger¹, B. P. Luo¹, G. E. Bodeker⁴, T. Egorova², W. Schmutz², T. Peter¹, S. Brönnimann¹

¹Institute for Atmospheric and Climate Science, ETH Zurich, Switzerland

²Physical-Meteorological Observatory/World Radiation Center, Davos, Switzerland

³Empa, Materials Science & Technology, Dübendorf, Switzerland

⁴National Institute of Water and Atmospheric Research, Lauder, Central Otago, New Zealand

(published in Atmos. Chem. Phys. Disc., 8, 14371-14418, 2008)

Abstract

Interannual-to-decadal variability in stratospheric ozone and climate have a number of common sources, such as variations in solar irradiance, stratospheric aerosol loading due to volcanic eruptions, El Niño Southern Oscillation variability and the quasi-biennial oscillation (QBO). Currently available data records as well as model simulations addressing stratospheric chemical climate variability mostly cover only the past few decades, which is often insufficient to address natural interannual-to-decadal variability. Here we make use of recently reconstructed and re-evaluated data products to force and validate transient ensemble model simulations (nine members) across the twentieth century computed by means of the chemistry-climate model SOCOL. The forcings included sea surface temperatures, sea ice, solar irradiance, stratospheric aerosols, QBO, changes in land properties, greenhouse gases, ozone depleting substances, and emissions of carbon monoxides, and nitrogen oxides. The transient simulations are in good agreement with

observations, reconstructions and reanalyses and allow quantification of interannual-to-decadal variability during the 20th century. All ensemble members are able to capture the low-frequency variability in tropical and mid-latitudinal total ozone as well as in the strength of the subtropical jet, suggesting a realistic response to external forcings in this area. The region of the northern polar vortex exhibits a large internal model variability that is found in the frequency, seasonality, and strength of major warmings as well as in the strength of the modeled polar vortex. Results from process-oriented analysis, such as correlation between the vertical Eliassen Palm flux (EP flux) component and polar variables as well as stratospheric ozone trends, are of comparable magnitude to those observed and are consistent in all analyzed ensemble members. Yet, trend estimates of the vertical EP flux component vary greatly among ensemble members precluding any robust conclusions. This suggests that internal variability in models must be accounted for in order to quantify the atmospheric model response in wave energy upon external forcings.

3.1 Introduction

The stratosphere exhibits chemical and dynamical variability on different time scales, ranging from day-to-day variability to interdecadal and longer variability, as well as exhibiting secular trends (*Solomon, 1999*). Through stratosphere-troposphere coupling, interannual-to-decadal variability originating from the troposphere can affect stratospheric climate (e.g. *Hadjinicolaou, et al., 2002*) and vice versa (see e.g., *Baldwin, et al., 2003*). For instance, volcanic eruptions (e.g. *Robock, 2000; Rozanov, et al., 2002*), solar variability (e.g. *Egorova, et al., 2004; Hood, 1999*), ozone depletion (*Gillett and Thompson, 2003*), or El Niño Southern Oscillation (ENSO) (e.g. *Sassi, et al., 2004*) may all affect both the troposphere and the stratosphere, and it is an open question to what extent climate changes are mediated by the stratosphere. Understanding the mechanisms underlying stratospheric interannual-to-decadal variability is important for detecting and attributing a possible ozone recovery as well as for assessing current and future climate change.

To study low-frequency variability in the stratosphere we have applied the new version of the chemistry-climate model (CCM) SOCOL (*Schraner, et al., 2008*) to simulate the 20th century in transient mode with a set of nine ensemble members. Most CCM-based studies focus on the past 30 years, analyzing the increase in anthropogenic ozone depleting substances (ODSs), the effects of volcanic eruptions, and of solar variability (e.g. *Austin, et al., 2003; Langematz, et al., 2003; Rozanov, et al., 2005; Rozanov, et al., 2002; Schnadt, et al., 2002; Shindell, et al., 1998*). This is also one of the goals of the “REF1-simulations” carried out in the CCM Validation Activity (CCMval) under the auspices of SPARC (see *Eyring, et al., 2006; Eyring, et al., 2005*). The past 30 years, however, is too short a time period to be representative of the full decadal variability of the stratosphere (see e.g., *Brönnimann, et al., 2004*). It is also the period with largest anthropogenic influences due to emissions of ODSs and greenhouse gases (GHGs) and thus less suitable for studying natural (solar, volcanic, ENSO) variability. There are a few transient CCM simulations that

go back to the 1960s or 1950s (*Austin and Wilson, 2006; Dameris, et al., 2005; Garcia, et al., 2007; Shindell, et al., 1998; Tegtmeier and Shepherd, 2007*). Yet, none of these simulations were carried out with a large set of ensemble members.

One aspect of scientific interest concerns changes in stratospheric wave driving over the past decades and future climate. As a response to increasing GHG concentrations, middle atmosphere models, irrespective of coupling with interactive chemistry, predict a positive trend in the total amount of wave energy reaching the stratosphere (*Butchart, et al., 2006*). Conversely, *Austin et al. (2003)* report on CCM simulations over 1979-2001 suggesting a reduction in stratospheric wave drag. However, the exact mechanisms for the circulation change suggested by the models remain unclear. The model spread is large and the trend over 1960-2000 is less clear than over future climate underscoring the need for ensemble member simulations to enhance the robustness of model results. Our simulations contribute to this discussion by allowing analysis of more simulations over a longer period. First results are shown in this paper.

While simulations covering the 20th century are standard for atmospheric general circulation models (AGCMs) (see also The Climate of the Twentieth Century (C20C) project, *Folland, et al., 2002; Scaife, et al., 2008*), this presents a challenge for CCMs as it requires additional data on boundary conditions as well as additional validation data. The necessary data, including information on the quasi-biennial oscillation (QBO) (*Brönnimann, et al., 2007*), upper-level geopotential height and temperature fields (*Griesser, et al., 2008*), as well as historical total ozone (TOZ) data (*Staehelin, et al., 1998; Vogler, et al., 2006; Vogler, et al., 2007*), are only now becoming available. For simulating the 20th century with SOCOL in transient mode we have specified solar irradiance, stratospheric aerosols, sea surface temperatures (SST) and sea ice (SI), emission of GHGs, ODSs, nitrogen oxides (NO_x) and carbon monoxide (CO), nudged QBO and time evolving land surface changes at the model's boundaries. The focus of the paper is on boundary conditions and analysis of long-term behavior in stratospheric ozone and dynamics.

The paper is organized as follows: Section 2 briefly describes the updated version of SOCOL, the compilation of boundary conditions, experimental model setup and observational data. Results of the long-term model performance in the stratosphere are shown in Sect. 3. Our conclusions and outlook can be found in the last section.

3.2 Descriptions of new model version, boundary conditions and observational data for comparison

A transient simulation over the 20th century (1901-1999) was carried out in ensemble mode (9 ensemble members) using the CCM SOCOL (*Schraner, et al., 2008*).

3.2.1 Model Description

The version of SOCOL used in the present work is essentially SOCOL Vs2 described in detail by Schraner et al. (2008). In brief, SOCOL Vs1 was first described and validated by Egorova et al. (2005a). It is a combination of the Middle Atmosphere version of the European Centre/HAMburg Model 4 (MA-ECHAM4) spectral AGCM (Manzini and McFarlane, 1998) and the chemistry-transport model (CTM) MEZON (Model for Evaluation of oZONe trends) (Egorova, et al., 2003). MA-ECHAM4 is a spectral model with T30 horizontal truncation and 39 vertical levels on a hybrid sigma-pressure coordinate system. The model spans the atmosphere from the surface to 0.01 hPa.

Chemical substances are transported by the hybrid numerical advection scheme (Zubov, et al., 1999), which consists of the Prather scheme in the vertical direction (Prather, 1986) and of the Semi-Lagrangian scheme in the horizontal direction (Williamson and Rasch, 1989). Through its flux-form, the Prather scheme is mass conservative enabling the maintenance of strong vertical gradients, whereas the Semi-Lagrangian scheme is not mass conserving. SOCOL was used for the CCMval REF1 simulation from 1975-2000 (Eyring, et al., 2006; Rozanov, et al., 2005).

The CCM intercomparison of Eyring et al. (2006) revealed several shortcomings in SOCOL compared to observations and other CCMs. A number of modifications of the transport and chemistry/micro-physics scheme in SOCOL have been applied to overcome these problems leading to SOCOL Vs2 (Schraner, et al., 2008). This included an improved parameterization of stratospheric water vapor condensation, extension of chemical transport to all species and a more sophisticated heterogeneous chemistry scheme. To overcome artificial mass redistributions leading to regional loss and accumulation caused by the Semi-Lagrangian transport scheme, a family-based mass fixing procedure for species of the nitrogen, chlorine, and bromine families was introduced. For ozone a similar mass fixing scheme, but restricted to latitudes between 40°S and 40°N, was introduced.

These modifications led to considerable improvements in key chemistry-climate parameters, most notably in high-latitude stratospheric chlorine (Figure 3.1). Compared to observations as well as to other CCMs, SOCOL has significantly improved in the region of the southern polar vortex. Any remaining discrepancies in stratospheric chlorine amounts have been attributed mostly to limitations of SOCOL's transport scheme. For a detailed description of the modifications and the results of the latest model version we refer to Schraner et al. (2008). In this study we performed one model run without the areal restriction (40°S to 40°N) of the mass fixing-procedure for ozone in order to analyze the effects of this implementation (see below).

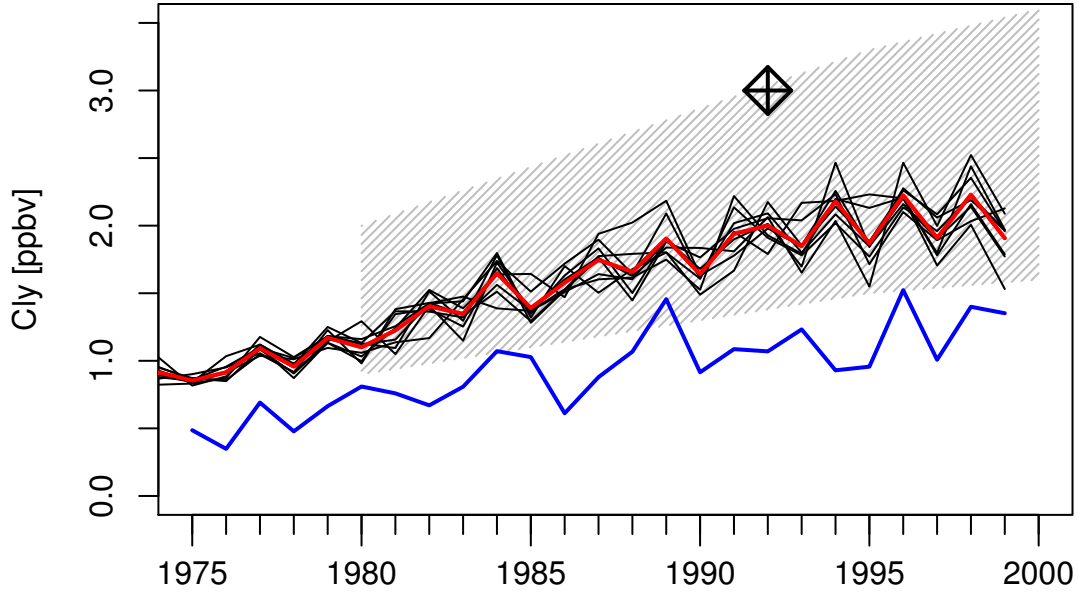


Figure 3.1 Time series of total inorganic chlorine in October at 50 hPa and 80°S for the ensemble members (black lines) and the ensemble mean (red line). The blue line shows the development predicted by the SOCOL version used for the CCMVal intercomparison published in Eyring et al. (2006). The grey hatched area indicates the range of all CCMs participating within CCMval except for SOCOL. An estimate of chlorine from HALOE HCl measurements in 1992 is indicated by the black diamond (see also Schraner, et al., 2008).

3.2.2 Boundary Conditions

Monthly and annually changing SST and SI distributions were obtained from the Hadley Centre HadISST data set (Rayner, et al., 2003). For the description of solar variability we used spectral solar irradiance data compiled by Lean (2000) (Figure 3.2a), which we applied to calculate the time evolution of solar heating and photolysis rates in the model.

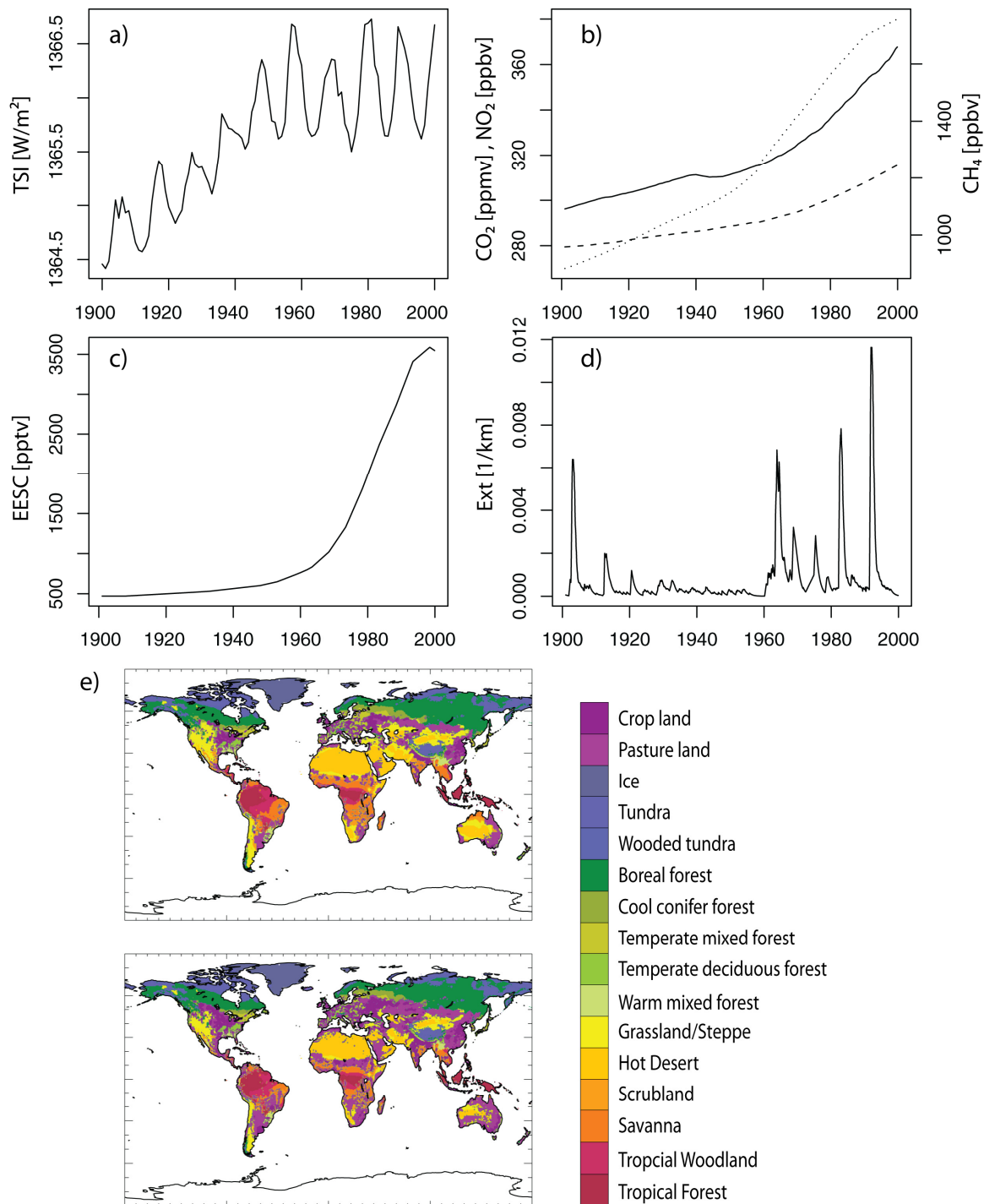


Figure 3.2 Boundary conditions used for the transient simulation: (a) Reconstruction of total solar irradiance (TSI in W/m²) (see Lean, 2000), (b) Greenhouse gas concentrations for CO₂ (solid, in ppmv), N₂O (dashed, in ppbv) and CH₄ (dotted, in ppbv), (c) Ozone Depleting Substances shown in equivalent effective stratospheric chlorine (EESC, in pptv), (d) Global mean extinction by stratospheric aerosols at 550 nm and an altitude of 22.5 km (Ext. in 1/km) (see Sato, et al., 1993), (e) Vegetation classes of HYDE (see Goldewijk, 2001) for the year 1900 (above) and 1990 (below).

Emissions

GHG (Figure 3.2b) and organic chlorine and bromine containing source gases (ODSs) are prescribed in SOCOL in the 5 lowermost model layers (corresponding to the lowermost ~ 1.5 km in the model). Figure 3.2c shows the time development of equivalent effective stratospheric chlorine (EESC) derived from ODSs mixing ratios. For 1959-2000 the monthly values of N₂O, CH₄, and CO₂ are based on WMO (2003) and obtained from the CCMval website (http://www.pa.op.dlr.de/CCMVal/Forcings/CCMVal_Forcings.html). For GHG mixing ratios before 1959, a combination of ice core and in situ measurements was used as described by Machida *et al.* (1995) and Etheridge *et al.* (1998; 1996) and provided on the GISS website (<http://data.giss.nasa.gov/modelforce/ghgases/>).

Sixteen organic chlorine and bromine source gases are taken into account for the representation of ODSs. Values based on the CCMval website (see above) for 1959-1999 were complemented with CH₂Br₂ and CHBr₃, two short-lived bromocarbons emitted naturally from the ocean, for which we assumed a constant contribution of 1.63 pptv and 1.21 pptv, respectively, throughout the century (see also Warwick, *et al.*, 2006). Prior to 1959, we extended the ODSs time series with data from WMO (2003) where available. For methylchloride and methylbromide a linear atmospheric trend was applied during the 20th century inferred from Antarctic firn air measurements (Butler, *et al.*, 1999; Sturges, *et al.*, 2001).

Surface emissions of CO and NO_x are represented by fluxes similar to those used for the CTM MOZART-2, representing values of the year 1990 (Horowitz, *et al.*, 2003). Natural sources were assumed to remain constant during the simulated period, while the time dependence of anthropogenic emissions was taken into account using data from EDGAR-HYDE 1.3 (van Aardenne, *et al.*, 2001), given on a 1° x 1° grid at 10 year intervals. These data include emissions from fossil fuel consumption, biofuel combustion, industrial processes, agricultural land, savannah burning, deforestation, and agricultural waste burning. The seasonal cycle of MOZART-2 was superimposed on the total emissions. Time-dependent aircraft NO_x emissions are identical to those used for the CCM E39/C (Dameris, *et al.*, 2005), regridded to the SOCOL grid. They are based on a data set by Schmitt and Brunner (1997).

Aerosols

The time evolution of stratospheric aerosols is prescribed by the GISS data set described in Sato *et al.* (1993) with later updates available on <http://data.giss.nasa.gov/modelforce/strataer/> (see also Figure 3.2d). For the period 1850-1999 these data contain monthly resolved and zonally averaged optical depths at 550nm for four altitude bands from 15 to 35 km height and a latitude grid spacing of 8°. Reference to the GISS data set is less accurate than using directly the gap-filled SAGE aerosol record of Thomason and Peter (2006), as was done by Schraner *et al.* (2008). However, that record dates back only to the late 1970s, which is why we decided in favor of the GISS

data set. Aerosol optical depths are estimated from optical extinction data for 1882-1990, whose quality increases with time. Since 1979 data are complemented with satellite observations of the Stratospheric Aerosol and Gas Experiment (SAGE I/II) and Stratospheric Aerosol Measurement (SAM II) (*Sato, et al.*, 1993).

The monthly stratospheric aerosol properties of SOCOL (as zonal cross sections) are prescribed with surface area densities as well as with extinction coefficients, asymmetry factors and single-scattering albedos for all 8 spectral bands (2 shortwave and 6 longwave bands). The computation of these parameters was performed offline using optical depths and effective radii of GISS as input parameters. Data of effective radii during major volcanic eruptions before 1980 were reconstructed based on observations during the eruptions of El Chichon and Mt. Pinatubo. These data were also obtained from the GISS website. The computation of aerosol properties is based on Mie theory assuming an H_2SO_4 concentration in the particle of 70 wt%, a width of a log-normal distribution of 1.8 and using temperatures from ERA40.

After the model runs discussed here had been performed, an analysis of the data set revealed an error in the single-scattering albedo, which was set to 1.0 (scattering only) instead of around 0.995 in the near infrared band during Mie calculation. This results in a slight underestimation of heating due to the presence of stratospheric aerosols. However, besides the volcanically most perturbed periods this error will not have any significant effect on the model results.

Tropospheric aerosols are prescribed by a climatology described by *Lohmann et al.* (1999), used for the calculation of local heating rates and shortwave backscatter.

Quasi-Biennial Oscillation

The oscillation of stratospheric equatorial winds is nudged in SOCOL according to *Giorgetta* (1996). The prescribed zonal mean zonal wind field includes 19 pressure levels (from 90 hPa up to 3 hPa). For the years 1957-1999 data were obtained from ERA40, and back to mid-1953 from the Free University of Berlin. Prior to that, we made use of a QBO-reconstruction that is based on historical pilot balloon wind data and on the QBO signature in the semidiurnal surface pressure oscillation which was extracted from historical sea-level pressure data. The reconstruction was validated with an independent reconstruction based on historical TOZ data, and it was found that after around 1910, the phase of the QBO in the middle stratosphere during peak phases should be correct around 80% of the time. Details on the final reconstruction and validation are given by *Brönnimann et al.* (2007).

Land surface changes

Effects of anthropogenic vegetation changes have been taken into account using the HYDE “A” data set (*Goldewijk*, 2001), which is compiled on a 0.5° by 0.5° grid. It includes pasture and cropland areas from 1700 to 1950 in 50 year intervals and additionally for 1970 and 1990. Wherever possible *Goldewijk* (2001) organized the allocation of cropland

and pasture on a country level using historical population density maps. Figure 3.2e illustrates the spread of pasture and cropland areas over the globe from 1900 to 1990 (violet colors). In order to assign the historical vegetation maps to ECHAM4, we mapped the 18 vegetation classes to the ECHAM vegetation classes (*Claussen, et al., 1994; Hagemann, 2002; Hagemann, et al., 1999*) and interpolated them to the model grid.

Vegetation parameters in ECHAM4 (*Roeckner, et al., 1996*) are implemented following estimates by *Claussen et al. (1994)*, prescribing land surface characteristics as a global field for present-day conditions. For our purpose, we follow later updates by *Hagemann et al. (1999)* and *Hagemann (2002)*, who made use of improved estimates of the dependence of vegetation parameters on different vegetation classes as well as of a much higher resolved global distribution of major ecosystem types (*Olson, 1994*).

Using the mapped and regridded historical vegetation maps we assigned tabulated estimates of surface background albedo, surface roughness length, vegetation ratio, forest coverage, leaf area index, soil water capacity and volumetric wilting point to each vegetation class (*Hagemann, 2002*). The aggregation of surface roughness length to the coarser grid was not performed by linear upscaling but using an inverse logarithmic formulation (*Claussen, et al., 1994*). As recommended by *Hagemann et al. (1999)*, we replaced the constant value of volumetric wilting point (as in *Roeckner, et al., 1996*) with a global spatially varying data set (*Patterson, 1990*). For years not included in the data set we interpolated the fields linearly in time.

3.2.3 Experimental Design

For spin-up we used the off-line CTM version driven by daily circulation, temperature and tropospheric water vapor representing the last year of the 25-year long time-slice experiment with CCM SOCOL described by *Egorova et al. (2005a)*. We have carried out a 10 year long run with this model using boundary conditions (NO_x - and CO- emissions as well as ODSs and GHG concentrations) for 1890-1899. All mixing ratios, except tropospheric water vapor, were set to zero for the initialization. The coupled simulation started in 1900 with a one-year spin-up of the GCM part. In the second year of the coupled simulation, we perturbed the CO_2 concentration during one month in the range of 0.01% to obtain the nine different ensemble members, which after 1901 were driven by identical boundary conditions. The simulations were run until December 1999.

3.2.4 Comparison to observational data

The focus of the present study is on the model's performance in simulating long-term stratospheric chemistry and climate. Our analysis focuses on ozone and dynamics for which a wealth of observational data are available. The chemical performance of SOCOL Vs2 was extensively validated by *Schraner et al. (2008)*. Key tropospheric climate parameters for the 20th century have been analyzed in SOCOL within the framework of the CLIVAR C20C Project (*Scaife, et al., 2008*). This intercomparison revealed a good

match with observations as well as with other atmospheric general circulation models on interannual and decadal time scales.

Modeled TOZ is compared against three observational data sets, the National Institute of Water and Atmospheric Research (NIWA) (*Bodeker, et al., 2005*) combined database, data from the Backscatter Ultraviolet (BUV) instrument on the Nimbus 4 satellite in the early 1970s (see also *Stolarski, et al., 1997*), and ground-based TOZ measurements prior to 1970, obtained from the World Ozone and Ultraviolet Radiation Data Centre (WOUDC). We contrast ozone distributions to the newly reprocessed Solar Backscatter Ultraviolet (SBUV) data set (version 8) (*Rosenfield, et al., 2005*) and to a combined data set of SAGE-I/SAGE-II (55°S-55°N) supplemented with high latitude ozonesonde measurements at Syowa (69°S) and Resolute (75°N) providing global coverage from 10 to 50 km altitude (referred to as SAGE data set, for details see *Randel and Wu, 2007*). Prior to 1970 we compare SOCOL results to ozonesonde measurements from several European and North American stations, obtained from WOUDC. In addition, for estimation of stratospheric ozone trends we make use of the Candidoz Assimilated Three-dimensional Ozone (CATO) data set (*Brunner, et al., 2006a*). This data set, providing global coverage, was reconstructed by assimilating TOZ satellite observations, corrected for offsets and drifts against the Dobson network, into an equivalent latitude – potential temperature framework.

To address dynamical features, fields of modeled zonal wind and zonal temperature are compared with the ERA40 reanalysis results (*Uppala, et al., 2005*). The northern subtropical jet index (referred to as “SJI” and measured as the maximum zonal mean zonal wind at 200 hPa in the 0°N-50°N belt) and polar vortex strength (referred to as “PVS” and measured as the difference between zonal mean geopotential height of the 100 hPa level averaged over 75°N-90°N and 40°N-55°N, respectively) were reconstructed as in *Brönnimann et al. (2006a)*, i.e. using the same predictor data and reconstruction method. The reconstructions cover the period 1922 to 1947 and were merged with NCEP reanalysis data (*Kistler, et al., 2001*) thereafter. Eliassen-Palm fluxes (EP flux) were calculated from ERA40 and NCEP data by I. Wohltmann and are based on formulations by *Andrews et al. (1987)*. Note that in the following we refer to reanalysis results of ERA40 and NCEP as “observations”, acknowledging that they are the output from a model based assimilation of observations.

3.3 Results

3.3.1 Analysis of Ozone

Figure 3.3 displays modeled climatologies (ensemble mean) of zonal mean TOZ over the century. From 1901 to 1960 the seasonal variation in TOZ remained almost unchanged. The increasing concentrations of ODSs in the atmosphere (see Figure 3.2c) initially led to depleted TOZ only in the region south of 70°S for August to October (climatology over 1961-1980). Compared to BUV data from 1970-1976 (in a period where ODSs

concentrations were still relatively low), SOCOL underestimates the TOZ peak in the Northern Hemisphere (NH) and the Southern Hemisphere (SH) which is probably connected to remaining mass fixing problems of the Semi-Lagrangian transport scheme (*Schraner, et al.*, 2008).

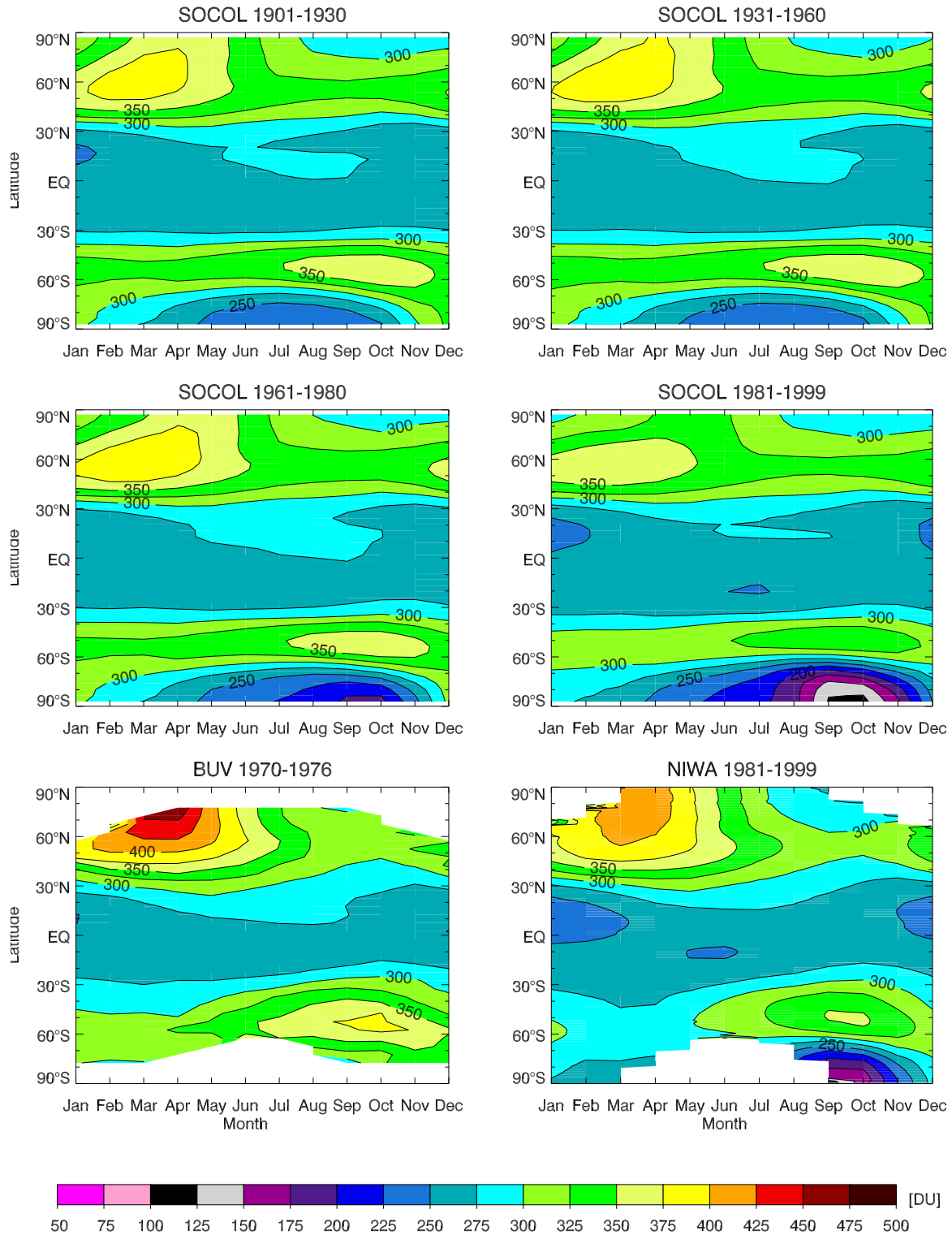


Figure 3.3 Climatologies of zonal mean TOZ (in DU) for the ensemble mean simulation of SOCOL for 1901-1930 (upper left), 1931-1960 (upper right), 1961-1980 (middle left) and 1981-1999 (middle right). Measurement onboard satellites of BUV (1970-1976) and NIWA (1981-1999) are shown in lower left and lower right panel, respectively.

For the more recent time period (1981-1999), modeled TOZ amounts dropped globally and hence altered the seasonal cycle at all latitudes in line with observations. However, the simulated ozone hole is somewhat deeper (values drop to 100 DU) and persists longer than in the NIWA climatology. In terms of latitudinal extent of the ozone hole, model and observations are in good agreement. In autumn over mid-latitudes TOZ is generally too high compared to NIWA, leading to an underestimation of the seasonal cycle. In general, the simulated TOZ climatologies over the past two decades are comparable to those simulated by other CCMs described in *Eyring et al.* (2006).

To address the evolution of TOZ in the nine different ensemble members and hence to qualitatively judge the internal variability of the simulations, we have analyzed TOZ anomalies back to 1970 with respect to 1979-1999 in five latitude bands (see Figure 3.4). This is compared with a special run with the ozone mass fixer applied to the global field (blue line) instead of the standard restriction to the latitude band 40°S-40°N as described above (for details of the mass fixing procedure see *Schraner, et al.*, 2008). For mid-latitudes and the tropics the low-frequency variability of all SOCOL ensemble members is in good agreement with the NIWA collection of observations. The TOZ reduction due to the volcanic eruptions of El Chichon (1982) and Mt. Pinatubo (1991) are visible in the tropical belt in the model and the observations. Yet, the modeled decay seems to be too dominant and too fast. In polar regions the amplitude of interannual variations is larger than at lower latitudes. Consistent with observations, a negative trend due to increasing ODSs concentrations is visible at all latitude belts. However, a shortcoming of SOCOL is the reduced amplitude of the seasonal cycle poleward of 30° in both hemispheres. The reason for this underestimation, which is independent of the detailed configuration of the mass fixer (compare blue and grey curves in climatologies of Figure 3.4), is presently not clear. The Arctic shows the largest internal variability of the seasonal cycle, especially in spring, reflecting different perturbations of the polar vortex among the ensemble members.

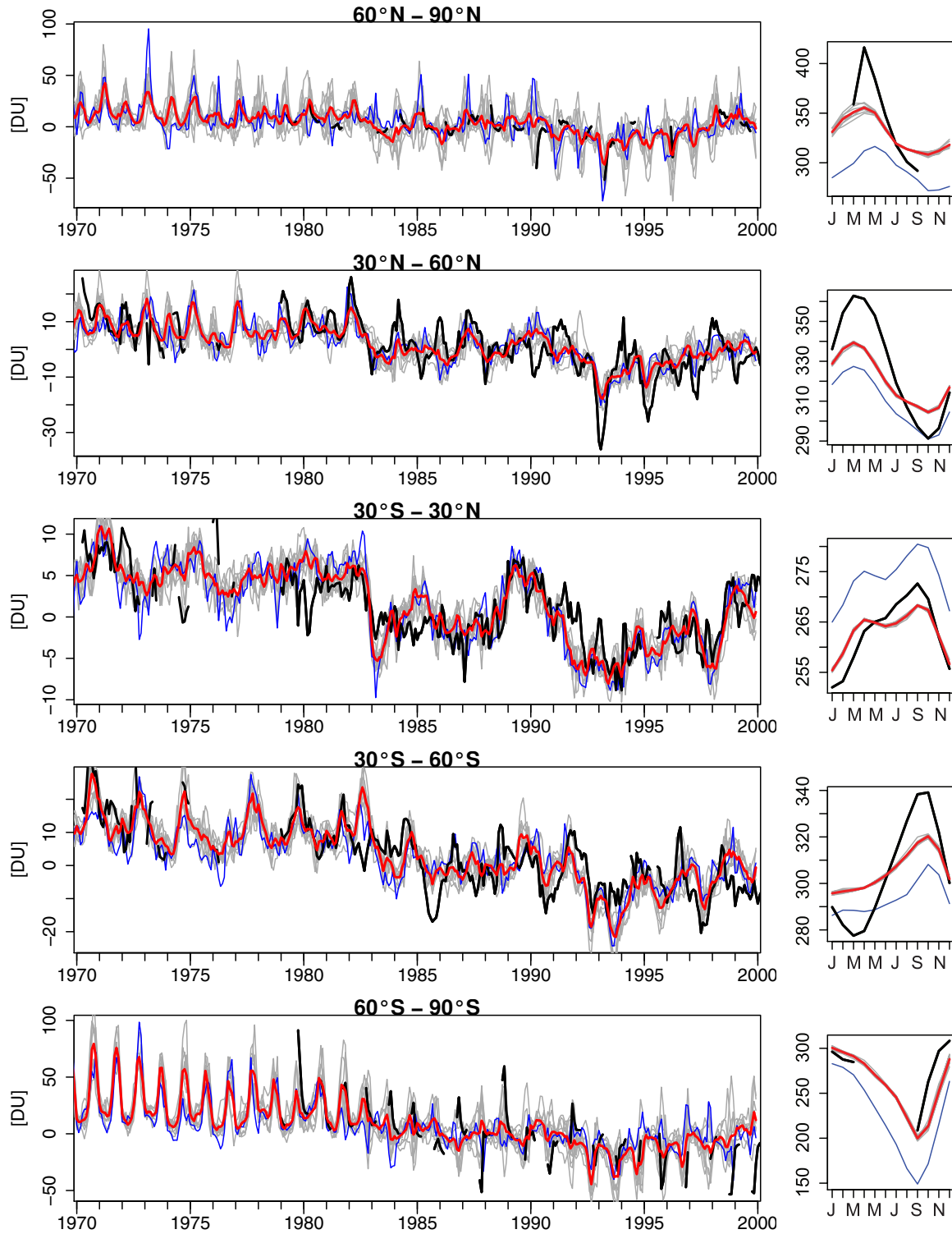


Figure 3.4 Left: Time series (1970–1999) of zonal mean TOZ anomalies (with respect to 1979–99, in DU) latitudinally averaged over 60°N–90°N, 30°N–60°N, 30°S–30°N, 30°S–60°S, 60°S–90°S (from top to bottom panel) for individual ensemble members (grey), ensemble mean (red) and satellite observations (black) of BUV (1970–1976) and NIWA (from 1979). The blue line denotes a simulation with a modified SOCOL version (mass fixing procedure for ozone changed from a mass fixer applied to the 40°S–40°N latitude band to a globally (90°S–90°N) applied mass fixer). Right: Climatologies over 1979–99 for the five latitude belts.

Due to the restriction of the ozone mass fixer to the 40°S-40°N band, where much of the Semi-Lagrangian transport error occurs (*Schraner, et al.*, 2008), the correction of the violation of mass conservation leads to a stronger downward adjustment of TOZ in the tropics compared to the scheme with global application of the fixer. Conversely, not applying the fixer to higher latitudes increases TOZ values, which leads to a more realistic seasonal amplitude. We have compared other fields of the ensemble mean and the run with globally applied mass fixer (e.g. zonal wind, temperature, ozone), but did not find any irregularities that would disprove an areal restriction of the mass fixing procedure for ozone. Therefore, in the following we address the results of the nine ensemble simulations with the constraint mass fixer.

To validate modeled TOZ before 1970 we have used NH ground-based stations of Svalbard, Tromsø, Uppsala, Oxford and Arosa that allow longer-term analysis (starting between 1924 and 1955) and cover a wide latitude range (46°N to 77°N, see Figure 3.5). The series of Svalbard and Oxford have only recently been reevaluated (*Vogler, et al.*, 2006; *Vogler, et al.*, 2007) and provide an excellent data source to validate decadal scale transient simulations with a CCM. By and large, the ensemble members of SOCOL are in reasonable agreement with observations. This is especially true for Svalbard, but less so for the autumn months in Uppsala, Oxford, and Arosa. In general, observed seasonal extreme deviations from the annual mean are well represented by some of the individual ensemble members.

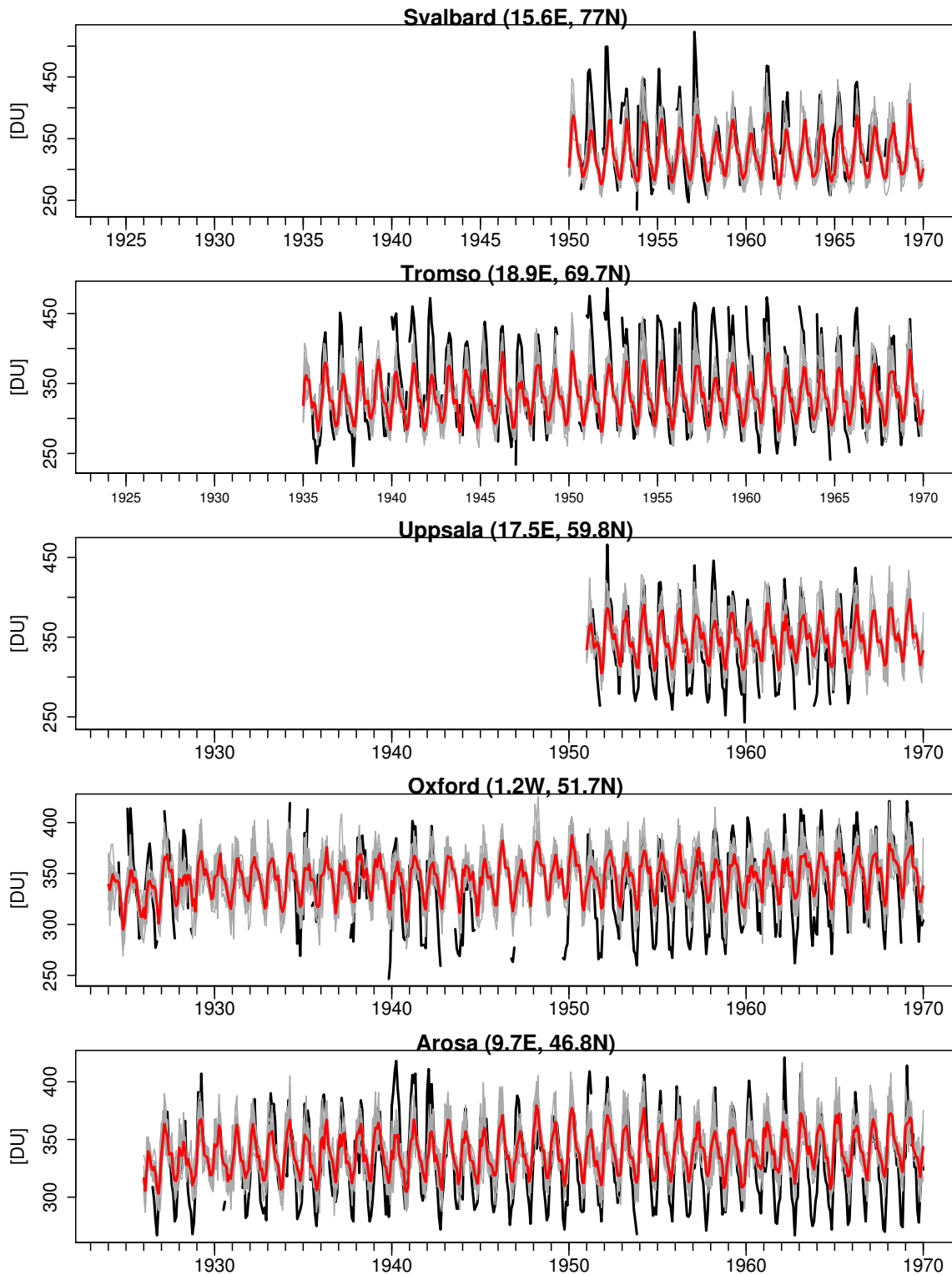


Figure 3.5 Modeled (ensemble members: grey; ensemble mean: red) and observed (black) time series of TOZ before 1970 at different locations in the NH: Svalbard (15.6°E and 77°N starting 1950), Tromsø (18.9°E and 69.7°N starting 1935), Uppsala (17.5°E and 59.8°N starting 1951), Oxford (1.2°W and 51.7°N starting 1924) and Arosa (9.7°E and 46.8°N starting 1926).

Similar to TOZ, zonally averaged vertical ozone also reveals little climatological change before the late 1970s. Conversely, over the past two decades ozone mixing ratios dropped significantly, e.g. for the month of January, by around 1 ppmv at 10 hPa for the latitudes north of 80°N (see Figure 3.6). Compared to observations of SBUV for the period of 1970-1976 and 1979-1999, the location and magnitude of the maximum ozone concentration in the tropics is well reproduced. Yet, model and observations diverge in the upper stratosphere (above the 10 hPa level), with largest discrepancies (up to 2 ppmv below observations) over the NH (SH) in boreal winter (summer). Below the 10 hPa level modeled ozone is too high (more than 1 ppmv), especially over the tropics and the SH (NH). This bias was already documented in *Eyring et al.* (2006) and *Schraner et al.* (2008) and is present in all months. The comparison of ozone number densities against observations of SAGE confirms these findings in the lower and upper stratosphere. It additionally shows an underestimation of ozone throughout the stratosphere in winter polar regions, leading to smaller than observed TOZ values (compare Figure 3.3).

Prior to 1970 we validated the model runs with ozonesonde observations from the 1960s of Hohenpeissenberg, Uccle, Payerne, Boulder, and Resolute, e.g. Figure 3.6e for the January intercomparison. Note, that a high quality for these old measurements is not assured and a validation to model results can therefore only be done in a qualitative way. For this comparison, only Brewer Mast measurements with a correction factor between 0.9 and 1.35 (0.9-1.2 in case of Hohenpeissenberg) were considered (similar to *Logan*, 1994). Brewer Mast data are more reliable than Regener type of measurements which were frequently applied at that time (S. Oltmans, personal communication) but excluded in the present study. The European stations in Figure 3.6e are at similar latitudinal location and shown together to obtain a more robust result.

In general, SOCOL is in qualitatively good agreement with these old station measurements. This is especially the case compared to European stations and Boulder throughout the year. In contrast to the Canadian station Resolute, which is located further north, modeled ozone mixing ratios in the lower stratosphere are comparable in winter but higher and outside the observed interannual standard deviation during summer (not shown). The model internal variability as well as the year-to-year fluctuation in station data is largest during wintertime and reduces in summer.

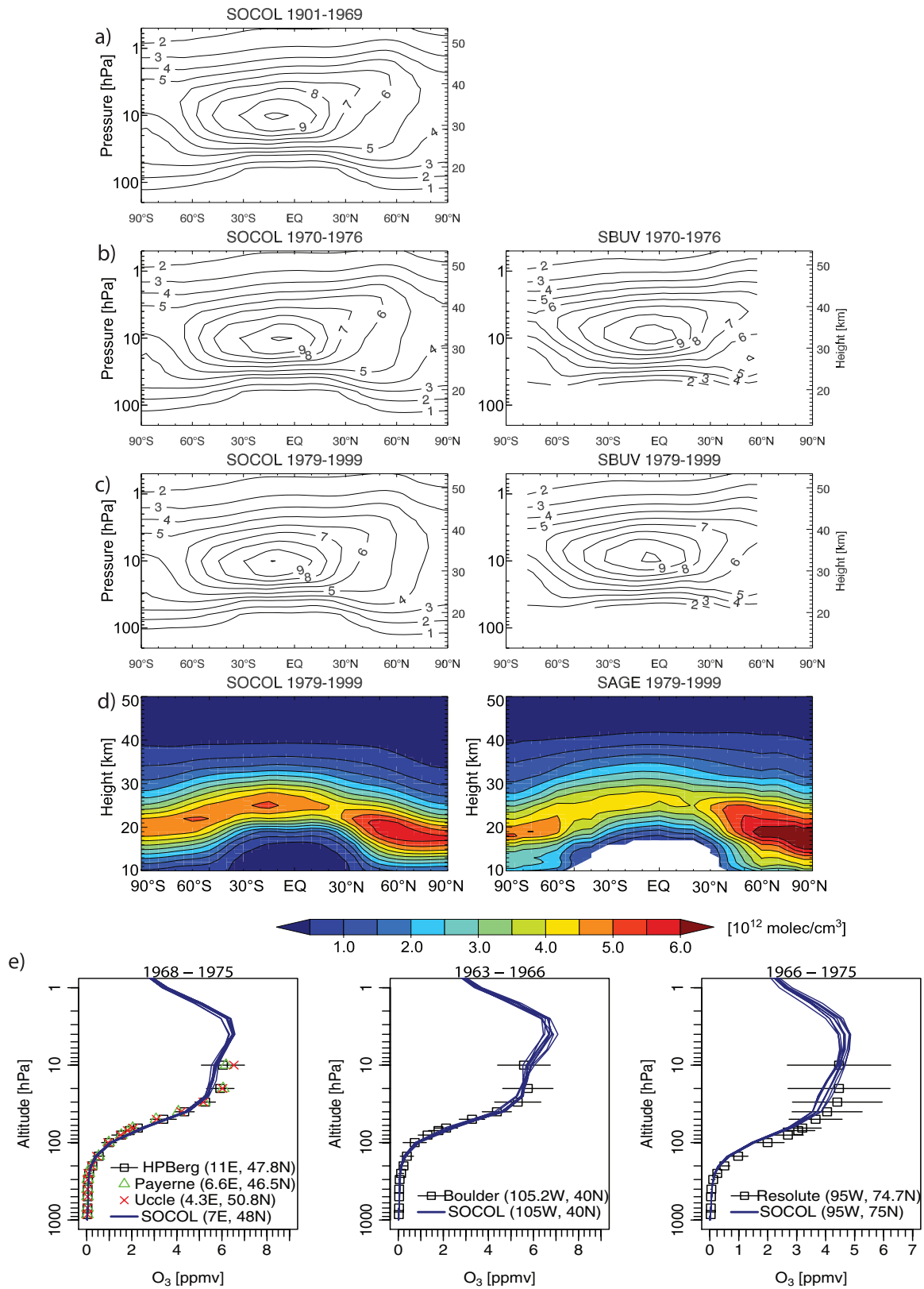


Figure 3.6 (a) – (c) Climatological zonal mean ozone distributions for January (in ppmv) for: (a) Socol over 1901-1969, (b) Socol (left) and SBUV version 8 (right) over 1970-1976, (c) Socol (left) and SBUV (right) over 1979-1999. January ozone number densities (in 10^{12} molecules per cm³) of Socol (left) and SAGE (right) are shown in (d) over 1979-1999. (e)

Climatological January ozone profiles (in ppmv, with horizontal bars indicating interannual standard deviations of observations) of Hohenpeissenberg (HPBerg), Payerne, Uccle (left panel), Boulder (middle panel), Resolute (right panel) and corresponding profiles from SOCOL.

To analyze the model runs in a process-oriented framework, we have tested whether the sensitivity of ozone upon increasing concentrations of ODSs is correctly reproduced. We estimated ozone trends from 1979-1999 by applying a multiple linear regression analysis with solar variability (see Figure 3.2a), two orthogonal QBO time series at 10 and 30 hPa, (method based on *Wallace, et al.*, 1993) and extinction from stratospheric aerosols (at 550 nm, see Figure 3.2d) as explanatory variables and zonally averaged ozone anomalies as target value.

$$O_3(t) = b \cdot EESC(t) + c \cdot solar\ cylce + d_1 \cdot QBO_{10} + d_2 \cdot QBO_{30} + e \cdot strat\ aer + \varepsilon(t)$$

The trend coefficient b is regressed upon EESC time series (see Figure 3.2c) and given in percentage per unit EESC. (Note that in a strict sense, the coefficient b is not itself a trend, but the sensitivity of ozone with respect to the trend prescribed by EESC, see *Maeder et al.* (2007). However, in the following for simplicity we refer to it as a trend.) Also note that percentage trends are calculated with respect to the average over the trend period. Autocorrelations within the residual time series $\varepsilon(t)$, which affects the significance level of the trend estimate (p-value), were eliminated by applying a third-order autoregressive process. The linear regression model was applied to individual ensemble members (not shown) and ensemble mean simulation of SOCOL as well as to observational data sets of SBUV, CATO and SAGE (see Figure 3.7).

The general pattern of estimated trends in zonal mean ozone is comparable in all ensemble member simulations. The upper stratospheric ozone trends in the ensemble mean and individual members of SOCOL show two significant local minima around 40 km altitude of up to -10%/ppbv EESC. This is in excellent agreement with SBUV and SAGE data. Upper stratospheric negative trends in both hemispheres are also appearing in CATO but the magnitude is much lower and probably an artifact of the reconstruction (*Brunner, et al.*, 2006b). In the Antarctic lower stratosphere a downward trend of more than -20%/ppbv EESC can be observed in SAGE and CATO which is generally underestimated in SOCOL (-14%/ppbv EESC averaged over all members). However, the variability among the ensemble members in this region is larger and three ensemble members reach the magnitude of observed trends. *Garcia et al.* (2007) also reported a too small downward trend in the ensemble mean simulation with the Whole Atmosphere Community Climate Model (WACCM). Note, that the lower than observed TOZ values over southern high latitudes mentioned above is a result of a negative bias (due to remaining artificial problems of the transport scheme), present throughout the century, rather than an effect of a negative trend. In the Arctic lower stratosphere the ensemble mean of SOCOL shows a significant negative trend that is only somewhat smaller than in SAGE and CATO.

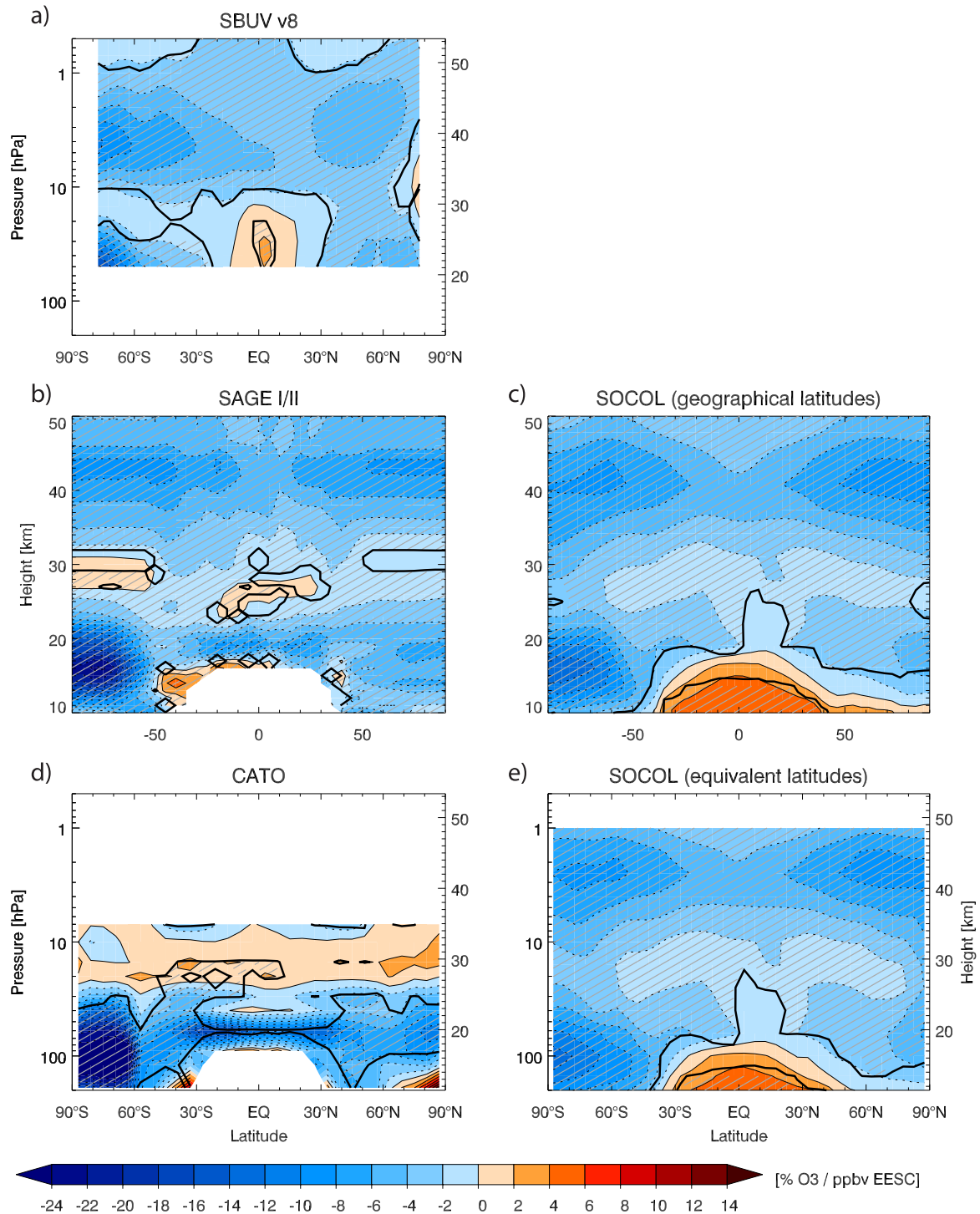


Figure 3.7 Modeled and observed trends (EESC coefficient) of zonal mean ozone (in % / ppbv EESC) over 1979-1999: (a) SBUV version 8, (b) SAGE I/II, (c) SOCOL on geographical latitudes, (d) CATO, (e) SOCOL on equivalent latitudes. Shaded areas together with black contour line mark statistically significant areas (p -value < 0.05).

3.3.2 Analysis of Dynamics

A realistic model representation of dynamical features is a prerequisite for a reliable simulation of ozone and other trace gases as well as for understanding the interaction between dynamics and chemistry. To assess the stratospheric model dynamics we first examined the well-known basic processes for the winter and summer hemispheres. Figure 3.8 illustrates the ensemble mean of zonal mean zonal wind for different climatic periods and in relation to ERA40 for the month of January and July. In SOCOL climatological zonal wind has hardly changed from 1901-1957 to 1958-1970. It simulates very well the main characteristics in both hemispheres and seasons. The northern winter polar vortex in SOCOL exceeds the observed wind speed by more than 7 m/s. This bias is less significant in the period 1958-70 than in the more recent period (1971-1999). In the winter SH zonal winds in the middle to upper stratosphere are weaker than observed for 1958-1970 but stronger for 1971-1999, especially in a latitude band of 55°S-75°S. Upper stratospheric easterlies are simulated in both summer hemispheres in agreement with ERA40. However, the areal extent is confined to the mid-latitudes in contrast to ERA40 where strong easterlies prevail over the whole hemisphere. A further discrepancy to ERA40 is a slight shift of the modeled subtropical jet towards the tropics in all periods (see also Brönnimann, *et al.*, 2006b). Its magnitude, however, looks reasonable compared to ERA40.

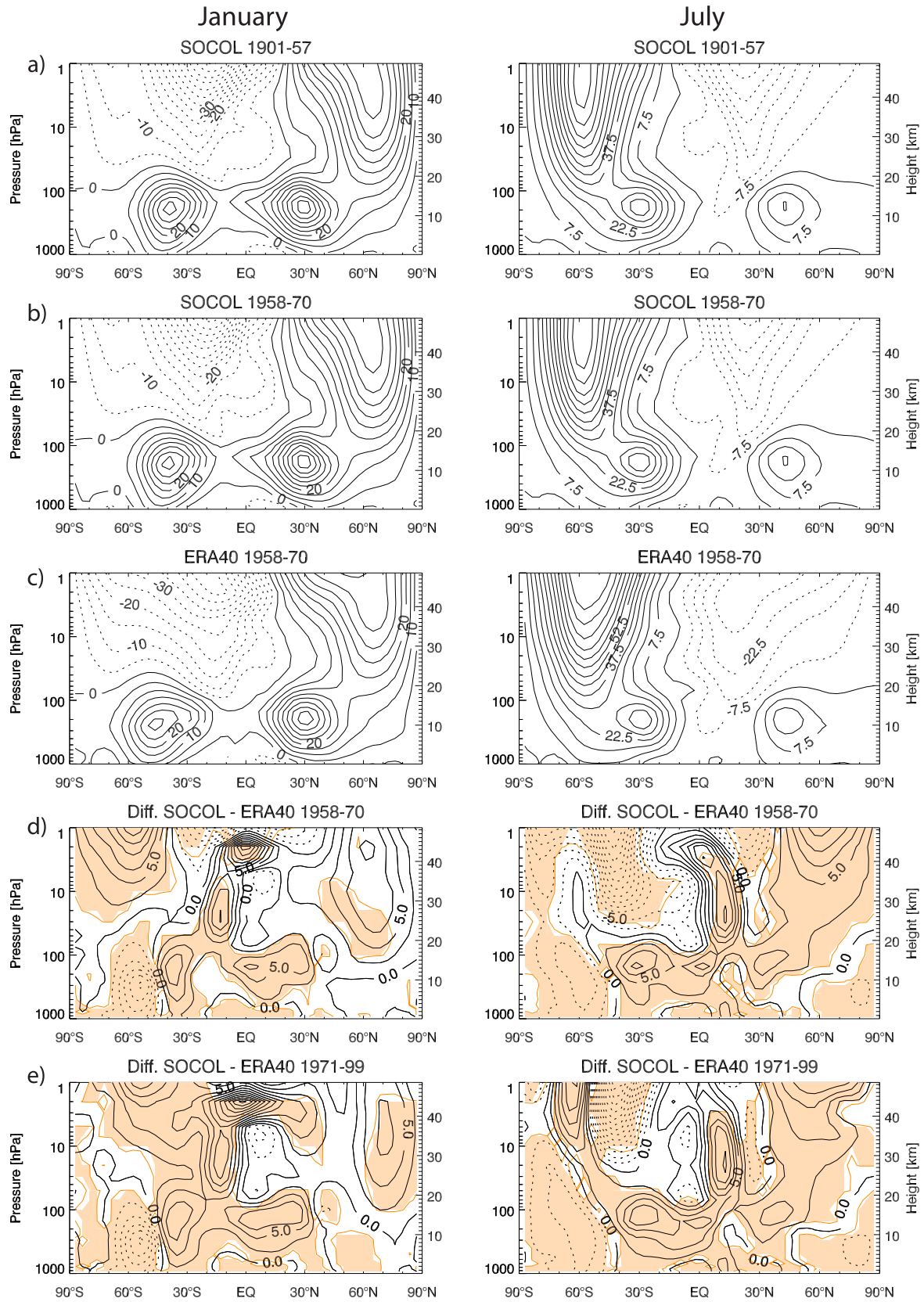


Figure 3.8 Absolute zonally averaged zonal wind (in m/s) for month of January (left) and July (right): (a) Socol 1901-57, (b) Socol 1958-70, (c) ERA40 1958-70 and climatological

differences between model and ERA40 during (d) 1958-70 and (e) 1971-99. Orange shading and contour line mark statistically significant areas (t -test, p -value < 0.05).

To further assess the model's performance in the stratosphere, we have analyzed zonal mean temperature (Figure 3.9) representing another important factor for the distribution of stratospheric chemical species. Similar to zonal wind, no big alterations in modeled zonal temperature can be observed for the first seven decades. In line with a stronger northern polar vortex, modeled temperatures show colder temperatures at northern high latitudes between 100 and 10 hPa suggesting too little downwelling over high latitudes. In the Antarctic stratosphere, above 100 hPa, higher temperatures are simulated than in the reanalyses in the period 1958-1970, but to a lesser degree for 1971-1999 reflecting again the sensitivity to the polar vortex. In general, agreement between ERA40 and SOCOL is better for July than January where a cold bias is present in the lower and upper stratosphere over almost all latitudes. A cold bias in the upper stratosphere might be connected to a rather simplified absorption scheme of MA-ECHAM4 for solar UV radiation (Egorova, *et al.*, 2005a). Note that the upper stratospheric temperatures are subject to a large variability among different CCMs, as well as observational data (Eyring, *et al.*, 2006). Negative model biases near the tropopause can be explained by the coarse vertical resolution in the upper troposphere-lower stratosphere (Egorova, *et al.*, 2005a). The modeled cold tropical tropopause temperature is well reproduced regarding location and magnitude and only slightly underestimated. In general, SOCOL is well able to capture the main dynamical characteristics in zonal mean wind and temperature back to 1901.

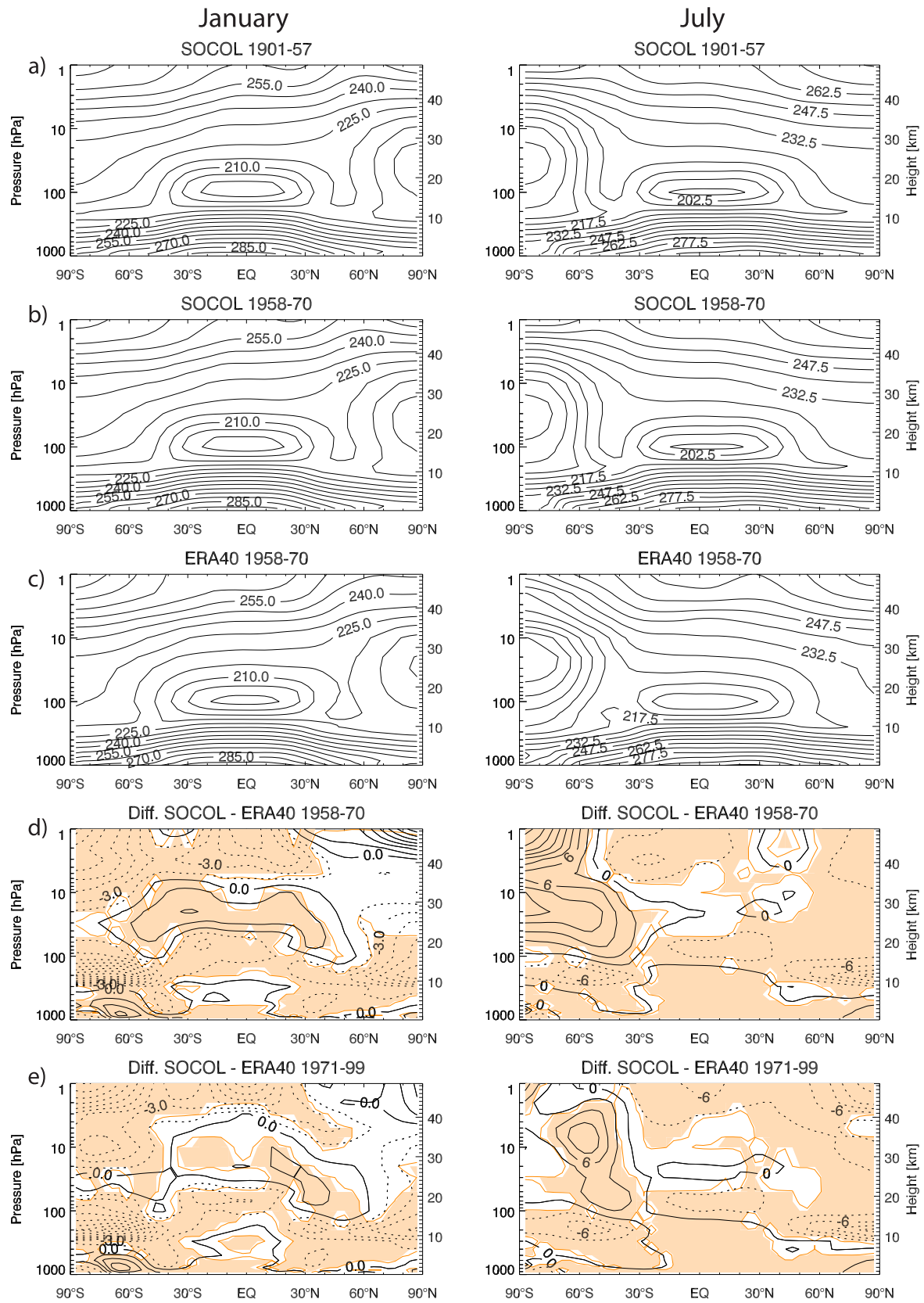


Figure 3.9 same as Figure 3.8 but for zonal temperature (in K).

To address interannual variability in all nine ensemble members back to 1920, we have analyzed boreal winter time series of SJI and PVS (Figure 3.10). Model results are compared to indices for the month of January to March (when reconstructions show sufficient skill, i.e. a reduction of error (RE) greater than 0.36) (see *Brönnimann, et al., 2006a*). Note that such a comparison is only possible for the Northern Hemisphere, where enough historical upper air station data is available. In the case of SJI the correlation between ensemble mean simulation and the observed index is high (0.74) and internal variability within SOCOL rather low. SJI is strongly related to tropical SST and hence ENSO via changes in the Hadley Circulation. SOCOL simulates a very strong ENSO response and thus agrees extremely well with the reconstructed index. SOCOL captures comparably little of the year-to-year variability in the PVS reconstruction, although observations mostly lie within the large ensemble spread. The correlation between the ensemble mean and reconstruction is far lower (0.25) than for SJI and does not increase for individual ensemble members. Yet, it is interesting to note that two individual deviations from the mean are modeled fairly well: winter 1976 and 1987, which are possibly linked to anomalous ENSO events (*Brönnimann, et al., 2006b; Fischer, et al., 2008b*).

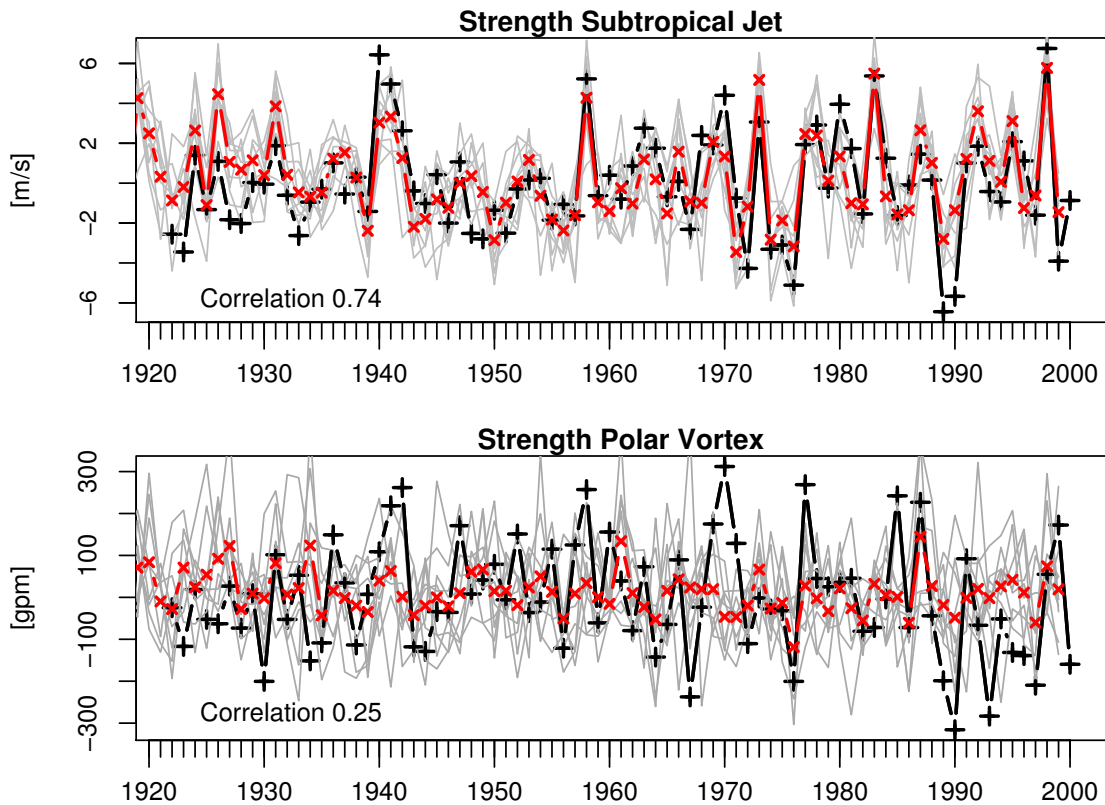


Figure 3.10 SJI (upper panel) (maximum zonal mean zonal wind at 200 hPa in the latitudinal region of 0°N - 50°N) and PVS (lower panel) (zonal mean difference between 75°N - 90°N and 40°N - 55°N in 100 hPa Geopotential Height), averaged from January to March and subtracted from a climatology of 1961-1990. Displayed are the individual ensemble members (grey lines), ensemble mean (red) and statistically reconstructed time series. The correlation coefficient of the ensemble mean and the reconstructions are indicated at the lower left of the plots.

To further elucidate the large model spread in the north polar region in TOZ and PVS, we have analyzed major warmings (MW), being a major source of interannual variability during boreal winter (see e.g., Matsuno, 1971). We have applied a standard WMO index with two criteria to diagnose MWs in the model and ERA40 for the months of November to March (see also Chaffey and Fyfe, 2001): 1) 10 hPa temperature difference between 60°N and 90°N is positive for four consecutive days (also referred to as “minor warming, note that due to horizontal model resolution we have extracted the fields at latitudes 61°N and 85°N) and 2) zonal mean zonal wind at 10 hPa and 60°N changes from westerly to easterly flow within the minor warming period (also referred to as the “central date”). The central dates were counted separately in each ensemble member and analyzed upon frequency and seasonality (Figure 3.11). Changes in zonal wind from westerly to easterly were counted only once within a minor warming period and possible final warmings in late March were excluded.

The total number of MWs for ERA40 over 1958-1999 amounts to 28, which is by a factor of 3-4 larger than in SOCOL averaged over all members for the same period. This is in agreement with the above mentioned findings of a too strong modeled northern polar vortex. On average, in 17% (66.6%) of analyzed years a MW is found in SOCOL (ERA40). For the period 1901-1957 the percentage is only slightly higher (22%). Dameris *et al.* (2005) also reported a too small number of modeled MWs in the E39/C model. Their model top, however, is at 10 hPa which hinders to fully capture the propagation of gravity waves and its interaction with the polar vortex.

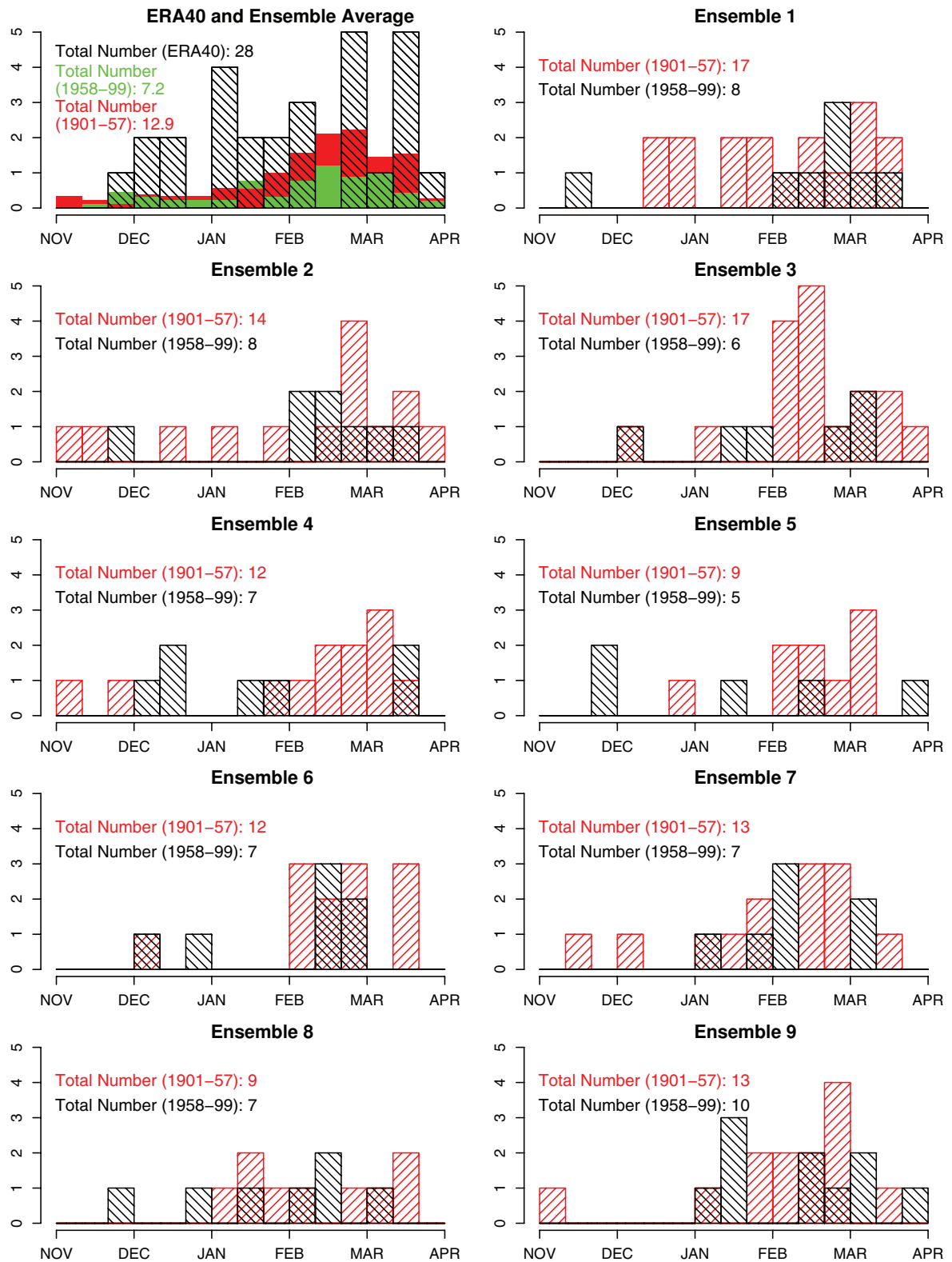


Figure 3.11 November to April histograms of major warmings in the NH for ERA40 (upper left panel) and the 9 different ensemble members over the period 1901–1957 (red) and 1958–1999 (black). The green (red) shading in the upper left panel denotes the averaged number of model occurrences for 1958–1999 (1901–1957).

A large fraction of MWs is normally observed in January/early February and in late February and mid-March. Five MWs occurred in late November to mid-December. Ensemble members diverge largely in the occurrence of MWs in early winter but show an increased frequency towards the end of winter on average in line with ERA40. In January the chance for a simulated MW, however, is generally low (similar to *Dameris, et al.*, 2005).

We defined four different parameters addressing the strength of individual MWs (Figure 3.12) in both periods, 1901-1957 and 1958-1999: a) Maximum zonal mean temperature at 85°N and 10 hPa, b) Maximum zonal mean temperature at 61°N and 10 hPa, c) Minimum zonal mean wind at 61°N and 10 hPa, and d) Maximum temperature increase at 10 hPa and 85°N within 5 days. In general the strength parameters in the ensemble members are in reasonable agreement with ERA40 (note that data distribution in Figure 3.12 is generally less skewed in ERA40 than in SOCOL). For temperature at 85°N (Figure 3.12a), SOCOL shows a slight positive bias for 1958-1999, whereas agreement is better for the latitude 61°N. The magnitude of average minimum easterly winds is somewhat lower in SOCOL than in ERA40. Good agreement is found for the fourth strength parameter (Figure 3.12d), where temperature increases in the range of 10 to more than 60 K per 5 day window are simulated and observed.

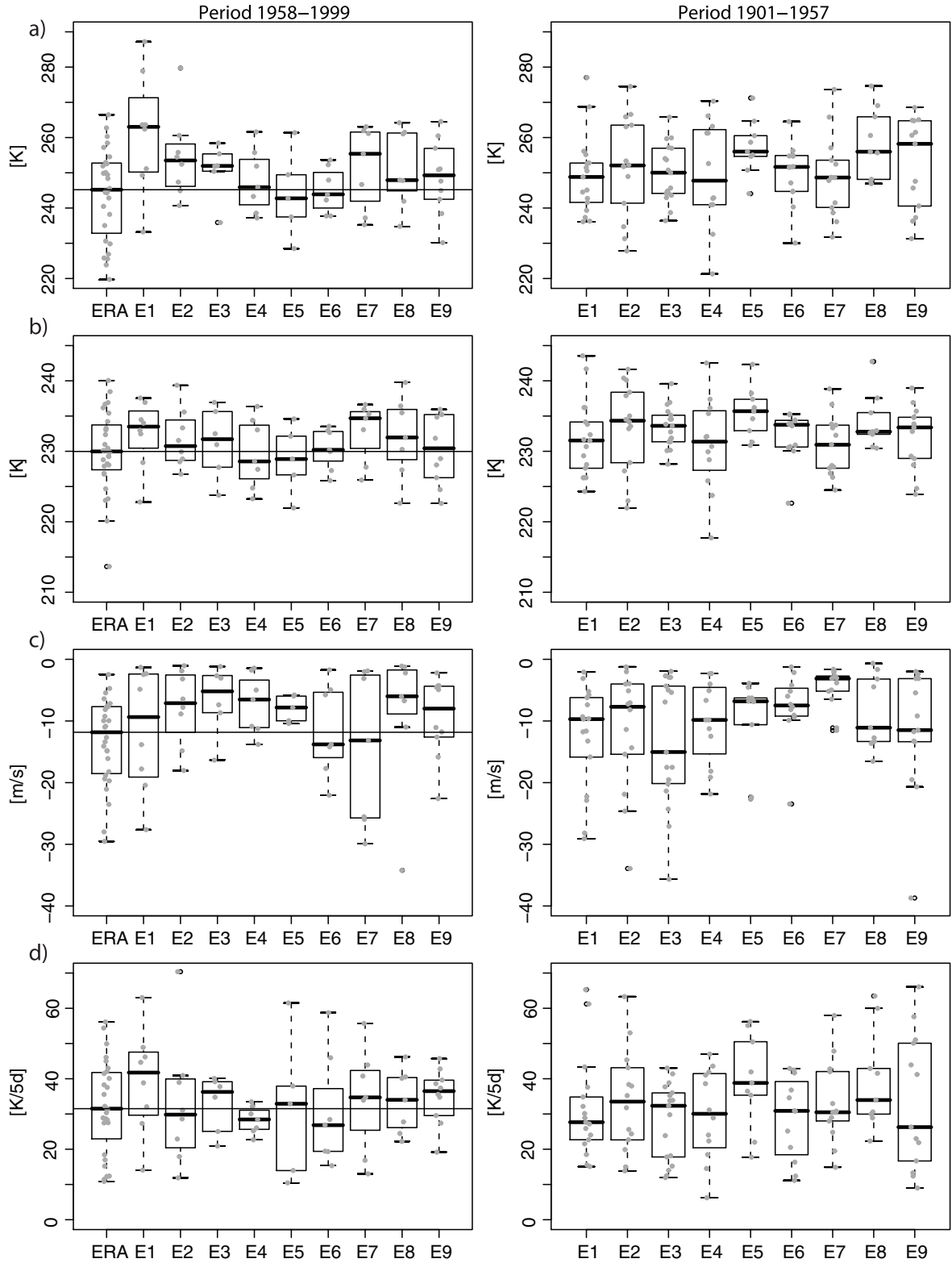


Figure 3.12 Strength parameters of major warmings in the NH for 1958–1999 (left, ERA40 and individual ensemble members, E1–E9) and 1901–1957 (right, for E1–E9): (a) Maximum zonal temperature (in K) at 85°N and 10 hPa, (b) same as (a) but at 61°N, (c) Minimum zonal mean zonal wind (in m/s) at 61°N and 10 hPa, (d) Maximum temperature increase at 10 hPa and 85°N within 5 days (in K/5d). The horizontal line in the boxplots displays the median, the upper and

lower edge of the box mark the 1st and 3rd quartile. The individual major warmings are indicated by grey dots.

Perturbations on the polar vortex and resulting MWs are caused by interaction of propagating waves, which is analyzed in the following. We have first evaluated the vertical component of the 100 hPa EP flux (EPz), averaged over 40°N-80°N and 40°S-80°S respectively, over the century to see whether the model captures the total midwinter wave activity that propagates from the troposphere into the stratosphere on an interannual-to-decadal scale. Time series of EPz during winter months are shown in Figure 3.13a. The overall magnitude of simulated EPz looks reasonable compared to observations of NCEP and ERA40 in both hemispheres. In the NH some individual developments in the averaged SOCOL time series appear as in observations: e.g., 1966, 1970-1975, 1983-1987. At least part of these anomalies are related to warm ENSO events which increase the vertical wave propagation in SOCOL and suggest again a strong model response to ENSO. In the SH interannual variation in the model and the reanalyses show a less good match, the latter showing a positive trend over the whole period. Yet, SH EP flux in the reanalyses are less reliable and the trend could be an artifact of the data assimilation, since more observational (satellite) data could be assimilated in later years which may influence the representation of waves. To overcome this, we have compared climatologies of EP flux diagnostics over the period 1990-1999 (not shown). In the NH (SH) modeled EPz is lower than ERA40 from 30°N – 60°N throughout the stratosphere (from 50°S-80°S up to 20 hPa). In addition, wave mean flow interaction measured by the divergence of the EP flux is attenuated in SOCOL (less negative) north of 40°N (in the SH the signal is also positive but less dominant). This may explain the stronger than observed polar vortex and the reduced number of MWs seen above. Conversely to this finding, we did not find a general weaker residual meridional circulation (RMC) as would be expected from reduced wave mean flow interaction. The tropical tape recorder exhibits too strong upwelling compared to observations (not shown). Yet, the estimated upward velocities are not constant in altitude but rather show stronger windspeed from 100 hPa to 40 hPa and reduced windspeed from 40 hPa and 10 hPa, similar to *Steil et al.* (2003) for simulation with MA-ECHAM4/CHEM model.

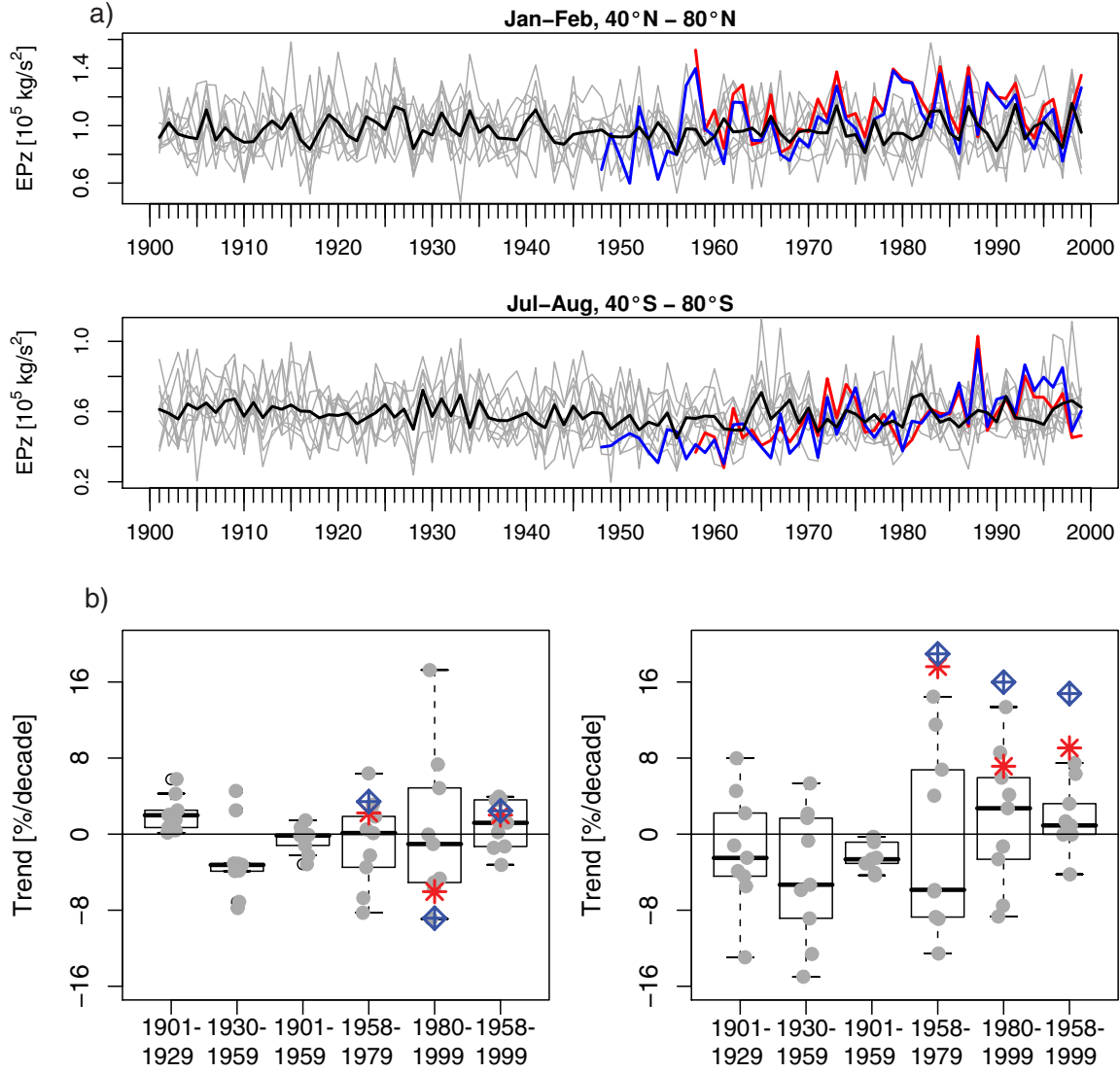


Figure 3.13 (a) Upper panel (lower panel): January to February (July to August) averaged time series (1901-1999) of the vertical EP flux component (in 10^5 kg/s^2) at 100 hPa, averaged over 40°N - 80°N (40°S - 80°S) for ensemble members (grey), ensemble mean (black), ERA40 (red) and NCEP (blue). (b) Boxplot of calculated Northern Hemisphere, left panel, (Southern Hemisphere, right panel) EP flux trends (in %/decade) for different time periods in the ensemble simulations (grey dots), ERA40 (red) and NCEP (blue).

Trends of EP flux and the RMC are presently a widely discussed topic of the scientific community (see e.g., Butchart, *et al.*, 2006). We have calculated trends of EPz (of Figure 3.13a) within the modeled and observed time series for different time windows to account for decadal variability (Figure 3.13, Table 3.1 and Table 3.2). Reanalyses show a positive NH EPz trend of around 2%/decade (not significant) over 1958-1979 and a negative trend over 1980-1999. Model realizations over the same period simulate trends of opposite signs (Table 3.1), which are mostly not significant. Over 1980-1999 the model realizations do not capture the negative trend as in the reanalyses. Note that most CCMs show a smaller than observed negative trend for the period 1979-2001 (Austin, *et al.*, 2003) which is not

significant in most models. Model results before 1958 are somewhat more conclusive: seven out of nine members show a negative trend over 1930-1959 and a positive trend over 1901-1929 for the whole set of ensemble members. Yet, statistical significance on the 5% level is again almost absent in all ensemble members.

In the Southern Hemisphere, for 1958-1999, SOCOL features a large model spread with trend estimates of both signs compared to very strong positive trends in the reanalyses (Table 3.2), which could be affected by data quality (see above). Note that ERA40 and NCEP show rather large dissimilar trends in the Southern Hemisphere. One realization shows a significant positive trend (on the 5% level) of 7.5%/decade over 1958-99. This is somewhat smaller than ERA40. Before 1958, all SOCOL members (two of them significantly on the 5% level) exhibit negative EPz trends for the trend period 1901-1959 similar to the Northern Hemisphere.

Table 3.1 NH trends (Beta, in %/decade) and standard error (se) in the 100 hPa vertical component of EP flux, averaged over 40°N-80°N and over January to February for different periods. Bright grey (dark grey) shading marks statistically significant estimates with p -value < 0.05 (0.1).

Simulations/ Observations	1901-1929		1930-1959		1901-1959		1958-1979		1980-1999		1958-1999	
	Beta	se	Beta	se	Beta	se	Beta	se	Beta	se	Beta	se
e1	2	3.9	-3.1	3.5	-1.2	1.3	0.5	7.2	4.9	7	1.4	2.5
e2	0.2	4.2	-3.9	4.2	-0.1	1.5	-6.7	5.8	17.3	7.5	3.7	2.5
e3	4.3	5.5	-7.1	3.5	-3.2	1.7	-2.2	6.6	-5.1	8.3	0.2	2.6
e4	2.1	3.6	-7.8	3.7	-0.1	1.3	-3.5	6.8	-1	7.4	-1.4	2.5
e5	5.8	2.7	4.5	2.6	1.5	1	6.4	6.1	-0.1	6	3.6	2.1
e6	1.5	5	-3.2	4.5	-0.2	1.7	3.1	4.4	7.3	8.1	-1.3	2.2
e7	2.5	4.5	-3.8	3.2	-0.1	1.4	0.1	6.8	-4.7	9.3	1.2	2.8
e8	0.4	4	-3.1	4.1	-2.2	1.4	-8.3	6.3	-5.7	6.4	-3.2	2.2
e9	0.7	4.6	2.5	4.3	0.7	1.6	1.9	6.6	-8.9	7	3.9	2.5
Ens. Mean	2.17	4.22	-2.8	3.7	-0.5	1.4	-1	6.3	0.44	7.4	0.9	2.4
ERA40							2.2	6.2	-6	5.5	2	2.1
NCEP							3.4	6.2	-8.8	6.4	2.4	2.3

Table 3.2 Same as Table 3.1 but for SH, averaged over 40°S-80°S and over July to August.

Simulations/ Observations	1901-1929		1930-1959		1901-1959		1958-1979		1980-1999		1958-1999	
	Beta	se	Beta	se	Beta	se	Beta	se	Beta	se	Beta	se
e1	-13	5.3	1.7	5.3	-3	1.9	-6	9	2.7	11	-0.1	3.5
e2	-5.5	5.6	-15	6.1	-2.6	2.2	14.4	10	-1.3	9.3	6.4	3.4
e3	2.2	5	5.4	5.5	-0.3	1.8	-8.9	8.9	-2.6	10	0.7	3.4
e4	8	5.5	2.2	5.7	-0.3	2	-5.9	5	8.6	13	7.5	3.5
e5	-3.9	5.5	-5.3	5.5	-0.8	1.9	4	9	-7.5	8.4	1.4	3.1
e6	4.6	5.4	-5.9	4.8	-4.3	1.8	11.5	8	4.1	6.5	0.9	2.7
e7	-4.4	5.5	-13	4.8	-3.1	1.8	-13	8.9	5.9	7.6	0	3
e8	-1.2	5.5	-8.8	6	-4.1	2	6.8	7.5	13.4	11	3.2	3.2
e9	-2.5	6.2	-0.7	5.1	-2.5	2	-8.7	7.5	-8.7	6.2	-4.2	2.5
Ens. Mean	-1.7	5.5	-4.3	5.4	-2.3	1.9	-0.6	8.2	1.62	9.3	1.76	3.1
ERA40							17.6	7	7.1	9.4	9.1	2.9
NCEP							19	7.1	16	8.1	14.8	2.6

Propagating waves affect the state of the winter polar vortex and related variables, such as temperature and TOZ. High correlation between meridional heat flux (proportional to EPz in the stratosphere) and 50 hPa polar temperatures has been documented by *Newman et al.* (2001) and addressed in several CCM-comparison studies (*Austin, et al.*, 2003; *Eyring, et al.*, 2006). Here we evaluate this process by showing scatter plots of January to February (July to August) 40°N-80°N (40°S-80°S) EPz and February to March (August to September) 50 hPa zonal temperature averaged over 60°N-90°N (60°S-90°S) (Figure 3.14a). In the NH the linear fit between modeled polar temperatures and EPz agrees extremely well with NCEP and ERA40 for the period 1958-1999 and also for 1901-1957. This is also true for the SH compared to NCEP. Differences in the intercept reflect deviations in polar temperatures. Note that the steeper slope in the SH for ERA40 is a result of a cold bias in the pre-satellite period, which is not present in NCEP (*Karpetchko, et al.*, 2005). Another useful diagnostic linked to wave propagation is the accumulation of TOZ as a function of EPz. *Randel et al.* (2002) examined the seasonal and latitudinal dependence of the correlation between TOZ and EPz. High correlation was found between TOZ accumulation over 60°N-90°N (over 60°S-90°S) in March (October) and EPz over 40°N-70°N in March (40°S-70°S in October), which is shown as scatter plots in Figure 3.14b for the individual ensemble members (black) and observations of NIWA TOZ and NCEP EPz (red). Note that TOZ accumulation in March (October) is measured here as monthly mean TOZ difference between April and February (November and September). The correlation in the model over 1979-1999 is in reasonable agreement with observations, showing correlation coefficients of 0.55-0.65 (0.46-0.62) compared to observed 0.76 (0.81) in the NH (SH). The linear fits are all statistically significant, except for two members which show a less steep linear dependency. The relationship between TOZ accumulation and EPz can also be found in the model for the period 1901-1978, underscoring the existence of dynamically controlled polar spring ozone variations on the interannual scale in the model caused by propagating waves.

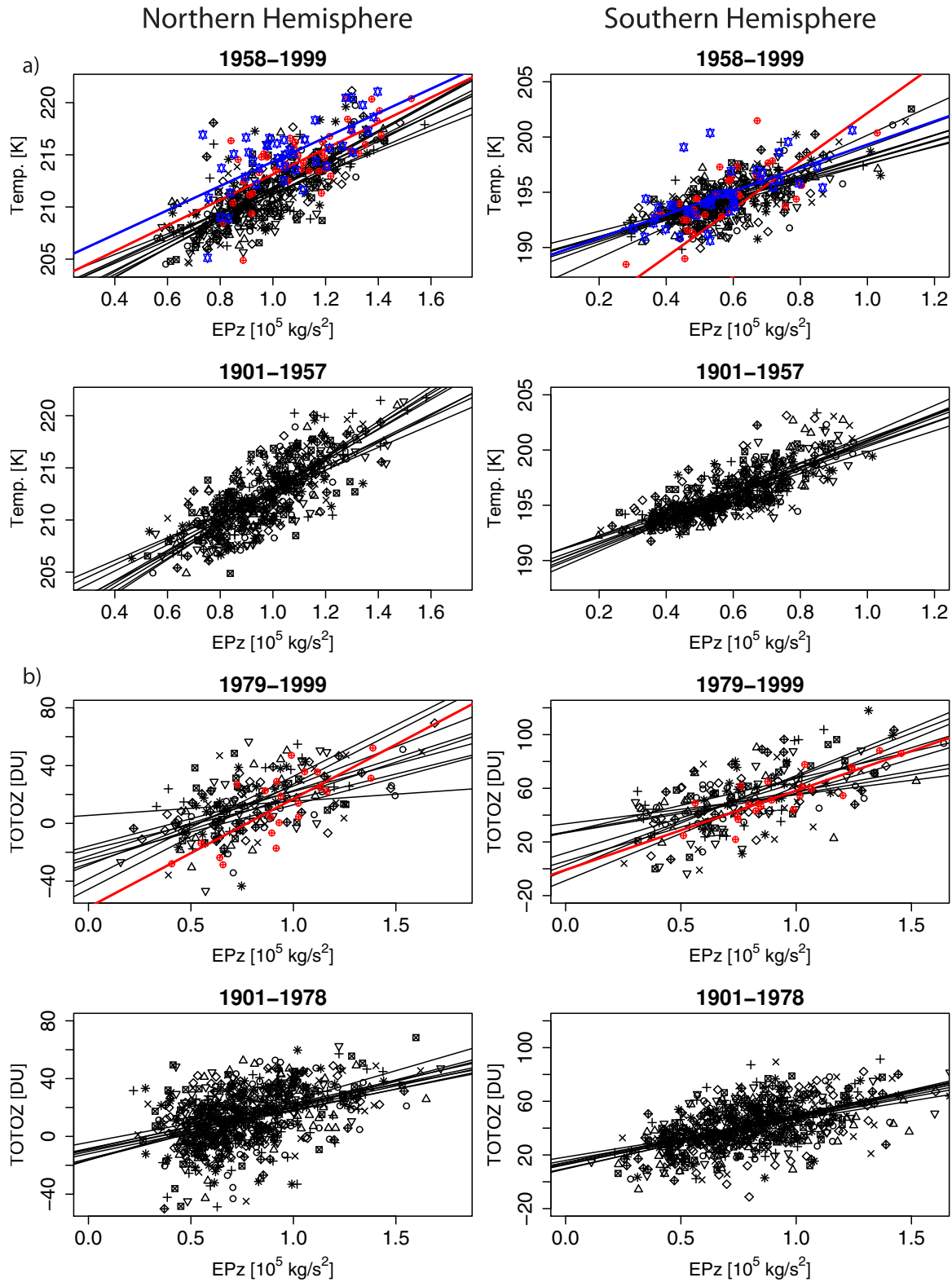


Figure 3.14 (a) Left panels (right panels): Scatter plots of Feb-Mar mean (Aug-Sep mean) 50 hPa temperature (in K), averaged over 60°N–90°N (60°S–90°S) against NH (SH) EPz (from Fig. 13a) for 1958–1999 (above) and 1901–1957 (below). Shown are ensemble members (black) and observations of ERA40 (red) and NCEP (blue). Lines indicate linear regression line for different

ensemble members and observations. (b) Scatter plots of April minus February (November minus September) TOZ difference (in DU) averaged over 60°N-90°N (60°S-90°S) against EPz, averaged over 40°N-70°N (40°S-70°S) for 1979-1999 (above) and 1901-1978 (below). Red symbols and line are observations of TOZ NIWA vs. EPz NCEP.

3.3.3 Summary and Discussion

In the first seven decades of the 20th century with still modest anthropogenic influence, modeled climatologies remain almost unaltered regarding TOZ, vertical ozone distribution, zonal mean zonal wind, and zonal temperature. SOCOL is able to capture TOZ development well compared to historic ground-based stations back to 1924, but the amplitude of the seasonal cycle is underestimated which is a remaining shortcoming of SOCOL Vs2. Compared to satellite observations back to 1970 the low-frequency variability in TOZ is well reproduced over the tropics and mid-latitudes. In the same region back to 1920, SJI in SOCOL is highly correlated (0.74) with the reconstructed index. Its interannual variability reflects to a large degree ENSO variability and corresponding changes in the Hadley and Walker circulations. The SJI allows validating model results in an insightful, process-oriented manner over long time-scales. It could potentially be further explored by other middle-atmosphere studies to test whether the response to oceanic forcing is correctly reproduced.

Zonal mean vertical ozone distributions are in reasonable agreement with SAGE and SBUV. Yet, they show a positive bias in the lower stratosphere and a negative bias in the upper stratosphere. Modeled stratospheric trends over 1979-1999 perform well compared to observations for all ensemble members. Trend estimates among the ensemble members vary most in the southern lower stratosphere where on average the observed negative trend is underestimated.

In general, the north polar region is where the largest internal model variability is found. This is revealed by the TOZ and PVS patterns suggesting that a sufficiently large set of ensemble members will be required if further progress in model development is sought for in this particular geographic region. For PVS the ensemble spread is almost as high as interannual variability in the reconstructed index (except for some ENSO related events) and hence not predictable. MWs in the NH being a major source of interannual variability were analyzed with respect to their frequency, seasonality and intensity. A much smaller number (factor 3-4 smaller) of MWs occurred in the model than in observations, though the seasonal distribution of the occurrence frequency looks comparable, except for January. No discrepancies to ERA40 were found for analyzed strength parameters of individual MWs. This means that SOCOL underestimates the total number of MWs but it evolves in a comparable way in case a MW occurs. The underestimation of MWs indicates a too strong northern polar vortex which is further endorsed by higher zonal wind speed and colder temperatures over the Arctic stratosphere compared to ERA40. EPz and EP flux divergence reveal less wave activity and less wave mean flow interaction during winter

months for 1990-1999 in the northern high latitudes and hence less perturbations of the polar vortex. In the SH the signal is less clear.

Time series of modeled EPz in the NH and SH exhibit a large internal as well as interannual variability. Modeled trends of EPz are generally not significant and the spread of estimates between different ensemble members is high. More sophisticated techniques are required to further explore the robustness of the trend estimates. The correlation between EPz and polar temperature as well as EPz and polar spring TOZ was examined, which shows good agreement with observations for both hemispheres and reveal comparable relationships for the pre-ERA40 and pre-satellite period.

3.4 Conclusion and Outlook

We have applied the CCM SOCOL Vs2 (*Schraner, et al., 2008*) with a set of 9 ensemble members covering the 20th century in transient mode using prescribed SSTs, SI distribution, NO_x- and CO-emissions, GHG and ODSs concentrations, QBO, and changes in land properties.

Despite its rather coarse horizontal and vertical resolution ($3.75^\circ \times 3.75^\circ$ (T30), 39 layers, 1000 - 0.1 hPa), simulations with the CCM SOCOL perform rather well compared to observations and allow addressing interannual-to-decadal variability during the twentieth century in relation to its forcing parameters. The model is in very good agreement in reproducing observed ozone anomalies and reconstructed dynamics in the (sub-) tropical belt. That means that in this region the response of SOCOL to forcings of QBO, ENSO, solar variability and volcanic eruptions is very realistic and predictable even with less than nine ensemble members. Also, process-oriented analysis of model output (i.e. positive correlation of polar TOZ with EPz, positive correlation of polar temperature with EPz and negative ozone trend estimates upon EESC) reveal only little changes between different ensemble members and hence represent robust model results. On the contrary, our analysis of the northern polar vortex system (i.e. PVS and MWs) show that in the Arctic the ensemble spread is very large which hinders to separate between internal and externally forced variability. The large ensemble range found for estimated trends in stratospheric wave drag, including estimates of opposite signs, reveals that the internal variability in models cannot be neglected when predicting the response in wave energy upon external forcings.

The presented model simulations provide a unique data set for further exploration of interannual-to-decadal variability. In particular, it is planned to quantify the impact of solar variability, ENSO variability and volcanic eruptions upon stratospheric ozone and climate individually over the whole twentieth century. The interaction between low-frequency variability in the stratosphere and tropospheric climate modes will be addressed in addition.

3.5 Acknowledgments

AF is funded by ETH Zurich (TH project CASTRO) and SB by the Swiss National Science Foundation. PK is supported by the S-ENETH project TUMMS, BPL and CSP by the EU projects SCOUT-O3 and QUANTIFY, respectively.

We would like to thank Ingo Wohltmann for EP flux calculations of ERA40 and NCEP and William Randel for providing us SAGE ozone data set.

4 Stratospheric Response to ENSO

Stratospheric Winter Climate Response to ENSO in three Chemistry-Climate Models

A. M. Fischer¹, D. T. Shindell², B. Winter³, M. S. Bourqui³, G. Faluvegi², E. Rozanov^{1,4},
M. Schraner¹, and S. Brönnimann¹

¹Institute for Atmospheric and Climate Science, ETH Zurich, Switzerland

²NASA Goddard Institute for Space Studies, New York, USA

³McGill University, Montréal, Canada

⁴PMOD/WRC, Davos, Switzerland

(published in Geophys. Res. Lett., 35, L13819, doi:10.1029/2008GL034289, 2008)

Abstract

Three different chemistry-climate models are compared with respect to their simulation of the stratospheric response to extreme cases of ENSO. Ensemble simulations of an unusually warm ENSO event (1940-1941) compared to a very cold event (1975-1976) reveal a weaker and warmer polar vortex in the Northern Hemisphere winter. This follows from anomalously propagating waves decelerating the zonal flow and strengthening the residual mean circulation. Models are in good agreement in simulating the observed (statistically reconstructed for the case 1941) flow in the lower stratosphere over the Pacific North American region, but less so over the North Atlantic European sector with insufficient reproduction of the wave structure. Modeled column ozone is reduced in the tropics and increased on average in the northern extra tropics in accord with the general pattern seen in observations and in line with an intensification of the Brewer-Dobson circulation.

4.1 Introduction

El Niño-Southern Oscillation (ENSO) is an important driver for modulating the stratospheric climate in the Northern Hemisphere (NH) on an interannual timescale.

Observational studies revealed that warm ENSO (wENSO) events are associated with a weak and warm polar vortex over the Arctic during boreal wintertime (*Van Loon and Labitzke, 1987*). Using models with sufficiently high vertical resolution it can be shown that ENSO is affecting the northern winter polar vortex by anomalously vertical propagating waves, thereby increasing wave mean flow interaction and the residual mean circulation (RMC) resulting in a colder (warmer) tropical (mid-latitudinal) stratosphere (*Brönnimann, et al., 2004; Garcia-Herrera, et al., 2006; Manzini, et al., 2006; Sassi, et al., 2004; Taguchi and Hartmann, 2006*). Disentangling the ENSO signal on the northern stratospheric climate from other perturbing factors (i.e. solar activity, QBO phase, stratospheric aerosol loading) is a particularly difficult task when analyzing transient chemistry-climate model (CCM) simulations as well as observational data (*Camp and Tung, 2007*). Studying the atmospheric response to a single ENSO cycle as in *Brönnimann et al. (2006b)*, requires comparable forcing conditions for both phases, wENSO and cold ENSO (cENSO), which occurs only rarely. Here we present a model intercomparison of an unusual wENSO event from 1939-1942 (*Brönnimann, et al., 2004*) with respect to a strong cENSO event from 1975-1976. A CCM simulation reproducing this extreme case not only leads to a better understanding on the processes prevailing but also serves as an insightful model test with respect to the communication of the ENSO signal, the propagation of planetary waves and the response in stratospheric ozone. The analysis involves three CCMs whose applicability lies in multi-decadal to centennial simulations or large ensemble sizes and which thus feature a coarser model grid than other state-of-the-art CCMs (see *Eyring, et al., 2006*). The focus of this paper is restricted to the effect of stratospheric climate and dynamics in the NH during boreal winter.

4.2 Methods

The model intercomparison comprises the CCMs SOCOL (based on *Egorova, et al., 2005a*), G-PUCCINI (*Shindell, et al., 2006*) and IGCM-FASTOC (*Taylor and Bourqui, 2005*). The horizontal resolution in SOCOL and IGCM-FASTOC is similar (about 3.75°) and slightly higher than in G-PUCCINI ($4^\circ \times 5^\circ$). In the vertical SOCOL has a resolution of 39 layers from the surface up to 0.01 hPa. This is higher than the vertical representation in G-PUCCINI (23 layers up to 0.01 hPa) and IGCM-FASTOC (26 layers up to 0.1 hPa) (Table 4.1; see the online supporting material for detailed information about these models).

Table 4.1 Overview of the model resolution, ensemble size and the considered external forcings. SST: Sea surface temperature, SI: Sea ice distribution, GHG: Greenhouse gases, ODS: Ozone depleting substances, strataer: stratospheric aerosols, Solar: total solar irradiance, SAT: Surface Air Temperature of the SOCOL ensemble mean simulation

Model	Resolution / Top	Ensemble Size	Forcings
SOCOL	T30L39 / 0.01 hPa	20	SST/SI, Solar, GHG, ODS, strataer
G-PUCCINI	4°x5°L23 / 0.01 hPa	20	SST/SI, Solar, GHG, ODS, strataer
IGCM-FASTOC	T31L26 / 0.1 hPa	50	SAT, GHG

The models were run from July 1940 until July 1941 (wENSO) and July 1975 until July 1976 (cENSO), and the analysis focuses on the respective late winter periods (1941, 1976). The simulations were performed in ensemble mode with 20 members in SOCOL and G-PUCCINI and 50 members in IGCM-FASTOC. The statistical significance of the simulated winter difference is calculated using Student's t-test.

For forcing SOCOL and G-PUCCINI we used monthly varying sea surface temperature (*Smith and Reynolds, 2004*) and sea ice distribution (*Rayner, et al., 2003*). IGCM-FASTOC was forced at the surface by monthly averaged surface air temperatures from an ensemble mean simulation using SOCOL in order to correctly simulate wave propagation. Changes in total solar irradiance were specified following *Lean (2000)* and for stratospheric aerosol loading we used compilations by *Sato et al. (1993)*. Both simulation periods were at solar minimum conditions and very similar in absolute terms. The aerosol loading in the stratosphere was low in both events but somewhat higher during 1975/1976 than 1940/1941.

The CCM results are compared to several observational and reconstructed data products. For geopotential height (GPH) and temperature fields in the stratosphere in 1941 we used statistical reconstructions that are based on upper-level data (*Brönnimann and Luterbacher, 2004*). The fields for 1976 are obtained from the ERA40 reanalysis data (*Uppala, et al., 2005*). We compared the signal in Total Ozone (TOZ) using several TOZ series in the NH, obtained from the World Ozone and Ultraviolet Radiation Data Centre (WOUDC).

4.3 Results

Figure 4.1 displays winter difference, 1941 – 1976, of 100 hPa GPH and temperature averaged over January to March. This is the time when largest ENSO anomalies are observed in the lower stratosphere due to downward propagation from higher altitudes (see *Manzini, et al., 2006*). The difference between reconstructions and ERA40 (referred to as “recERA”) reveals elevated pressure over the Arctic region and over low latitudes and thus a weakening of the polar vortex accompanied by anomalous warm temperatures in line with previous modeling and observational studies (*Brönnimann, et al., 2004*; *Garcia-*

Herrera, et al., 2006; *Manzini, et al.*, 2006; *Sassi, et al.*, 2004; *Van Loon and Labitzke*, 1987). The increase in temperature is zonally symmetric at northernmost latitudes and the magnitude of the signal is comparable to the results by *Sassi et al.* (2004) for February. Similar to *Manzini et al.* (2006) (for ERA40), at mid-latitudes, a wave 2 component can be found with strong negative GPH anomaly centres over the Northern Pacific and Central Europe. In the tropics a negative temperature anomaly stretches northwards over the Atlantic towards Asia.

In general CCM results of the ensemble mean are in reasonable agreement with these patterns, though the magnitude is less strong. Unlike G-PUCCINI the internal variability of SOCOL and IGCM-FASTOC is quite large and some of its members capture the strong response in GPH and temperature as observed (see Figure 4.4, online supplementary material). In the ensemble mean the models show a significant increase in tropical GPH together with the well-known positive (negative) dipole structure over the Eastern Tropical Pacific in GPH (temperature) (*Claud, et al.*, 1999). Note, that IGCM-FASTOC was forced with surface temperatures of SOCOL. In SOCOL, the weaker polar vortex during wENSO is manifest over the whole Arctic region, in contrast to IGCM-FASTOC and G-PUCCINI where it is restricted to the region west of Greenland. It is also interesting to note that the negative temperature anomaly band over tropical Pacific, Atlantic, North Africa and East Asia is very well reproduced by all CCMs. At mid-latitudes the wave imprint in GPH and temperature over the Pacific North American region is in remarkably good agreement with recERA, but the models diverge in correctly simulating the wave structure over the North Atlantic European sector. The observed GPH anomaly over Central Europe is shifted westward in SOCOL and G-PUCCINI and northward in IGCM-FASTOC (though not significantly), accompanied by a GPH increase over the Mediterranean and Europe. This mismatch is most probably caused by insufficient planetary wave propagation characteristics due to coarse model resolutions. Applying the same ENSO experiment with IGCM-FASTOC at a resolution of T21 instead of T31 resulted in a complete failure in reproducing any of the aforementioned characteristics (not shown). This emphasizes the importance of the horizontal model resolution in correctly reproducing the wave patterns in the NH during an ENSO cycle (see also *Merkel and Latif*, 2002).

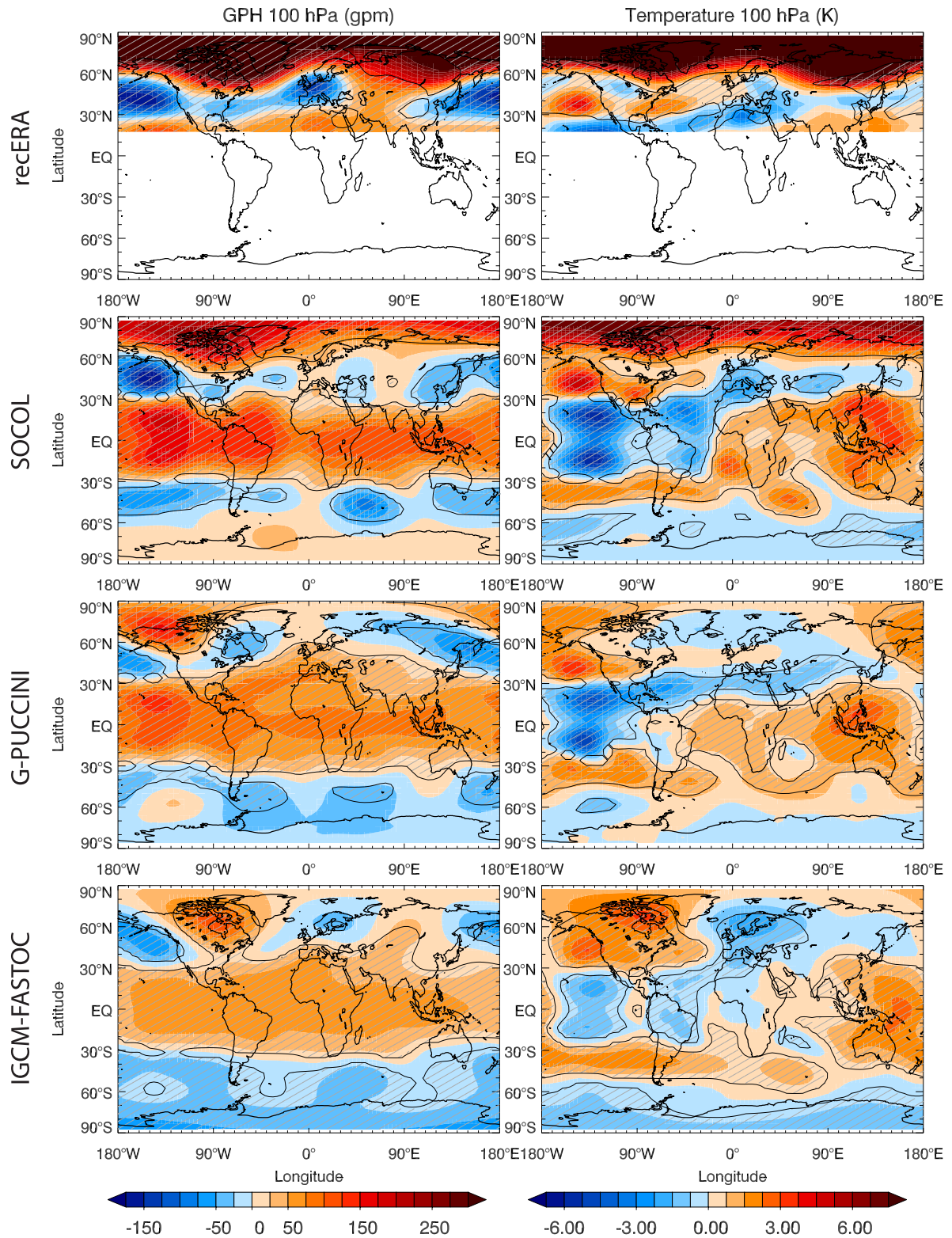


Figure 4.1 Difference between 1941 and 1976 in GPH (left, in m) and temperature (right, in K) at 100hPa, averaged from January to March, for recERA (uppermost), and SOCOL, G-PUCCINI and IGCM-FASTOC. Shaded areas together with contour lines in lower three panels mark statistically significant areas (t-test, p -value < 0.05). Shading with lines in uppermost panel denotes a high reconstruction skill (reduction of error > 0.2).

Several TOZ series are available in the NH for either the 1940s or 1970s, but only two for both periods. Therefore, the best way to compare the TOZ series during these events is by analyzing (smoothed) standardized anomalies with respect to a 7yr time window surrounding each event (see *Brönnimann, et al.*, 2004). Figure 4.2 reveals that in the 1940s (1970s) strong positive (negative) anomalies are observed at all sites.

For the winter difference between wENSO and cENSO all three CCMs exhibit a negative response over the tropics (strongest over Pacific), which is, zonally averaged, of similar magnitude in SOCOL and G-PUCCINI and stronger than in IGCM-FASTOC. The signal north of 30°N becomes less clear due to a large ensemble spread in G-PUCCINI and IGCM-FASTOC (only the TOZ increase in response to the deepening of the Aleutian Low is significant in all models), but displays, zonally averaged, elevated TOZ over mid- to high latitudes in the ensemble means. In SOCOL this increase is a significant dominant signal over the whole Polar region covering the northernmost European TOZ stations. Note, that the rather different responses at high latitudes in G-PUCCINI and in IGCM-FASTOC (particularly the negative anomalies over Alaska and Northern Europe) are not significant. It is interesting to note that a positive signal over East China and the southern tip of Japan (compare stations Shanghai and Tatenos) as well as over the Northeast of the US (compare New York and Caribou) can be found in some of the models. This increase was also observed in satellite data, described in a similar ENSO study (see *Brönnimann, et al.*, 2006b). Agreement between model responses and TOZ stations, however, is poor for Central Europe which is possibly linked to the miss-representation of the wave structure in this region.

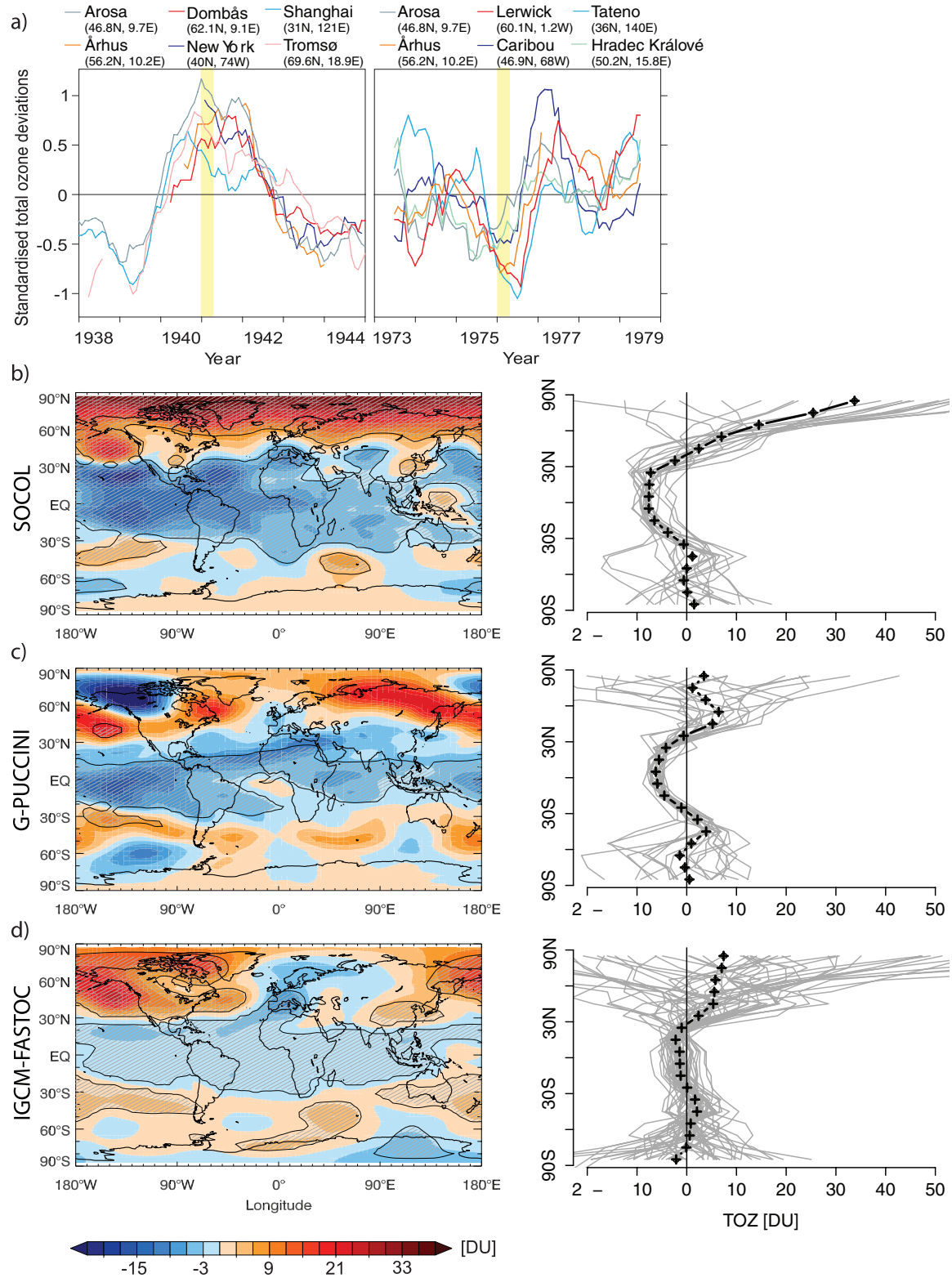


Figure 4.2 a) TOZ deviations from a climatology derived from the displayed time window for several stations in the NH (standardized for each station and smoothed with a 12-month moving average, Brönnimann et al. (2004)) for 1938-1944 (left) and 1973-1979 (right). Yellow shading marks the analyzed winter. b) – d) Difference between 1941 and 1976 TOZ (in DU), averaged from January to March, for ensemble mean field (left, shaded areas together with contour lines mark

statistically significant areas, t-test, p-value < 0.05) and zonally averaged ensemble members (right in grey, ensemble mean in black and plus symbols) in SOCOL, G-PUCCINI and IGCM-FASTOC (all interpolated to 10° bins).

To elucidate dynamical and chemical changes, we have analyzed zonal mean zonal wind, ozone and RMC (see Figure 4.3). All CCMs show a significantly reduced zonal wind speed at polar latitudes, underlining the pattern of large-scale circulation anomalies at polar regions. At most, zonal flow is decelerated by more than 15 m/s (in SOCOL) at around 10 hPa. Similar to *Manzini et al.* (2006) we found that the decrease in wind speed proceeds to tropospheric layers in the mid-latitudes and thus directly affects climate at the ground. A strengthening of the subtropical jet is apparent in all models, but displaced southwards in SOCOL (see also *Brönnimann, et al.*, 2006b).

Ozone in the equatorial lower stratosphere is significantly reduced in all CCMs resulting in the TOZ decrease in the tropics seen above. Further northward at the same altitude ozone concentration is much enhanced in the response of all models (in G-PUCCINI not significantly). The response at higher altitudes is weaker and reverses in IGCM-FASTOC and G-PUCCINI. SOCOL simulates enhanced ozone throughout the NH with strongest changes at northernmost latitudes. The pattern of reduced ozone over the tropics together with increased ozone and weakened zonal flow at higher latitudes in the stratosphere suggests a strengthening of the RMC, caused by anomalously vertical propagating waves (e.g. *Garcia-Herrera, et al.*, 2006). The RMC difference, averaged over November to February, and thus accounting for possible time lags, shows an enhancement throughout the stratosphere in the NH, which increases the transport of ozone from the source region in the tropics towards higher latitudes where the lifetime is considerably longer. EP flux divergence reveals a more convergent pattern in large part of the middle and upper stratosphere and a strengthening of the convergence zone at around 500 hPa resulting from both vertical and horizontal component (see Figure 4.5, online supplementary material). This result gives evidence of increased wave mean flow interaction eventually weakening the zonal flow and driving the RMC in all three CCMs.

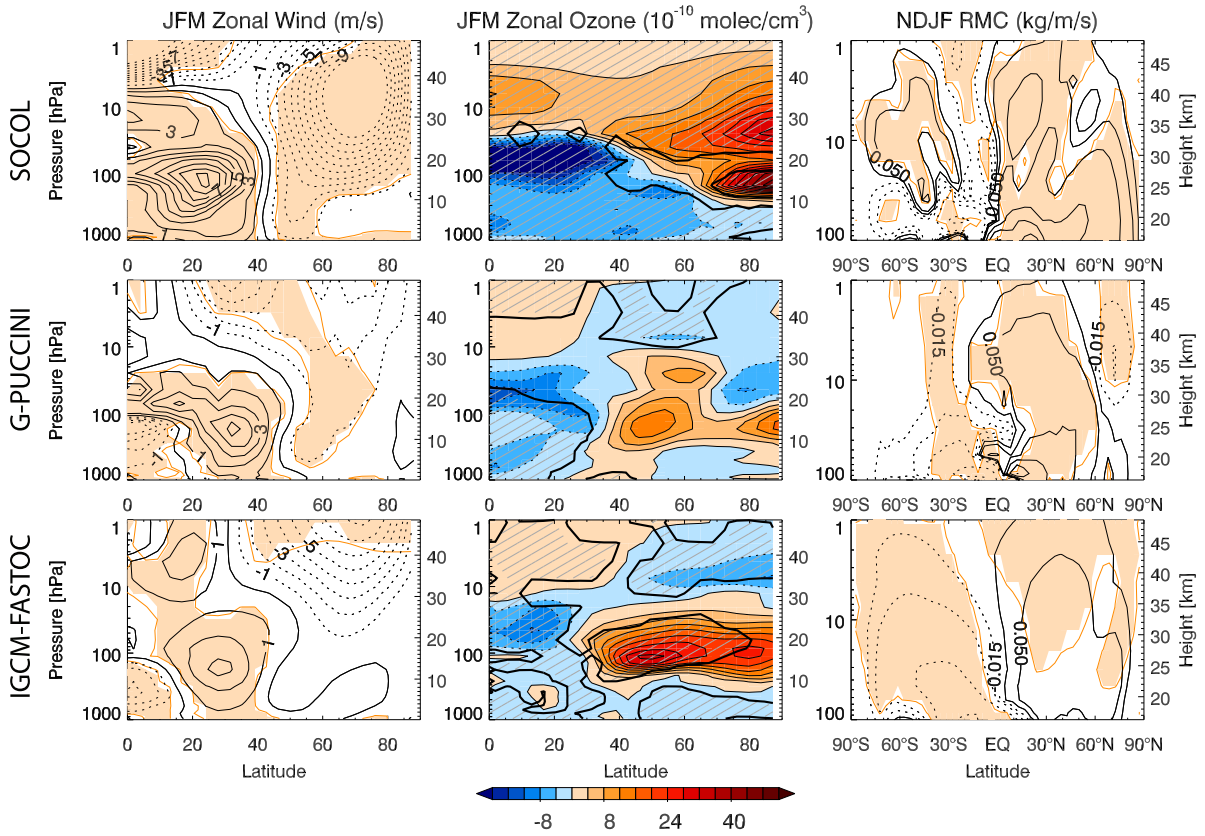


Figure 4.3 NH difference between 1941 and 1976 in zonal mean zonal wind (left, in m/s), zonal mean ozone number densities (middle, in 10^{-10} molecules/cm³), and RMC (right, in kg/m/s), averaged from January to March (left and middle panel) and November to February (right panel), for Socol (top), G-PUCCINI (middle) and IGCM-FASTOC (bottom). Shaded areas together with contour lines (orange on the left and right) mark statistically significant areas (t-test, p-value < 0.05).

4.4 Conclusion

The presented models participating in this intercomparison are in reasonable agreement with recERA as well as previous model and observational studies of the ENSO imprint on stratospheric chemistry and climate. The detected main responses (acceleration of the RMC, weakening of the polar vortex, enhanced Equator to Pole transport of ozone) are most pronounced in Socol which has the highest resolution in the vertical. At mid- to high latitudes, within model variability for TOZ in IGCM-FASTOC and G-PUCCINI is large whereas for GPH and temperature the spread of ensemble members differs among the models but the bulk of it shows a weaker signal than in recERA. Over the Pacific North American sector agreement between the ensemble means and recERA is very promising, but less so over the North Atlantic European sector with respect to the wave pattern. The rather low horizontal resolution could explain some of the discrepancies. *Merkel and Latif (2002)* showed that increasing the horizontal model resolution can improve the reproduction of eddy-mean flow interaction over this region. Yet, the presented models are

designed and used for multi-decadal and longer simulations, and thus have a grid resolution imposed by computational costs. For the application of long-term simulations we conclude that the presented models are suitable for capturing ENSO variability in the NH stratosphere given a sufficiently large set of ensemble simulations. Reproducing correctly strong SST-forced signals is a prerequisite for analyzing externally forced signals in CCMs. Note, that by setting up this case study we have isolated the effect of ENSO from other potential sources of stratospheric variability (i.e. QBO, solar variability, volcanic eruptions). Thus, in a transient long-term simulation and corresponding composite study we expect the ENSO signal to be much less distinct. It may also be weaker during other ENSO cycles (e.g. *Brönnimann, et al., 2006b*), as we have chosen here two extreme cases of ENSO. The variability calls for a large number of ensemble simulations when detecting and attributing ENSO effects on NH stratospheric climate in transient CCM simulations.

4.5 Acknowledgments

AF is funded by ETH Zurich (TH project CASTRO) and SB by the Swiss National Science Foundation. We are grateful for valuable comments by Thomas Peter (IACETH).

MB and BW are grateful to Chris Bell, University of Reading, UK, who updated the IGCM to the T31 resolution, and to the Canadian Foundation for Innovation and Recherche Québec for financing the computing infrastructure used in this study.

BW was funded by the Canadian Foundation for Climate and Atmospheric Sciences.

DS and GF acknowledge support from NASA's ACMAP.

We thank WOUDC for providing TOZ station data. ERA40 data have been obtained by ECMWF.

4.6 Online Supplementary Material

4.6.1 Model Spread

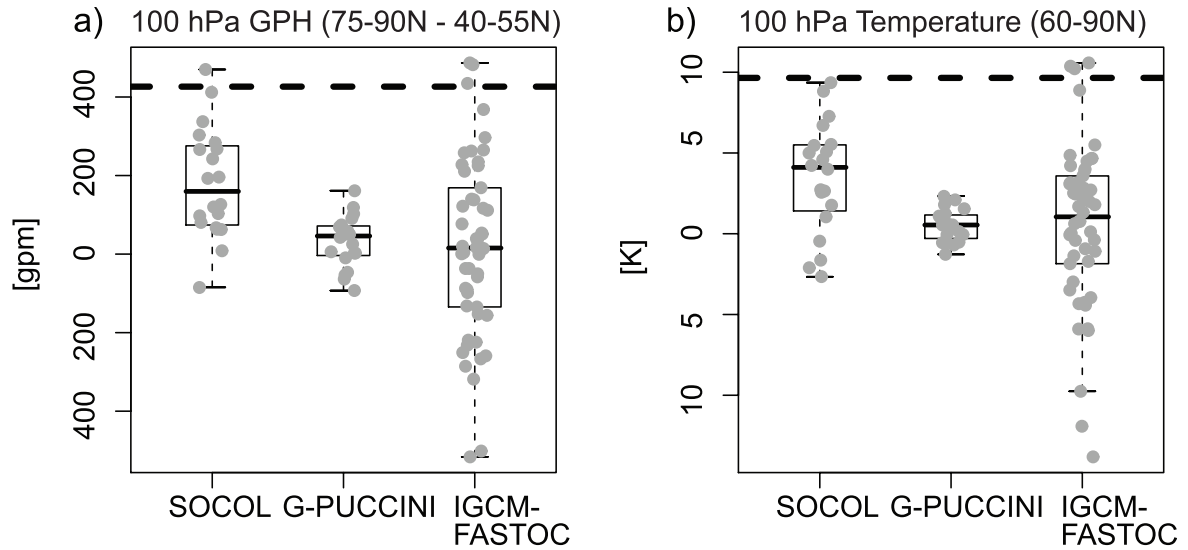


Figure 4.4 Difference between 1941 and 1976, averaged over Jan.-March, in a) geopotential height (zonal mean difference of averaged area 75N-90N and 40N-55N at 100 hPa) and b) temperature (zonal mean of averaged area 60N-90N at 100 hPa) for Socol (left), G-Puccini (middle) and IGCM-FASTOC (right). Shown are boxplots (horizontal line in box: ensemble mean, upper and lower edge of box: 1st and 3rd quartile) together with individual ensemble members (grey dots). Result from recERA is indicated by the horizontal dashed line.

4.6.2 Eliassen Palm Flux

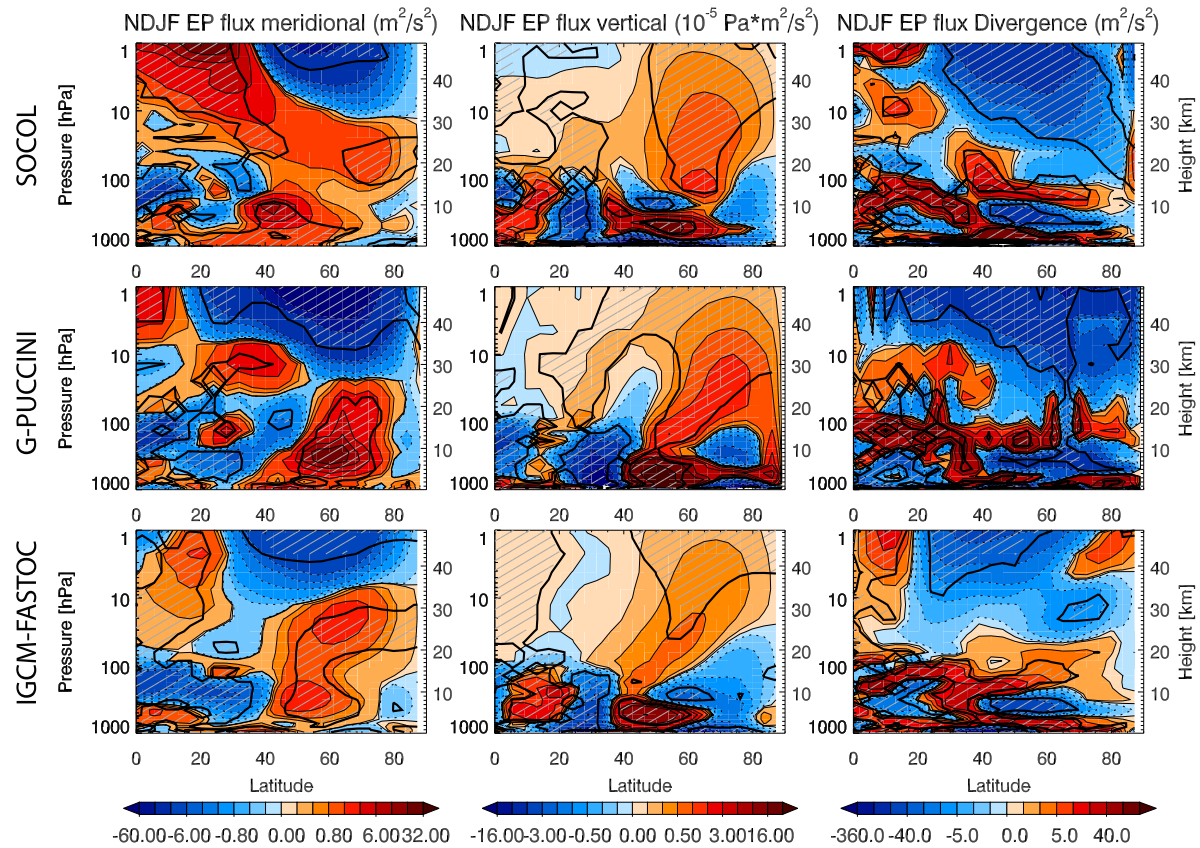


Figure 4.5 Northern Hemispheric difference between mean of Nov.-Feb. 1940/41 and 1975/76 in meridional component (left, in m^2/s^2) and vertical component (middle, in $\text{Pa} \cdot \text{m}^2/\text{s}^2$) of EP flux and EP flux divergence (right, in m^2/s^2) for SOCOL (top), G-PUCCINI (middle) and IGCM-FASTOC (bottom). Shaded areas together with contour lines mark statistically significant areas (t -test, p -value < 0.05).

4.6.3 Model Descriptions

SOCOL

The chemistry-climate model SOCOL (described in Egorova, *et al.*, 2005a) has been developed as a combination of a modified version of the MA-ECHAM4 GCM (Manzini and McFarlane, 1998) and the chemistry-transport model MEZON described in detail by Rozanov *et al.* (1999) and Egorova *et al.* (2003). It is a spectral model with T30 horizontal truncation and 39 vertical levels in a hybrid sigma-pressure coordinate system. The model lid is at 0.01 hPa. Time step for dynamical and physical processes is 15 min and 2 hours for radiative transfer calculations and chemical reactions. With respect to the standard MA-ECHAM4, the gravity wave source spectrum of the Doppler spread parameterization has been modified. MEZON simulates 41 chemical species, which are determined by 118 gas-phase reactions, 33 photolysis reactions and 16 heterogeneous reactions on/in sulphate aerosol (binary and ternary solutions) and polar stratospheric cloud (PSC) particles. The

transport of all considered species is performed using the hybrid numerical advection scheme of Zubov *et al.* (1999). The scheme for calculating photolysis rates covers the spectral region 120-750 nm and specifically includes the Lyman- α line. The GCM and CTM components of SOCOL are coupled via the three dimensional fields of wind, temperature, ozone, water vapor, N₂O, methane and CFCs.

Compared to the model version described in Egorova *et al.* (2005a) a nudging of the QBO (Giorgetta, 1996) and a new parameterization of heterogeneous chemistry was later included. Recently, several failures in SOCOL including artificial mass loss over Polar regions were discovered (see also Eyring, *et al.*, 2006; Schraner, *et al.*, 2008). The problem is most pronounced when heterogeneous chemistry and hence ozone hole chemistry is dominant. For the experiment presented here, the effect is expected to be small, since both simulation periods (wENSO and cENSO) are in the pre-ozone hole period.

G-PUCCINI

G-PUCCINI is based on the NASA Goddard Institute for Space Studies (GISS) composition and climate model used recently for simulations of preindustrial, present-day and 2100 conditions (Shindell, *et al.*, 2006). It has been expanded from the earlier troposphere-only version (Shindell, *et al.*, 2003) by more than 70 stratospheric chemical reactions and by coupling trace gas and sulphate aerosol chemistry. Interactions between chemistry and mineral dust are now considered, too. More than 50 species are included in the model, 27 of which are being transported. Coupling to radiative transfer calculations is established for ozone, methane, aerosols and dust. Photolysis rates of water and nitric oxide in the Schumann-Runge bands are parameterized. G-PUCCINI follows the new modelE project (Schmidt, *et al.*, 2006), which shows improvements in the physics, convection, and boundary layer scheme. The resolution of the model amounts to a grid spacing of 4 by 5 degree in the horizontal and 23 layers in the vertical. The model top is in the mesosphere at 0.01 hPa. Climatology for the mean meteorological state in the stratosphere is generally quite good (Schmidt, *et al.*, 2006), but the variability is generally too small. The latter appears to be due to overly strong gravity-wave drag.

IGCM-FASTOC

The IGCM-FASTOC is based upon the Intermediate General Circulation Model (IGCM) of the University of Reading UK (Forster, *et al.*, 2000; Hoskins and Simmons, 1975) coupled to the chemical scheme FASTOC (Bourqui, *et al.*, 2005; Taylor and Bourqui, 2005). The IGCM is characterized by parameterizations of an intermediate level of complexity. The resolution is T31 with 26 vertical layers from the surface up to 0.1 hPa, and Rayleigh friction is applied in the top three levels. FASTOC is a fast input-output model where explicit functions linking input variables to output variables replace the computationally expensive differential equation solver. Input variables are: temperature, pressure, day length, noon solar zenith angle, and overhead ozone column in addition to O₃, NO_x, HNO₃ and N₂O₅. Output variables are O₃, NO_x, HNO₃ and N₂O₅. Note, that the

current version does not include chlorine and bromine chemistries. O_3 is coupled to the radiative scheme.

5 The Main Drivers of Stratospheric Variability

5.1 Introduction

Stratospheric variability is observed on different temporal and spatial scales (*Solomon, 1999*). Yet, little is still known about long term stratospheric processes mostly due to the absence of high quality upper air data. An improved knowledge on the driving mechanisms of stratospheric variability is important with respect to detection and attribution of a possible recovery of the ozone layer as well as for assessing current and future climate change.

Over the recent years CCMs and middle atmosphere models with a high vertical resolution and extent up to the mesosphere have proven to be indispensable tools for investigating middle atmospheric processes in the stratosphere (*Austin, et al., 2003; Butchart, et al., 2006; Eyring, et al., 2006*). Valuable insights on the impacts of forcings on stratospheric climate and feedback mechanisms could be gained from sensitivity studies as well as composite studies (e.g. *Langematz, et al., 2003; Rozanov, et al., 2005; Sassi, et al., 2004; Shindell, et al., 2001; Stenchikov, et al., 2002*).

Here we investigate the main drivers of stratospheric variability in a 100 year transient CCM simulation (*Fischer, et al., 2008a*). To separate the different forcings a simple multiple linear regression model is applied as done in several observational and modeling studies (e.g. *Brunner, et al., 2006b; Crooks and Gray, 2005; Garcia, et al., 2007*). However, the time frame of this analysis is much extended backwards compared to previous studies which not only enhances the robustness of the resulting stratospheric imprints but also allows analyzing the stratospheric effect of decadal scale variations in SSTs, such as the Atlantic Multidecadal Oscillation (AMO) (*Enfield, et al., 2001*) and the Pacific Decadal Oscillation (PDO) (*Mantua, et al., 1997*).

The focus of the presented study is on the stratospheric Northern Hemisphere and its main driving processes during boreal wintertime.

5.2 Data and Methods

We applied a multiple linear regression model to the ensemble mean of a transient simulation with the CCM SOCOL over the 20th century (*Fischer, et al., 2008a*). Since our focus here is on dynamical and radiative mechanisms and feedbacks, we have applied the regression model to zonally averaged zonal wind, temperature and ozone over January to

March. The set of explanatory variables used in this study is shown in Figure 5.1. It includes drivers with variability on different time scales, ranging from interannual to decadal variability and trends. The explanatory variables used here are extracted from the datasets used to force the transient simulation. For detailed information on these forcings we refer to *Fischer et al.* (2008a). The quasi-biennial oscillation (QBO), which is nudged in SOCOL, is represented by two orthogonal time series (method based on *Wallace, et al.*, 1993) on 10 hPa (QBO10) and on 30 hPa (QBO30). The anthropogenic perturbation of the stratosphere is taken into account by two long-term trend components: equivalent effective stratospheric chlorine (EESC) as a measure for the amount of ozone depleting substances (ODS) and CO₂ concentration representing the emissions of greenhouse gases (GHG). The pattern of stratospheric aerosols is prescribed in the model simulation as monthly meridional cross sections of surface area densities (*Fischer, et al.*, 2008a). To account for the meridional transport of aerosols towards higher latitudes during wintertime, we have taken into account the latitudinal variation of optical depth in the layer between 15 and 35 km altitude. The time series in Figure 5.1 displays the optical depth averaged over the globe. The effect of solar variability is considered with total solar irradiance reconstructions by *Lean* (2000). This not only shows the well-known 11 year solar cycle but also a long-term increase in the first half of the 20th century. To study the role of SSTs in driving stratospheric climate we have included three time series with variability on different time-scales. ENSO was computed as area average of SST anomalies (with respect to 1961-90) over 170°W to 120°W and 5°S to 5°N, also known as the NINO 3.4 index. The AMO index is representative for the SST anomalies averaged over the North Atlantic region (7.5°W to 75°W and 0°N to 60°N) and filtered with a 121 month filter. To remove any GHG signal from this time series, the index was first regressed upon GHG alone. The PDO is defined as the standardized first principal component of SST anomalies in the North Pacific basin (100°E to 100°W and 20°N to 60°N). Positive index phases are associated with anomalous cold SSTs over the interior North Pacific and warm temperatures off the North American West Coast. Here, the GHG signal was subtracted from the time series by a separate regression upon global averaged SSTs. One complication when including the PDO is its strong relation with ENSO. The PDO and ENSO indices are highly correlated, but show dissimilarities in the low-frequency variability as can be observed in the power spectra (not shown). Since the focus here is to study a possible relationship between the decadal scale variability in the Pacific Ocean basin and the stratosphere, we filtered the PDO index with a 180 month filter.

To take into account that variations on the interannual scale (i.e. QBO, ENSO and optical depth from stratospheric aerosols) could lead the stratospheric response by some months, we first made individual regressions of lagged explanatory variables and the target variables in the polar stratosphere, which is the main focus of this study. This revealed higher correlations with ENSO when lagged by 1 month and with QBO30 lagged by 2 months. All other explanatory variables are averaged over January to March. To encounter possible autocorrelations within the residual time series of the multiple regression model,

affecting the significance level of the trend estimate (p-value), we have applied a first order autoregressive process.

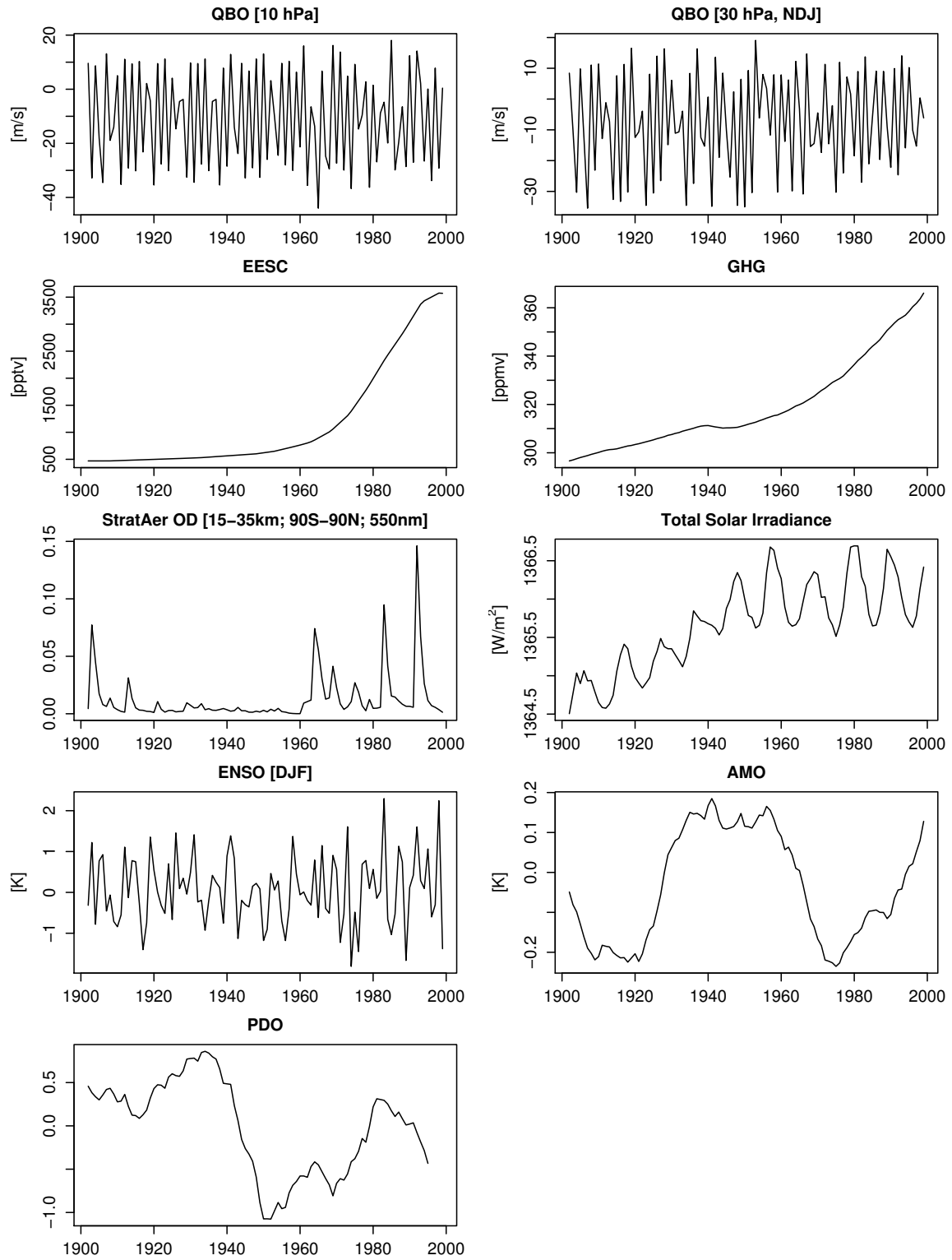


Figure 5.1 Set of explanatory variables used for the multiple regression analysis at annual temporal resolution. All variables are averaged over January to March, except for ENSO which is

lagged by 1 month (DJF) and QBO30 by 2 months (NDJ). For more details on the individual time series, see text.

5.3 Results

The purpose of this section here is to discuss the patterns of the obtained regression coefficients and to qualitatively judge them with previous studies. At the end of this section an overview and a discussion of the relative impact among the different drivers will be provided.

Figure 5.2 displays the regression coefficients (in unit change per standard deviation) of zonally averaged zonal wind, temperature and ozone upon QBO10 and QBO30. The QBO is a dominant variability pattern in the tropical stratosphere with downward propagating easterly and westerly wind regimes with a period of around 28 months (*Baldwin, et al., 2001*). This characteristic can be seen in the zonal wind's response in SOCOL which shows a latitudinal symmetric dipole structure from around 20°S to 20°N which is at a lower altitude in QBO30 than QBO10 due to downward propagation. Through thermal wind balance the largest positive (negative) temperature anomalies are correlated with the most positive (negative) vertical wind shear, which can be found here in the lower (upper) equatorial stratosphere. It is also the region where we find two local ozone maxima connected to weakened (strengthened) vertical transport: these increases are a consequence of the vertical ozone profile shape with a maximum at around 10 hPa (see also *Butchart, et al., 2003*). As an effect of these findings tropical column ozone is highly correlated with the stratospheric equatorial zonal winds as observed in satellite data, maximizing when taking the winds at 20 – 30 hPa (*Randel and Wu, 1996*).

For QBO30 in the extra tropics (northward of 50°N) we find a statistically significant acceleration of zonal winds at all altitude levels. This is also known as the “Holton-Tan effect” (*Holton and Tan, 1980*), showing a strengthened polar vortex when the QBO at 50 hPa is in its westerly phase. Since the phase of QBO10 at 50 hPa is less determined (switching from westerly to easterly below 50 hPa) compared to QBO30, the enhanced zonal wind speeds at polar latitudes are less manifest and statistical significance is mostly absent. It is interesting to note that the enhancement of the polar vortex for QBO30 also has a significant signal down to the Earth's surface. In line with a strengthened polar vortex, Arctic upper air temperature anomalies are negative up to around 5 hPa and positive in the upper stratosphere, indicating less downwelling over high latitudes. The temperature anomalies from 20-60°N for QBO10 and QBO30 are out of phase with those over the equator which is a well-known response to the QBO variation in winter and spring also seen in satellite observations (*Baldwin, et al., 2001; Randel and Cobb, 1994*). The ozone response reveals a statistically significant decrease in the stratosphere over the whole hemisphere with largest ozone losses in the sub-tropics. This is again in agreement with total ozone satellite data of TOMS showing decreases over the mid-latitudes when the QBO is in its west phase (*Baldwin, et al., 2001; Randel and Cobb, 1994*). *Butchart et al.*

(2003) showed that the negative anomalies in this region are connected to the vertical transport anomalies which are out of phase compared to the tropics (vertical transport reduced above and enhanced below ozone maximum during westerly QBO phase). Unlike in satellite data where total ozone losses at high latitudes are observed but statistical significance is missing, we find in SOCOL for QBO30 significant ozone losses throughout the polar stratosphere.

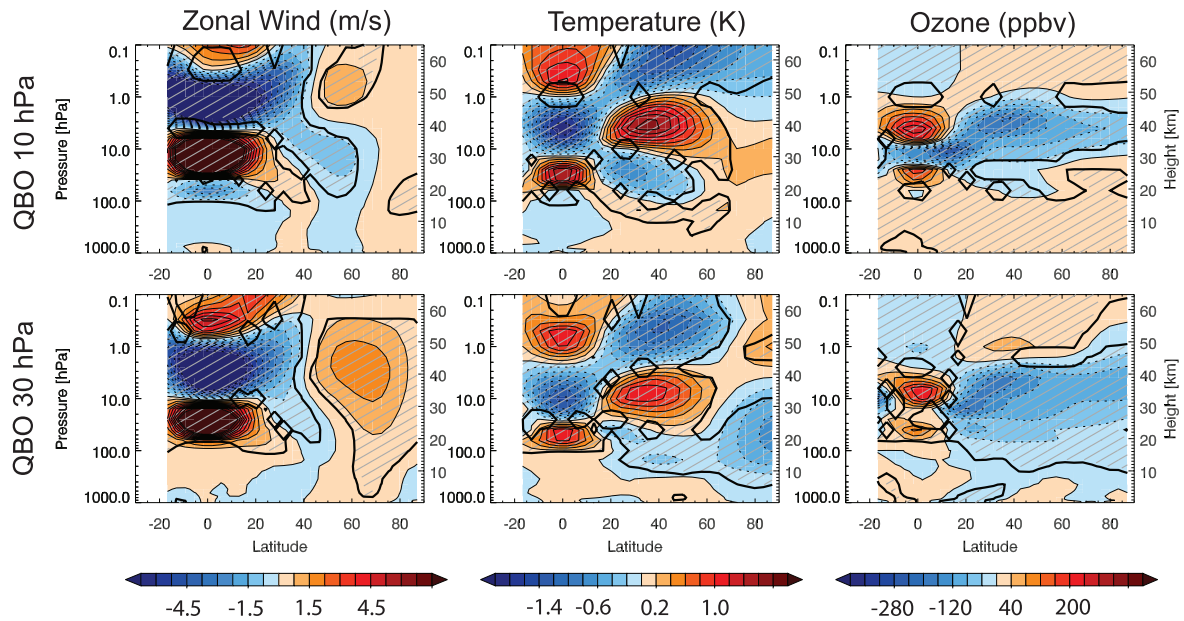


Figure 5.2 Regression coefficients of zonally averaged wind (left), temperature (middle) and ozone (right) upon explanatory variables of QBO at 10 and 30 hPa in the winter Northern Hemisphere (averaged over JFM). Units of coefficients are with respect to one standard deviation of the explanatory variable. Shaded areas together with black contour line mark statistically significant areas (p -value < 0.05).

The stratospheric response to the anthropogenic releases of ODS and GHG is shown in Figure 5.3. Note that due to the long-term trends over the century in the explanatory variables the coefficients are given in unit change per 100 pptv EESC and 1 ppmv GHG. The zonal wind response reveals patterns which are almost opposite phase. This could be an effect of collinearity between the two explanatory variables (Kerzenmacher, *et al.*, 2006; Maeder, *et al.*, 2007). The tropical zonal wind signal for GHG (i.e. strengthened westerlies in the mesosphere and easterlies in the middle stratosphere) is similar to the one found by Langematz *et al.* (2003) who did idealized model simulations with imposed ozone and CO₂ changes for the period 1979-2001 in order to separate the contributions to observed stratospheric temperature and circulation trends. According to this study the response in zonal wind to EESC and GHG should be fairly similar, which is not the case here. In contrast to previous modeling and observational studies which reported of a strengthening of the polar vortex (e.g., Kodera and Koide, 1997; Langematz, *et al.*, 2003) over recent decades, the signals here are small with differing signs at different altitudes and not significant.

As in Figure 5.2 the temperature response in the tropics follows the phase of the vertical shear in zonal wind. For EESC the pattern resembles the one of QBO which could be due to inappropriate separation between the two explanatory variables (see also *Crooks and Gray, 2005*). Thus, the response in the middle and upper stratosphere is different to previous studies. *Langematz et al. (2003)* showed that due to ozone depletion (as seen in the last column of Figure 5.3) and subsequent changes in the heating rates from the short- and longwave radiation maximal cooling is occurring near the subtropical stratopause. In the lower stratosphere the cooling effects are more intense at higher latitudes than over the tropics, which is in agreement with the findings of *Langematz et al. (2003)*. In a global annual mean view temperature trends due to ozone depletion show a distinct pattern with maximal cooling at around 1 hPa, minimum cooling at 10 hPa and a second but smaller maximum in the lower stratosphere (*Shine, et al., 2003*).

The effect of increased GHG concentration is to enhance the cooling trend due to increased emission of longwave radiation. These additional temperature changes are minor in the lower stratosphere but increase with height and therefore lead to strongest cooling trends at the stratopause (*Shine, et al., 2003*). For SOCOL the enhancement of negative temperature trends due to GHG are manifest in the upper stratosphere (Figure 5.3, middle lower panel). In addition negative trends can be observed in the tropical and polar mesosphere. In the lower stratosphere the signal is less clear showing an increase in temperatures (though almost not significant) towards northern latitudes. Note that this is also the region where large model to model variability are found and where the uncertainty of trend estimates in observations are high (*Shine, et al., 2003*). The lower polar stratosphere is an area being pre-dominantly dynamically controlled. An analysis of the 100 hPa Eddy heat flux revealed that CO₂ contributes to an enhancement of the planetary wave activity and the RMC in late winter / early spring (*Langematz, et al., 2003*), which could be a reason for warmer modeled temperatures than observed. In the troposphere temperatures are rising due to GHG as observed and show at low latitudes a faster warming in the upper troposphere than at the surface. The latter is qualitatively in line with other climate models and was recently evidenced with trends deduced from thermal winds measured with radiosondes (*Allen and Sherwood, 2008*).

Mid-latitude ozone is strongly decreased in response to EESC. Negative contributions are largest in the lower and upper stratosphere, which is in agreement with previous observational and modeling studies (*Fischer, et al., 2008a; Randel and Wu, 2007*). In the troposphere the ozone increase observed in the late 20th century (*Oltmans, et al., 2006*) is taken up by the GHG term whereas the EESC coefficient shows ozone decline in the whole Northern Hemispheric troposphere.

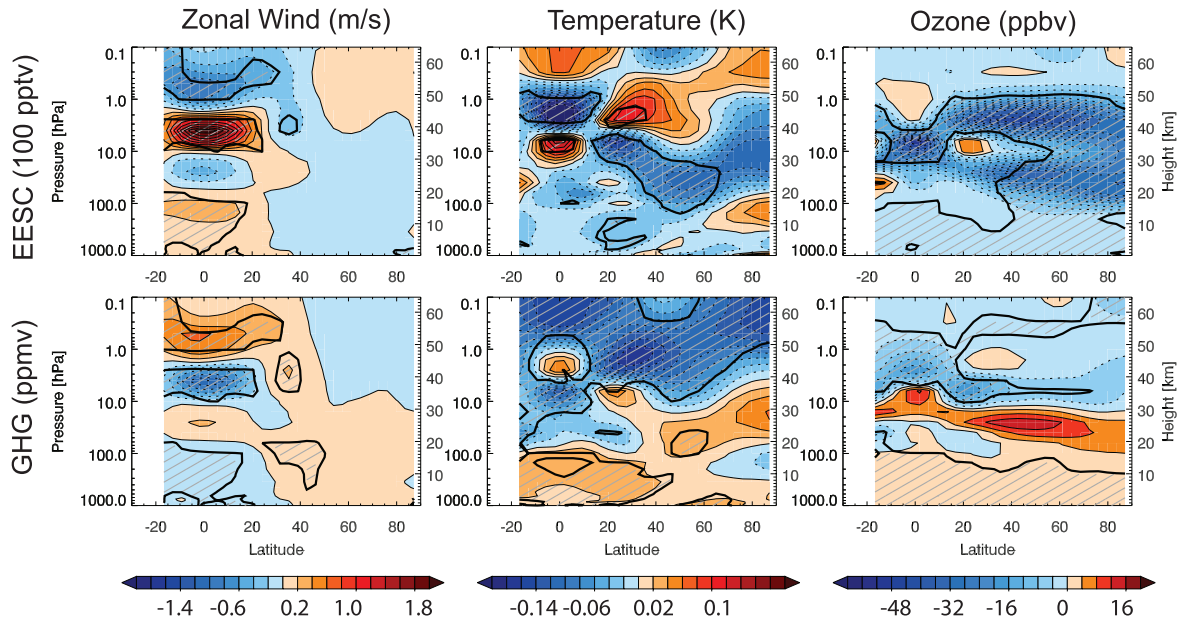


Figure 5.3 the same as Figure 5.2 but for EESC and GHG as explanatory variables. Units of the coefficients are with respect to 100 pptv and 1 ppmv, respectively.

Figure 5.4 displays the extracted solar signal over the twentieth century. As a prominent response we find a significant strengthening of the polar vortex with maximum wind increases in the upper stratosphere. At the same time temperatures in the lower and middle Arctic stratosphere are strongly reduced but increased in the upper stratosphere and lower mesosphere. This is in agreement with previous studies extracting the solar signal in composite studies, idealized model simulations and multiple regression analysis (e.g., *Crooks and Gray, 2005; Egorova, et al., 2004; Kodera, 1995*). *Kodera and Kuroda (2002)* have shown that the anomalies in the polar stratosphere are related to a stronger polar night jet in the upper stratosphere during solar maximum conditions, which modulates the build-up of the polar vortex during winter by propagating planetary scale waves. The stronger jet at the stratopause is a consequence of an increased meridional temperature gradient in the winter hemisphere. The dipole structure in polar temperature and the positive temperature anomaly in the equatorial lower stratosphere suggests reduced downwelling and a deceleration of the RMC (*Kodera and Kuroda, 2002*). Furthermore, the vertical shape of the tropical temperature increase in SOCOL reveals a maximum near the stratopause and a local minimum (though not significant) at around 20 hPa which is in rough agreement with TOVS data analyzed by *Scaife et al. (2000)*. In the troposphere, similar to studies by *Crooks and Gray (2005)* for ERA40 reanalysis, we find a vertically banded structure with a significant easterly zonal wind response in the sub-tropics and enhanced westerlies (though not significant) at higher latitudes, which is explained by a latitudinal shift of the Hadley Cell during solar maximum conditions (*Haigh, 1996*).

Ozone mixing ratios are significantly increased in the upper stratosphere due to an intensification of the oxygen photolysis with a latitudinal maximum at around 25°N. Enhanced UV radiation also leads to an increase in tropospheric ozone levels at solar

maximum. Note that the ozone decline in the middle stratosphere in mid- to high latitudes is not significant. In the tropical and subtropical mesosphere ozone is significantly decreasing which is a consequence of intensified HO_x destruction cycles (*Egorova, et al., 2005b*). The equatorial stratospheric ozone increase with two maxima and a minimum at around 20 hPa is in good agreement with satellite data (*Soukharev and Hood, 2006*) as well as with a recent CCM simulation investigating the solar signal (*Austin, et al., 2007*).

SOCOL simulates maximal heating due to increases in stratospheric aerosol loading at around 70 hPa in the equatorial stratosphere and negative temperature anomalies in the troposphere as a result of enhanced backscattering of shortwave radiation (Figure 5.4). (Note that due to an error in the radiation code of ECHAM4, heating is generally overestimated in SOCOL.) The strongest temperature increases are located at a lower altitude than was observed after the Pinatubo eruption (*Robock, 2000*). The modeled response in the lower stratosphere displays an enhanced equator-to-pole temperature gradient and a significant strengthening of the polar vortex. This is in agreement with previous studies (*Robock, 2000*), which show as a consequence a positive phase of the Arctic Oscillation and anomalous warming in surface air temperatures over continents during wintertime. *Stenchikov et al. (2002)* suggested a tropospheric feedback mechanism (i.e. reduction of the meridional temperature gradient and subsequent reduction of vertical flux of planetary wave energy) reinforcing the strengthened polar vortex in presence of a volcanically disturbed stratosphere. However, *Graf et al. (2007)* recently analyzed the boreal winters after strong volcanic eruptions in the NCEP reanalysis and found contradictory results to *Stenchikov et al. (2002)*: they observed more planetary wave energy originating from the troposphere and passing through the stratosphere during volcanically disturbed winters. To reconcile with observed AO patterns they suggest that these waves are being reflected instead of breaking. They also note that the biggest volcanic eruptions coincide with ENSO positive phases which could contribute to the observed findings (see below). In the Arctic stratosphere SOCOL simulates positive (negative) temperatures in the upper (lower) stratosphere which is most probably a result of the strengthened polar vortex and less air descending from the upper stratosphere. The negative temperature response in the lower stratosphere, however, is not significant. A negative anomaly was observed in the second winter after the Pinatubo eruption, but this could also be an effect of the QBO which was switching from East to West phase (*Stenchikov, et al., 2004*).

The regression coefficients of ozone upon stratospheric aerosol loading reveal stratospheric ozone increases over almost the whole hemisphere. This is due to the fact that in the pre-CFC period the dominant effect of enhanced N_2O_5 hydrolysis, as usually observed on sulphate particles after volcanic eruptions, is to reduce the NO_x induced ozone destruction cycle (see also *Tie and Brasseur, 1995*). This enhances the ozone column in mid- to high latitudes which is opposite to what has been reported from observational and modeling studies on the effects of the well studied volcanic eruptions of El Chichon and Pinatubo (*Robock, 2000*). Under high chlorine loading reduced NO_x leads to an enhanced $\text{ClO} /$

ClONO₂ partitioning. Furthermore, the increases of sulphate particles provide additional surfaces for the activation of chlorine (Solomon, 1999). The ozone signal after the Mt. Agung eruption (1963) was investigated in modeling studies with somewhat contradictory results: Dameris *et al.* (2005) found ozone depletion in the northern mid-latitudes despite low chlorine loading and explained that with an enhancement of increased water vapor and HO_x cycle ozone destruction. Austin and Wilson (2006), however, reported an increase in stratospheric ozone in accordance with Tie and Brasseur (1995). The tropical ozone signal in SOCOL which shows positive (negative) anomalies above (below) 20 hPa could be due to a lift of the ozone profile as a result of a strengthening of the RMC as found in Dameris *et al.* (2005). Note that overall, the increases in stratospheric ozone and hence reduced ozone depletion contribute to a less enhanced meridional gradient and a less dominant AO pattern. Stenchikov *et al.* (2002) could reproduce an AO positive pattern in an idealized model simulation imposing only the observed ozone anomalies.

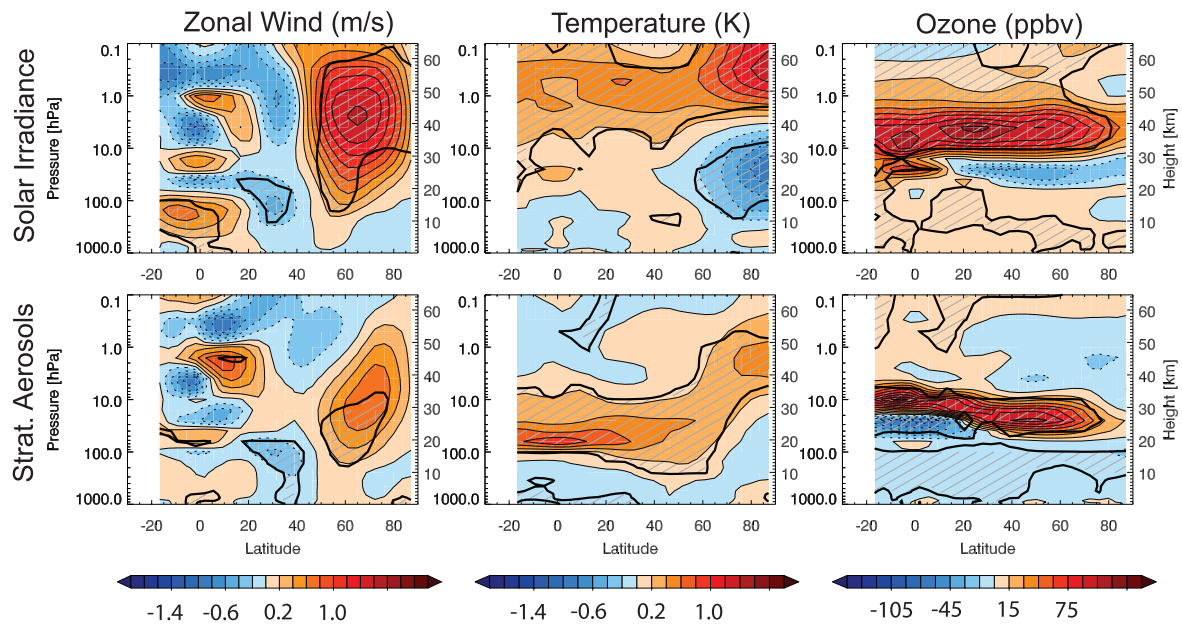


Figure 5.4 the same as Figure 5.2 but for solar irradiance and stratospheric aerosols as explanatory variables.

The climate imprint of interannual and decadal scale variations in SSTs can be inferred from Figure 5.5. ENSO variability leaves a clear signature on the high latitudinal stratosphere in SOCOL with decreased zonal flow and warm anomalies. This result is in agreement with previous observational and modeling studies (Brönnimann, *et al.*, 2006b; Camp and Tung, 2007; Garcia-Herrera, *et al.*, 2006; Sassi, *et al.*, 2004; Van Loon and Labitzke, 1987). In simulations of warm and cold ENSO events with the CCM SOCOL it could be shown that these characteristics are associated with an acceleration of the RMC and increased wave-mean flow interaction (Brönnimann, *et al.*, 2006b; Fischer, *et al.*, 2008b). It is interesting to note that the high latitude anomalies in wind and temperature observed in the stratosphere are extending towards the troposphere leaving significant

climate anomalies at the Earth's surface. The ENSO signal in the equatorial stratosphere reveals lower temperatures than normal which can be understood in the context of a strengthened RMC (*Brönnimann, et al.*, 2006b). In the tropical troposphere warming is amplified at upper levels in line with studies showing that tropical tropospheric temperatures are lagged by some months compared to the ENSO index (e.g., *Chiang and Sobel*, 2002). Through the intensification of the RMC during ENSO positive phases it was suggested that ozone transport from the equatorial stratosphere towards higher latitudes is increased (*Brönnimann, et al.*, 2006b; *Fischer, et al.*, 2008b). This can be partly seen in the regression analysis with negative anomalies over the tropics and an ozone increase in the polar stratosphere. The signal, however, is less dominant than e.g. in *Fischer et al.* (2008b), who did a model intercomparison with three CCMs simulating two extreme phases of ENSO.

The last two rows of Figure 5.5 show the climatic response to decadal scale variability in the ocean. Large multidecadal variations in regional climate could be linked to multidecadal variations in Atlantic SSTs and hence AMO (*Knight, et al.*, 2006; *Sutton and Hodson*, 2005). Moreover, the connection between the PDO and North American and North Pacific decadal variability was the topic of many studies. *Latif and Barnett* (1994) showed that positive SSTs in the interior North Pacific (negative PDO phase) cause a weakening of the Aleutian Low and subsequent surface air temperature decreases (increases) in the northeastern (southeastern) part of the North American continent. To our knowledge no studies have been performed analyzing the impacts of the AMO or the PDO on the stratosphere. In the tropical and subtropical stratosphere the response upon AMO resembles a QBO-like pattern as already seen for EESC as explanatory variable (Figure 5.3). This feature is most probably caused by insufficient separation between the two variables (see above). At high northern latitudes we find a significant weakening of the polar vortex together with a slight increase in temperatures and ozone. Furthermore, a warming in the troposphere and a northward displacement of the subtropical jet can be observed. The PDO signal in the stratosphere is small and statistical significance is mostly absent. The polar vortex system seems to be shifted southward. However, only an increase in the mid-latitude lower stratosphere is statistically significant. In the troposphere northward of 20°N a significant cooling is found which is connected to anomalous cold SSTs in the interior North Pacific during positive phases of the PDO.

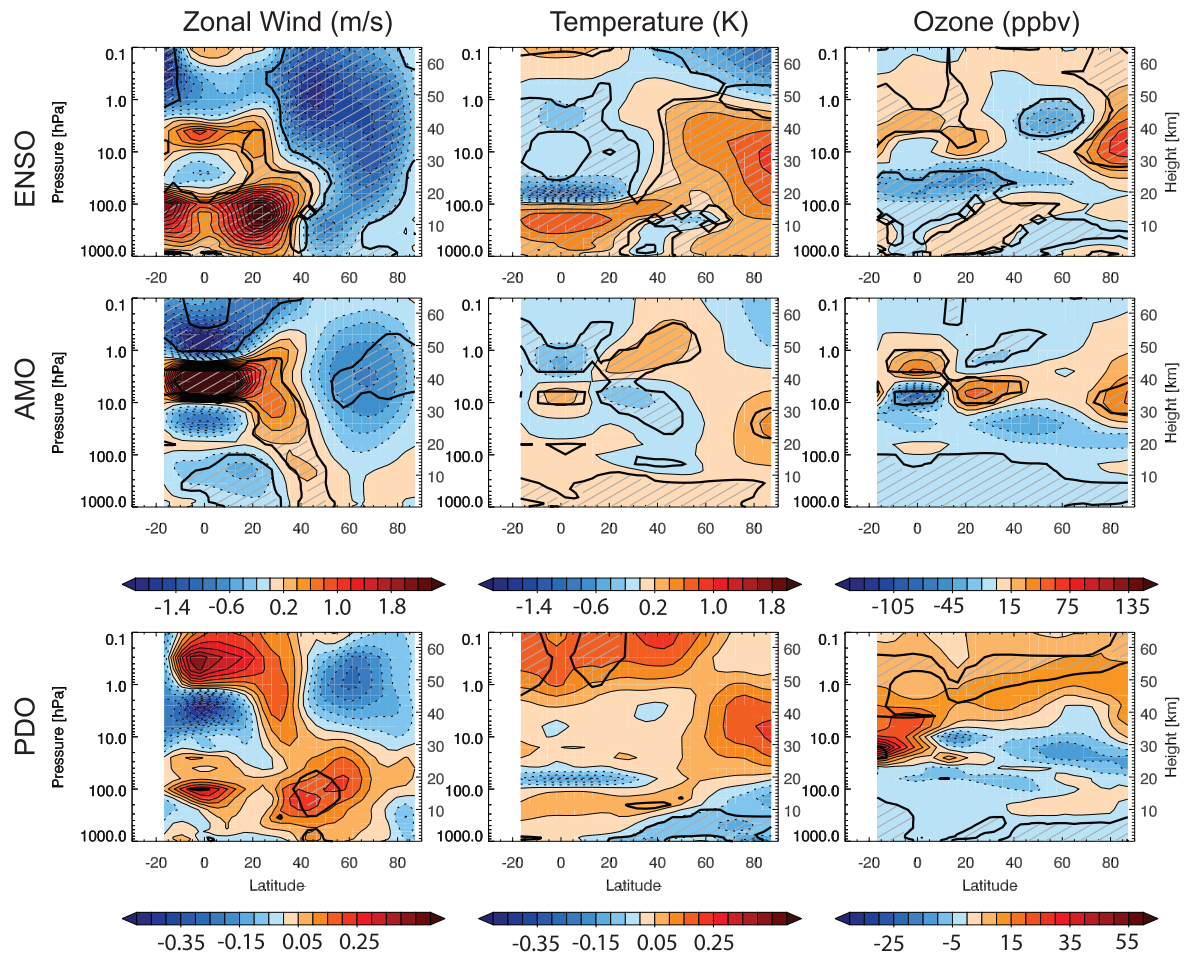


Figure 5.5 the same as Figure 5.2 but for ENSO, AMO and PDO as explanatory variables.

5.3.1 Summary and Discussion

ENSO, solar variability and QBO30 could be identified as the largest contributors to modeled variability of zonal winds at the high latitudinal stratosphere. Both QBO30 and solar cycle variations lead to acceleration of the polar vortex of more than 1.5 m/s per standard deviation in the explanatory variable. A comparable magnitude with opposite sign is seen for ENSO. It is interesting to note that all of these effects are to some degree extending to tropospheric levels (though not significant for solar variability). AMO and increases in stratospheric aerosols have a weaker impact on high latitude zonal winds. Their magnitude is similar but with opposite effects. Temperatures in the Arctic lower stratosphere are connected to the strength of the polar vortex (i.e. warming signal when vortex is weak and vice versa) and hence show a similar ranking.

The subtropical jet is most dominantly affected by ENSO, displaying an acceleration of zonal winds in its positive phases. Variability in solar irradiance, stratospheric aerosols and AMO are negatively correlated with the jet strength and show less strong signals.

In the equatorial stratosphere a large fraction of variability in temperatures are explained by the QBO. However, a considerable part of equal magnitude is caused by ENSO and stratospheric aerosols in the lower stratosphere. In the upper stratosphere and lower mesosphere solar variability significantly contributes to temperature variability with a positive signal during solar maximum. QBO, solar variability, and stratospheric aerosols are also essential for explaining stratospheric temperature variability in mid-latitudes.

Explanatory variables with variations on the interannual scale leave an imprint in stratospheric ozone most dominantly seen in solar irradiance, stratospheric aerosols and the QBO. ENSO also contributes to the modeled variability but its magnitude is smaller. Moreover, the low-frequency variabilities of SSTs have only little effect on the ozone distribution during wintertime.

6 Conclusions and Outlook

6.1 Conclusions

This thesis has focused on interannual-to-decadal variability in the stratosphere during the 20th century. Results and conclusions are based on numerical simulations with the CCM SOCOL. Time-slice experiments and 100 year transient runs in ensemble mode were performed to investigate the relation between forced and internal variability in the climate system.

The output of the 100 year transient runs has been analyzed with respect to tropospheric climate variability. SOCOL is in very good agreement with other state-of-the-art AGCM simulations as well as with observational data over the 20th century. This especially holds for the strength of the SOI – ENSO signature, NAO trends and global temperature development.

With respect to the stratosphere, the output has first been validated with observational and reconstructed data to account for model biases. It has further been checked for temporal consistencies over the century. A direct comparison to observations revealed by and large reasonable agreement regarding modeled fields of stratospheric ozone, temperature, and zonal wind. Modeled climatologies of these variables remained almost unaltered in the first seven decades of the 20th century. Some shortcomings of the model were reported concerning the seasonal cycle of TOZ and biases in zonally averaged ozone in the upper and lower stratosphere. The runs were also successfully validated in a process-oriented view by looking at the relationship between upward propagating wave energy and polar temperatures and ozone. Trends of ozone over the time period 1979-1999 were estimated in all ensemble members, which agree well with satellite observations in the upper stratosphere but on average underestimate the observed negative trend in the southern lower stratosphere.

Special emphasis was set on the investigation of forced and internal variability. Trends of the vertical EP flux component were estimated in individual ensemble members over different time windows. Our results show that these estimates vary greatly among ensemble members and statistical significance is mostly absent which hinders to make reliable conclusions. However, it suggests that previous studies on EP flux trends based on model results should be interpreted with caution since these are mostly results of one model realization only. The spread of internal variability is strongly dependent on the analyzed parameter and may manifest regionally differently. It could be shown that the strength of the subtropical jet is pre-dominantly externally forced and presumably develops

in response to ENSO via changes in the Hadley and Walker circulation. Agreement between individual ensemble member simulations and the reconstructed index is therefore high regarding magnitude and interannual variations. On the contrary, the north polar stratosphere is the region where largest ensemble variability was found. This not only holds for the strength of the polar vortex but also for TOZ development over this region. Capturing the year-to-year fluctuation of the reconstructed polar vortex strength index is unlikely precluding potential prediction of it. However, the ensemble members are consistent with reconstructions (index mostly lies within the ensemble spread) suggesting that the strength of the polar vortex is well modeled and internal variability is a dominant source of variability. To further characterize the climatic conditions in the polar stratosphere, frequency, seasonality and intensity of major warmings (MWs) were analyzed. It was shown that a much smaller number of MWs was occurring in the model compared to observations suggesting a less disturbed polar vortex. No major discrepancies could be identified regarding seasonality and intensity of MWs in a climatological view implying that in case a MW occurs, it evolves in a comparable way as in observations. Yet, the exact timing of individual MWs across the 20th century remains variable among individual ensemble members.

Despite regionally large internal variability in some of the analyzed variables, the contributions of externally forced drivers to stratospheric interannual-to-decadal variability could be identified. A multiple regression model was applied to zonally averaged zonal wind, temperature, and ozone of the ensemble mean simulation in the winter Northern Hemisphere to track the role of the main drivers. Several aspects of the different responses were found to match qualitatively well with previous studies. Part of the variability in zonal wind and temperature at the high latitudinal stratosphere can be attributed to different sources: the westerly phase of the QBO at 30 hPa and positive phases of solar activity lead to an acceleration of the polar vortex, whereas warm ENSO events are associated with decreased zonal flows. Through intensification of the meridional temperature gradient in the lower stratosphere, an increase of stratospheric aerosol loading contributes to a strengthening of the polar vortex, though the magnitude is smaller. Our results further show that the imprint of the AMO is associated with a weakened zonal flow at high latitudes. Yet, no statistical significant signal could be found for the response upon the anthropogenic trend components (GHG and ODS) in this region. Similarly, the stratospheric signal of low-frequency variability in North Pacific SSTs remains less clear. The extraction of the solar signal in ozone further shows a qualitatively good match with observations in the tropics. Interestingly, the signature of stratospheric ozone in response to volcanic eruptions is marked by a significant positive anomaly in mid- to high latitudes, which is suggested to be an effect of the reduced ozone destruction cycle induced by NO_x.

A main focus of this thesis was on the role of ENSO on the high-latitude stratosphere. A model intercomparison with a large set of ensemble members using the CCMs SOCOL, IGCM-FASTOC and G-PUCCINI was carried out to investigate this issue. The intercomparison of the northern hemispheric winter stratospheric response upon two

unusually strong opposite phases of ENSO (1940-1942 and 1975-1976) confirms previous observational and modeling studies. As a main response an increased wave-mean flow interaction accelerating the residual mean circulation and weakening the zonal flow at northern high latitudes could be detected in all models. This is accompanied by anomalous warm temperatures over the Arctic stratosphere and by an enhanced equator-to-pole transport of ozone during warm ENSO events. The results were compared to reconstructions of geopotential height and temperature fields as well as to historical TOZ observations at several locations in the Northern Hemisphere. Agreement between models and reconstructions is especially promising over the tropics and the Pacific North American sector at mid- to high latitudes. However, the wave structure over the North Atlantic European sector is not correctly reproduced in any of the analyzed CCMs. The role of the rather low horizontal grid resolution was discussed and suggested to be responsible for the mismatch over this region. Out of the three CCMs SOCOL displays the strongest of the aforementioned signals which might be an effect of the higher vertical grid resolution. Investigations of the ensemble spread in temperature, geopotential height and TOZ suggest that a large number of ensemble simulations must be carried out to detect and attribute ENSO effect on the northern stratospheric climate in transient CCM simulations.

6.2 Outlook

The output of the 100 year transient ensemble simulations provides a unique data set for further exploration. Based on the presented thesis several succeeding studies could be performed.

It would be interesting to perform the presented regression analysis to all individual ensemble members. This would allow putting the uncertainty arising from the regression model in relation to the ensemble spread. Much further effort could be set on the development of the regression model. This involves analyzing the inclusion of interaction terms, which in case of QBO and solar variability could add more information on the interpretation (*Smith and Matthes, 2008*). A further extension of the model concerns the different response of ozone upon stratospheric aerosol loading under high and low halogen concentrations. Information on the different behavior could be added to the regression model in a theory-guided way. It would also be interesting to calculate the individual responses in spatially different areas (rather than zonal averages). Such an analysis might be especially beneficial with respect to the low-frequency variability of SSTs in different northern hemispheric basins. Finally, the regression model could be applied to the Arctic Oscillation to better understand the manifestations of the stratospheric signal in the troposphere. Any such further studies must be complemented with an analysis of observational data, which is presently not yet done.

It would also be valuable to further investigate the relation between external forcings and stratospheric climate and its effects separately for each forcings, looking at individual events and making composite studies. Many interesting scientific issues could be addressed. For instance could individual warm ENSO events across the 20th century be

compared with respect to their influence on the North Atlantic European sector. Such a study could provide detailed information on how the events differ among each other but also how differently they evolve with regard to the processes described in this thesis. An analysis of ensemble members could potentially help to better understand why some warm ENSO winters are accompanied by different climate anomalies over Europe than others according to observations. It could contribute to the discussion if this is a modulating factor or rather a nonstationary behavior (see *Brönnimann, 2007*). A further interesting topic is the climatic effect of volcanic eruptions which could be addressed in a composite study. It would be very interesting to see whether the model reproduces a winter warming pattern over continents (*Robock, 2000*) after major volcanic eruptions. Dissimilarities among the events could provide useful insights in the relative importance of stratospheric processes during volcanic eruptions. The output of the 100 year transient simulation also provides an ideal opportunity to investigate in detail the climatic effects of the high-latitude volcanic eruption Mt. Katmai in 1912 which has only little been investigated in the past (*Oman, et al., 2005*). Yet, due to a model error detected in the radiation code of ECHAM4, concerning absorption in the near infrared, these individual volcanic events would first have to be re-simulated.

The ensemble simulations can be further compared to sensitivity runs with the CCM SOCOL which will be performed in the near future. Several of such simulations are planned with different forcings switched on and off (i.e. evolving in transient mode and set to a climatological mean state). It is of particular interest to compare the results of these simulations to the extracted signals from the 100 year transient ensemble simulations. Such a comparison would greatly improve our understanding of forced and internal variability during the 20th century.

The model results are also highly valuable for analyzing tropospheric climate anomalies in the 20th century. The runs were used to analyze the US “Dust Bowl” droughts of the 1930s (*Brönnimann, et al., 2008*). Other interesting topics that could be tackled with this dataset are for instance stratospheric memory effects on tropospheric weather and climate (*Baldwin, et al., 2003*) or the Arctic warming in the troposphere from 1920-1945 with a focus on the vertical temperature structure (*Grant, et al., 2008*).

Finally, large scientific benefits would be gained from a comparison of the transient simulations to ensemble climate simulations of a fully coupled ocean-troposphere-stratosphere GCM (*Huebener, et al., 2007*), as it additionally allows to investigate the effects of feedbacks between the stratosphere and the ocean.

To sum it up, the output of the presented 100 year transient simulations provide the fundament for a variety of pursuing projects. Nevertheless, it would also be highly interesting to update the model simulations until today and to simulate further backwards in time. A continuation of the model run to recent times could substantially improve the discrimination between GHG and ODS signals in a regression analysis, since ODS has peaked in the late 1990s and GHG has continued to increase. Model simulations extending back to the 1880s could eventually re-visit the discussions on upper air processes during

the devastating Krakatoa eruption, which, thanks to the pioneers at that time, paved the way for our today's comprehensive view of stratospheric variability.

Appendix A

The 1986-1989 ENSO cycle in a chemical climate model

S. Brönnimann¹, M. Schraner¹, B. Müller¹, A. Fischer¹, D. Brunner¹, E. Rozanov^{1,2}, and T. Egorova²

¹Institute for Atmospheric and Climate Science, ETH Zürich, Universitätsstr. 16, CH-8092 Zürich, Switzerland

²PMOD/WRC, Dorfstr. 33, CH-7260 Davos, Switzerland

(published in Atmos. Chem. Phys., 6, 4669-4685, 2006)

Abstract

A pronounced ENSO cycle occurred from 1986 to 1989, accompanied by distinct dynamical and chemical anomalies in the global troposphere and stratosphere. Reproducing these effects with current climate models not only provides a model test but also contributes to our still limited understanding of ENSO's effect on stratosphere-troposphere coupling. We performed several sets of ensemble simulations with a chemical climate model (SOCOL) forced with global sea surface temperatures. Results were compared with observations and with large-ensemble simulations performed with an atmospheric general circulation model (MRF9). We focus our analysis on the extratropical stratosphere and its coupling with the troposphere. In this context, the circulation over the North Atlantic sector is particularly important. Relative to the La Niña winter 1989, observations for the El Niño winter 1987 show a negative North Atlantic Oscillation index with corresponding changes in temperature and precipitation patterns, a weak polar vortex, a warm Arctic middle stratosphere, negative and positive total ozone anomalies in the tropics and at middle to high latitudes, respectively, as well as anomalous upward and poleward Eliassen-Palm (EP) flux in the midlatitude lower stratosphere. Most of the tropospheric features are well reproduced in the ensemble means in both models, though the amplitudes are underestimated. In the stratosphere, the Socol simulations compare well with observations with respect to zonal wind, temperature, EP flux, meridional mass streamfunction, and ozone, but magnitudes are underestimated in the middle stratosphere.

With respect to the mechanisms relating ENSO to stratospheric circulation, the results suggest that both, upward and poleward components of anomalous EP flux are important for obtaining the stratospheric signal and that an increase in strength of the Brewer-Dobson circulation is part of that signal.

A.1 Introduction

On a global scale, the most important (and potentially predictable) mode of interannual climate variability is El Niño/Southern Oscillation (ENSO). It affects not only climate in tropical regions, but also in the extra tropics and in the stratosphere. While the climatic influence in the Pacific-North American sector is well known and understood (e.g., *Alexander, et al.*, 2002), the effects in other parts of the world are less well established. Understanding these effects is important, e.g., with respect to seasonal climate forecasting. As to the stratosphere, the ENSO signal is relevant as it affects the ozone layer as well as stratospheric dynamics (*Brönnimann, et al.*, 2004).

The ENSO signal in the stratosphere is neither well known nor completely understood. Many El Niño events are accompanied by a weak and warm polar vortex both in models and observations; a signal that appears in the upper stratosphere in early January and then propagates downward and dominates the lower stratosphere in late winter (e.g., *Brönnimann, et al.*, 2004; *Garcia-Herrera, et al.*, 2006; *Manzini, et al.*, 2006; *Sassi, et al.*, 2004; *Taguchi and Hartmann*, 2006; *Van Loon and Labitzke*, 1987). In climate models, ENSO affects stratosphere-troposphere coupling (e.g., *Pyle, et al.*, 2005) and stratospheric chemistry (e.g., *Sassi, et al.*, 2004). However, the signal is not reproduced in all model studies (see references in *Manzini, et al.*, 2006) and in observation-based studies it has been found difficult to separate the ENSO signal from other effects such as the Quasi-Biennial Oscillation (QBO) or volcanic eruptions. The effect on Arctic ozone has only rarely been addressed.

The circulation in the Arctic stratosphere is closely related to the tropospheric circulation in the North Atlantic-European sector (e.g., *Ambaum and Hoskins*, 2002; *Baldwin and Dunkerton*, 2001; *Hartmann, et al.*, 2000) and hence understanding the stratospheric ENSO signal requires an understanding of the ENSO climate signal in the North Atlantic-European area. The latter, however, is a matter of ongoing discussion. In statistical studies, several authors found a symmetric signal that resembles the North Atlantic Oscillation (NAO) and supposedly results from a downstream propagation of a wave disturbance from the Pacific-North American sector in the form of a stationary wave-train, possibly maintained by a transient-eddy feedback (*Fraedrich*, 1994; *Fraedrich and Muller*, 1992). However, others found an asymmetric signal (e.g., *Wu and Hsieh*, 2004) or a signal that is strong for La Niña but weak or absent for El Niño (e.g., *Pozo-Vazquez, et al.*, 2005). This is important with respect to the interpretation of the stratospheric signal. Hence, trying to reproduce the ENSO signal in the North Atlantic-European area and the stratosphere with climate models not only serves as a model test but also promotes our understanding of ENSO mechanisms.

In this study we analyse the effects of a pronounced El Niño/La Niña cycle on the circulation of the extra tropics and the northern stratosphere using ensemble simulations with a chemical climate model (CCM). Ensemble simulations provide multiple realisations of numerical predictions of the atmospheric state, which allows analysing probabilities and frequency distributions. The observed state ideally should fall within the ensemble spread. Although standard for atmospheric general circulation models (AGCMs), ensemble simulations are less common for CCMs and, to our knowledge, have not yet been systematically used for addressing ENSO effects. We compare our results with observations as well as with existing large-ensemble simulations performed with an AGCM. The latter comparison serves as a test for the robustness of the modelled tropospheric signal, which is a prerequisite for analysing the stratospheric signal.

Before models can be analyzed with respect to inter-event variability or combinations of influences, they should be able to reproduce a standard ENSO cycle. For our study we therefore chose an ENSO cycle that follows the “canonical” case with respect to the observed circulation anomalies in the Pacific-North American and North-Atlantic European sectors and the stratosphere. However, the “canonical” case is primarily a statistical construct and rarely occurs in nature. With respect to the ENSO signal in the stratosphere (but also at the Earth’s surface), volcanic eruptions as well as the QBO have a modulating effect. The same might be true for anthropogenic influences, most importantly ozone depletion. Nevertheless, a close to “canonical” ENSO cycle occurred 1986-1989, which comprises an average El Niño in the winter 1986/87 and a relatively pronounced La Niña in the winter 1988/89. The cycle was not coincident with volcanic eruptions, the two opposite ENSO events both occurred during easterly phases of the QBO, and greenhouse gas concentrations, aerosol loadings, and stratospheric chlorine loading were not very different for the two events. Note, however, that solar irradiance was different for the two cases, 1986/87 being close to a minimum, 1988/89 close to a maximum of the sunspot cycle.

One or both events have been studied by many others using oceanographic and atmospheric data (e.g., *Kousky and Leetma*, 1989; *Mc Phaden, et al.*, 1990; *Miller, et al.*, 1988) and models (e.g., *Hoerling, et al.*, 1992; *Hoerling and Ting*, 1994; *Sardeshmukh, et al.*, 2000). Climate effects in Europe have also been addressed (e.g., *Compo, et al.*, 2001; *Fraedrich*, 1994; *Mathieu, et al.*, 2004; *Palmer and Anderson*, 1993; *Sardeshmukh, et al.*, 2000). The latter studies have demonstrated that atmospheric circulation over the North Atlantic-European sector during this ENSO cycle was in relatively good agreement with the “canonical” ENSO effects found in other studies (e.g., *Brönnimann, et al.*, 2004; *Fraedrich and Muller*, 1992; *Merkel and Latif*, 2002). Hence, this ENSO cycle provides a good opportunity to assess the ability of current models to reproduce the ENSO effects and in addition helps to better understand the observed dynamical and chemical effects in the polar stratosphere.

The paper is organised as follows. Section 2 describes the observational data sets used and the set-up of the model experiments. In Sections 3.1 and 3.2 we analyse the results for the

troposphere and for the stratosphere, respectively. Discussion and conclusions are presented in Sections 4 and 5, respectively.

A.2 Observational data and model description

The main tool for our analysis is the CCM SOCOL (for details see *Egorova, et al., 2005a*). It combines a modified version of the AGCM MAECHAM4 (*Manzini, et al., 1997*) and the chemistry-transport model MEZON (*Egorova, et al., 2003; Rozanov, et al., 1999*). The radiation scheme is based on the ECMWF radiation code (*Fouquart and Bonnel, 1980; Morcrette, 1991*). The model was run with a horizontal resolution of T30 and 39 levels (model top at 0.01 hPa). A 26-year long (1975-2000) transient simulation (*Rozanov, et al., 2005*) was used as climatology (termed S0, note that no detrending was performed on this simulation). The solar forcing was taken from (*Lean, 2000*). For each of the two winters an ensemble of 11 simulations was performed (S1). A second ensemble of 11 simulations per winter (S2) was later performed with an updated version of the model, which allows addressing the robustness of the results with respect to changes in the model stratosphere. These include a different aerosol forcing (SPARC stratospheric aerosol data (*Thomason and Peter, 2006*) instead of NASA-GISS data (*Sato, et al., 1993*)) and a nudging of the QBO (*Giorgetta, 1996*). A known problem of SOCOL concerns artificial stratospheric total chlorine loss in October over the southern high-latitudes caused by the mass-fixing procedure of the applied semi-lagrangian transport scheme (*Eyring, et al., 2006*). The problem mostly affects ozone hole chemistry. It is much less important for the analysis presented here because the focus is on ozone in the Northern Hemisphere and because we do not specifically address the effects of heterogeneous chemistry.

All simulations were started from S0 in August 1986 and 1989, respectively (in the case of S1), or in January 1986 and 1989, respectively (S2, in order to allow another seven months of spin-up with the modified model). Initial conditions for the ensemble members were obtained by perturbing global CO₂ concentration within 0.01% for one month (August 1986 and 1989, respectively). The final simulations were then performed from September to March in each winter. Meteorological variables were stored at 12-hour intervals and chemical variables as monthly means (S1, based on the original 2-hourly data) or at 12-hour intervals (S2).

In the context of this paper, S1 and S2 are considered as multi-set-up experiments. Even though the ensemble means were generally very similar, there are some differences in the stratosphere that preclude us from combining the runs into one large sample.

As discussed in the introduction, our focus on stratosphere-troposphere coupling requires that the tropospheric signal is well captured. In order to test whether a standard GCM reproduces the main features of the tropospheric response in the chosen cases, we compared our simulations to existing runs performed with the AGCM MRF9. Apart from the fact that MRF9 does not include chemistry, there are also other differences to SOCOL.

MRF9 was run at a higher horizontal resolution than SOCOL, but with fewer levels in the vertical.

A detailed description of the MRF9 model may be found in *Kumar et al.* (1996) and references therein. The simulations are described in more detail in *Sardeshmukh et al.* (2000) and *Compo et al.* (2001). The model was run at a T40 horizontal resolution with 18 sigma levels. The model top was at 50 hPa, which imposes important constraints when analysing the stratosphere. As climatology we used a set of 90 runs performed with climatological SSTs (M0). For each of the two winters, a total of 180 simulations were performed. Apart from the initial conditions, also the starting month varied. We chose sets of 45 simulations per winter that started on 1 November and were performed through March (M1). Similar ensembles starting on 1 December or 1 January gave almost the same results, but are not further described in the following. All simulations were detrended with respect to the initial fields (see *Compo, et al.*, 2001; *Sardeshmukh, et al.*, 2000). Note, however, that the trend is the same for each set and hence subtracts out when analysing El Niño-La Niña differences. Table 6.1 gives an overview of the model experiments.

Table 6.1 Overview of the model experiments

Run	SSTs	Description	Resolution/top (hPa)	No.
M0	Climatological Nov-Mar	MRF9 reference	T40L18/50	90
M1	Nov-Mar 1986/87 and 1988/89	MRF9 ENSO	T40L18/50	2x45
S0	Transient (1975-2000)	SOCOL reference	T30L39/0.01	1
S1	Sep-Mar 1986/87 and 1988/89	SOCOL ENSO	T30L39/0.01	2x11
S2	Sep-Mar 1986/87 and 1988/89	SOCOL ENSO (modified model)	T30L39/0.01	2x11

In order to address the circulation of the troposphere and stratosphere we used ERA40 reanalysis data (*Uppala, et al.*, 2005), which are somewhat incorrectly referred to as observations in the following (we performed all comparisons also with NCEP/NCAR reanalysis data (*Kistler, et al.*, 2001), but refer to these comparisons only occasionally). For precipitation we used the Global Precipitation Climatology Project (GPCP) Version 2 data (*Adler, et al.*, 2003). The signal in stratospheric ozone was analyzed in TOMS Version 8 total ozone data (Nimbus-7) and SAGE II (Version 6.2) ozone profiles. In addition, we also used the CATO assimilated ozone data (*Brunner, et al.*, 2006a) on an equivalent latitude coordinate system, which allows focusing on changes in the diabatic mean circulation and chemical effects. The overlapping period of all data sets, i.e., 1979-2002 (no detrending was performed), was used as a reference period.

Results from the two models and observations are compared mostly with respect to late-winter (January to March) averages, when a consistent signal is expected over the North Atlantic and in the lower stratosphere (e.g., *Gouirand and Moron*, 2003; *Manzini, et al.*, 2006; *Sassi, et al.*, 2004; *Van Loon and Labitzke*, 1987). Note that the expected signal is different, in fact opposite in many respects, in November and December (e.g., *Manzini, et al.*, 2006; *Mariotti, et al.*, 2002; *Moron and Plaut*, 2003). In order to correctly interpret the

stratospheric signal, it is important that the tropospheric signal is reproduced correctly. Hence, we first analyzed 1000 hPa temperature and geopotential height (GPH) as well as precipitation. In order to address the stratospheric signal we analyzed temperature, zonal wind, GPH, ozone, the components and divergence of the Eliassen Palm (EP) flux as well as the meridional mass streamfunction based on Transformed Eulerian Mean residual winds (*Andrews, et al.*, 1987).

A.3 Results

A.3.1 The troposphere

Figure A.1 displays observed anomalies of temperature and GPH at 1000 hPa as well as precipitation for January to March 1987 and 1989. The two winters exhibit the well known ENSO imprint in the North Pacific area such as a strong (weak) Aleutian low for El Niño (La Niña), accompanied by high (low) temperatures in Alaska. Temperature anomalies in northeastern Europe were strongly negative for the El Niño winter and positive for the La Niña winter. The 1000 hPa GPH field shows a pronounced negative (positive) NAO pattern in the two winters. This is in excellent agreement with the “canonical” effect of ENSO on Europe in late winter. The El Niño winter also resembles the strong 1940-1942 case (*Brönnimann, et al.*, 2004). A strong precipitation signal is found especially for the La Niña winter, with negative anomalies throughout the Mediterranean area and positive anomalies in northwestern Europe. The El Niño case shows anomalies of opposite sign, but slightly weaker in amplitude. In general, the results show a close to symmetric response for these two winters with respect to most of the features, and they again suggest that 1986-1989 was a “classical” ENSO cycle with respect to its effect on the circulation over the North Atlantic-European sector.

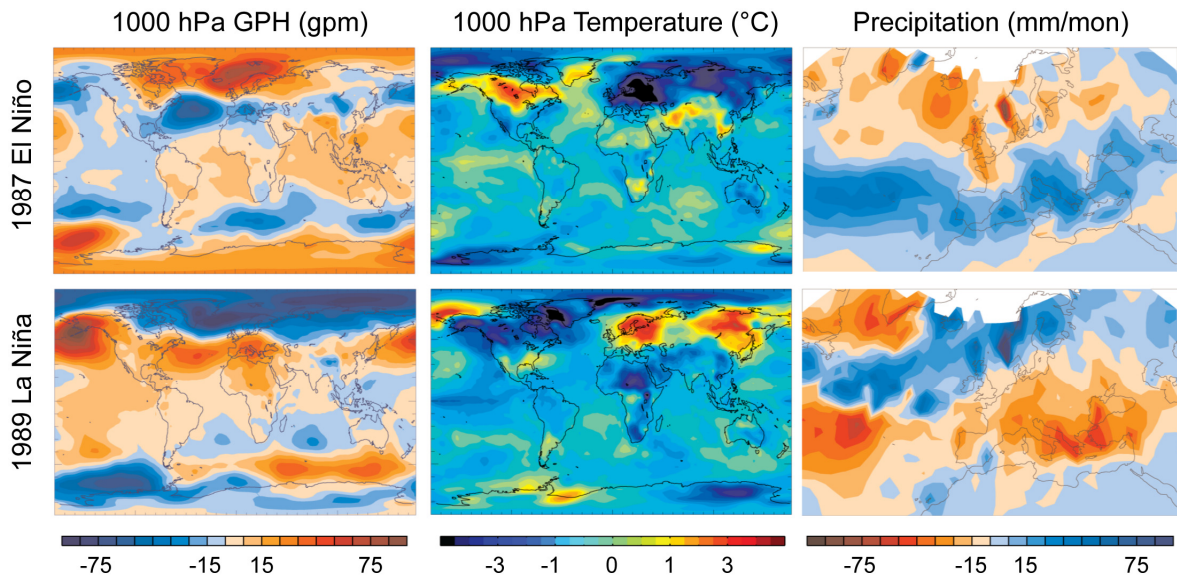


Figure A.1 Observed anomalies of 1000 hPa geopotential height (left) and air temperature (middle) as well as precipitation (right) for January to March 1987 (top) and January to March 1989 (bottom) with respect to the 1979-2002 period.

Comparisons between simulations and observations for the two individual winters are not possible in a strict sense (and therefore not shown here) because of the different climatologies used. Nevertheless, it is interesting to note that similar to the observations, both models show a response that is close to symmetric around the respective climatology in the two winters. Model results (ensemble means) are compared to the observations in Figure A.2 in the form of the difference between the El Niño winter (1987) and the La Niña winter (1989). The amplitudes of the anomalies are generally smaller in the ensemble means than in the observations, which is expected due to averaging. The patterns, however, are relatively well reproduced by both models. For El Niño minus La Niña, all experiments show cold winters in northeastern Europe, stretching all across northern Eurasia, and a dipole pattern in 1000 hPa GPH resembling the negative mode of the NAO (see *Compo et al.* (2001), for a discussion of related changes in subseasonal variability). In the SOCOL experiments as well as in the observations (but not in M1) the anomaly centres lie close to Iceland and the Azores.

For precipitation (Figure A.2), all experiments reproduce the observed decrease in Norway and the increase in the Mediterranean area. The precipitation signal over the Atlantic reflects a southward shift in the Atlantic storm track for El Niño relative to La Niña, which was also shown by *Compo and Sardeshmukh* (2004). As for the other fields, the magnitudes of the precipitation anomalies is underestimated. Nevertheless, in all three fields (temperature, GPH, and precipitation) the main differences between El Niño and La Niña found in the observations are also statistically significant (t-test, $p < 0.05$) in the model experiments.

Several features, on the other hand, are not well reproduced in the SOCOL model. This concerns in particular surface air temperature over the sea ice north of Alaska (also in

MRF9). Also, the warming signal for El Niño minus La Niña stretching from Sudan to the Middle East is not well reproduced (again by both models).

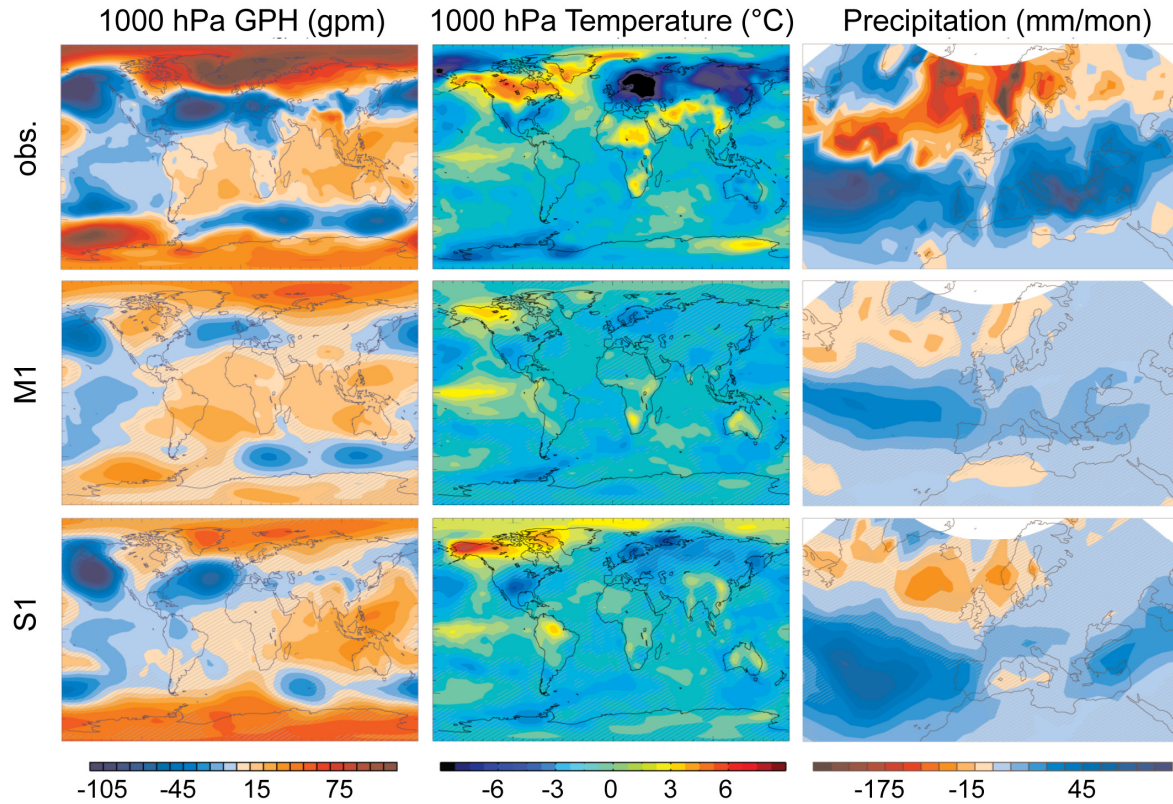


Figure A.2 Difference between January to March 1987 (El Niño) and January to March 1989 (La Niña) in 1000 hPa geopotential height (left) and air temperature (middle) as well as precipitation in the observations (top), M1 ensemble mean (middle), and S2 ensemble mean (bottom). Hatched areas are not significantly different from zero (t -test, $p < 0.05$).

In addition to the significance of the ensemble mean differences, it is advisable also to look at the distribution functions (see also *Melo-Goncalves, et al., 2005*). Figure A.3 shows histograms of temperatures at a grid point near Dalarna, Sweden ($60^\circ \text{ N}/15^\circ \text{ E}$), which is close to the location of the maximum 1000 hPa temperature difference in the observations. Note, however, that the grid point is close to the Baltic Sea, where SSTs were prescribed. We therefore include a second location near Moscow, Russia (55.8° N , 37.6° E). In order to obtain a larger sample we merged S1 and S2, which show a similar mean response, into one figure (but with different hatchings). First of all, it becomes obvious that the models differ both with respect to absolute values as well as variability. The surface temperature is lower in SOCOL compared to MRF9. On the other hand, the variability is higher in SOCOL than in MRF9. The low variability in M1 for the grid point near Dalarna is most likely due to the proximity of the ocean, but also for Moscow the variability is smaller in M1 than in S1/S2. The observed temperatures are indicated as coloured lines. Here we use both ERA40 and NCEP/NCAR reanalysis data. They are outside the ensemble spread in many of the comparisons. While the models reproduce the sign of the difference between

the two winters, they clearly underestimate the magnitude. However, it should be noted that the two observation-based data sets (i.e., two depictions of the same “realisation”) also show quite substantial differences (up to 2.5 °C) and that the observed magnitude amounts to 10 °C. This is extreme for a 3-month average. In fact, long temperature records from nearby stations sites (not shown) indicate that the two winters were both close to the record minima and maxima, respectively.

With respect to the interpretation of ensemble means, it is clear that the modelled temperature signal shown in Figure A.3 does not arise from a few outliers, nor does it mask a bimodal behavior.

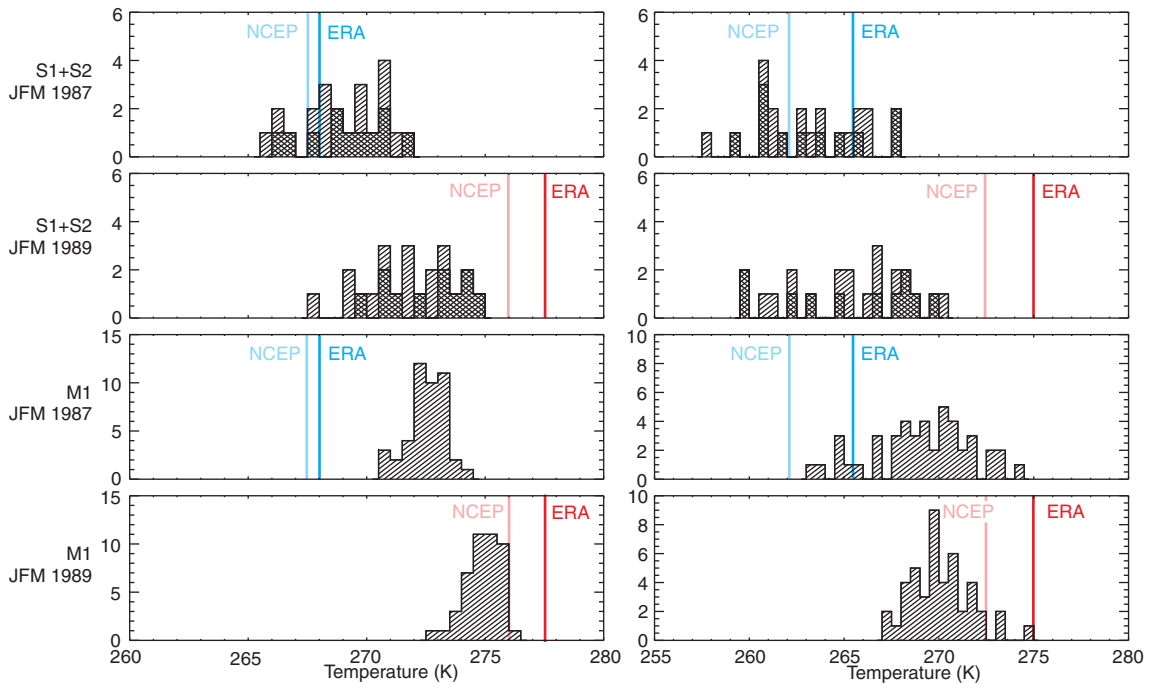


Figure A.3 Histograms of 1000 hPa temperature near Dalarna (Sweden, left) and Moscow (Russia, right), averaged from January to March, for S1 and S2 (cross hatched) and M1 for 1987 (El Niño) and 1989 (La Niña). The blue and red lines give the corresponding values from ERA40 and NCEP/NCAR reanalysis.

A.3.2 Stratospheric dynamics and chemistry

In the following, we focus on the stratospheric dynamics and chemistry. Figure A.4 shows difference fields for GPH and temperature at 100 hPa. For the El Niño case, temperatures were lower and GPH higher above the eastern tropical Pacific than for the La Niña case (see also *Claud, et al.*, 1999). At mid-latitudes, a clear wave structure is visible in the 100 hPa GPH field, with its main anomaly centres in the North Pacific and central Europe. Temperatures were high over northern Eurasia, but low over the North Atlantic, similar as in the case of the 1940-1942 El Niño (*Brönnimann, et al.*, 2004). The main feature at high latitudes is a weak and meridionally expanded polar vortex, which is consistent with statistical analyses (*Van Loon and Labitzke*, 1987) and model studies (*Manzini, et al.*,

2006; *Sassi, et al.*, 2004) and again similar to the 1940-1942 case (*Brönnimann, et al.*, 2004). In line with a weak polar vortex and again in agreement with the above mentioned studies, ERA40 temperatures were much higher in 1987 compared to 1989 over much of the Arctic. This is in part due to a major warming in January 1987.

The models reproduce the patterns in tropical temperature and GPH anomalies fairly well. MRF9 underestimates the magnitudes in both fields, whereas SOCOL slightly overestimates the GPH response. Both models also show a similar wave-structure as the observations in temperature and GPH over the North American-Pacific sector. Further downstream, over the North Atlantic, the wave-pattern is shifted westward in the models compared with the observations. The cooling over the North Atlantic is pronounced and significant in M1 and S2. In the high Arctic, however, the observed temperature signal is not well reproduced in the ensemble means. No significant effect is found except over eastern Siberia. The weak polar vortex at 100 hPa GPH is better reproduced, with a statistically significant signal in all ensemble sets. However, the magnitude is again smaller than in the observations, especially in M1. The fact that even MRF9 with a low model top shows a significantly weaker polar vortex confirms that this is a very robust part of the stratospheric ENSO signal.

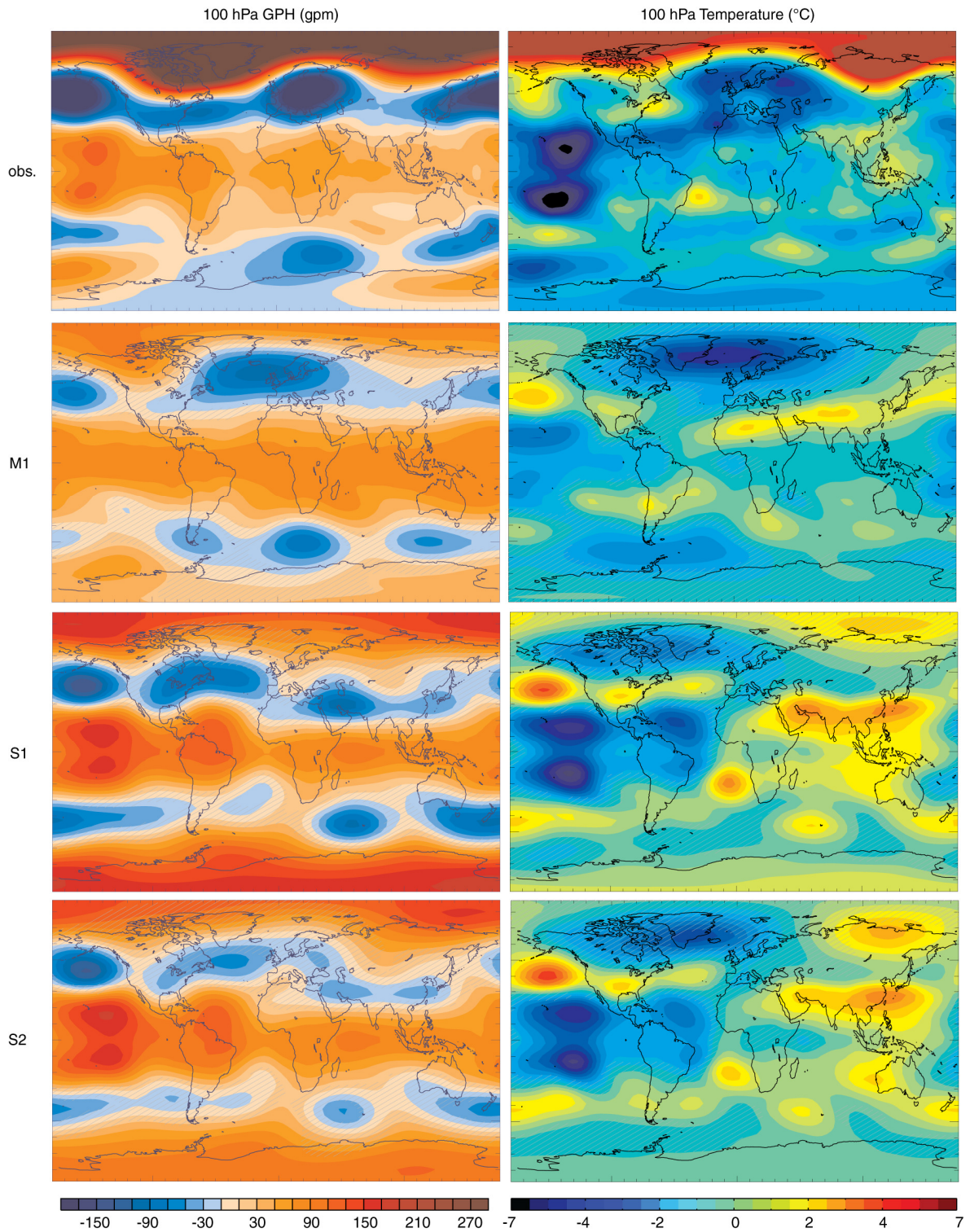


Figure A.4 Difference between 1987 and 1989 in GPH (left) and temperature (right) at 100 hPa, averaged from January to March, in ERA40, M1, S1, and S2. Hatched areas are not significantly different from zero (t-test, $p < 0.05$).

In the following we focus more closely on stratospheric dynamics. This was done only for the SOCOL model, but not for MRF9, which due to its low model top is not expected to

realistically reproduce processes related to wave-mean flow interaction in the middle stratosphere. In order to assess whether the propagation of quasi-steady wave-like structures into the stratosphere is correctly reproduced, we analyzed the longitudinal variation of GPH at 50° N at 100 and 30 hPa for each individual run and compared it to ERA40 data. The observations show clear differences between the two cases, with a wave number one pattern dominating in the El Niño case and a wave number two pattern in the La Niña case, most pronounced at 30 hPa. In the model, GPH is underestimated at 100 hPa but overestimated at 30 hPa. The former could be due to a somewhat too large polar vortex whereas the latter could be affected by the vertical interpolation (the nearest model levels are 25.12 hPa and 39.81 hPa). The wave structure during the El Niño case is very well reproduced by S1 and S2 both in terms of amplitude and position, particularly at 100 hPa. A clear dominance of wave number one is found. Discrepancies arise, however, for the La Niña case. At 100 hPa, a pronounced feature in the observations is the absence of the trough over western Russia. Both S1 and S2 reproduce a trough in the majority of the runs, though weaker (more so in S1 than S2) than for the El Niño case. In addition, the wave over the Atlantic-European sector is shifted westward in the model and the observed westward shift of the ridge over the Rocky Mountains is not similarly reproduced. In contrast to the observations, wave number one is dominating (but in agreement with observations, wave number four is strongly reduced compared to the El Niño case). At the 30 hPa level, both S1 and S2 fail to reproduce the planetary wave structure during La Niña and the difference between El Niño and La Niña vanishes.

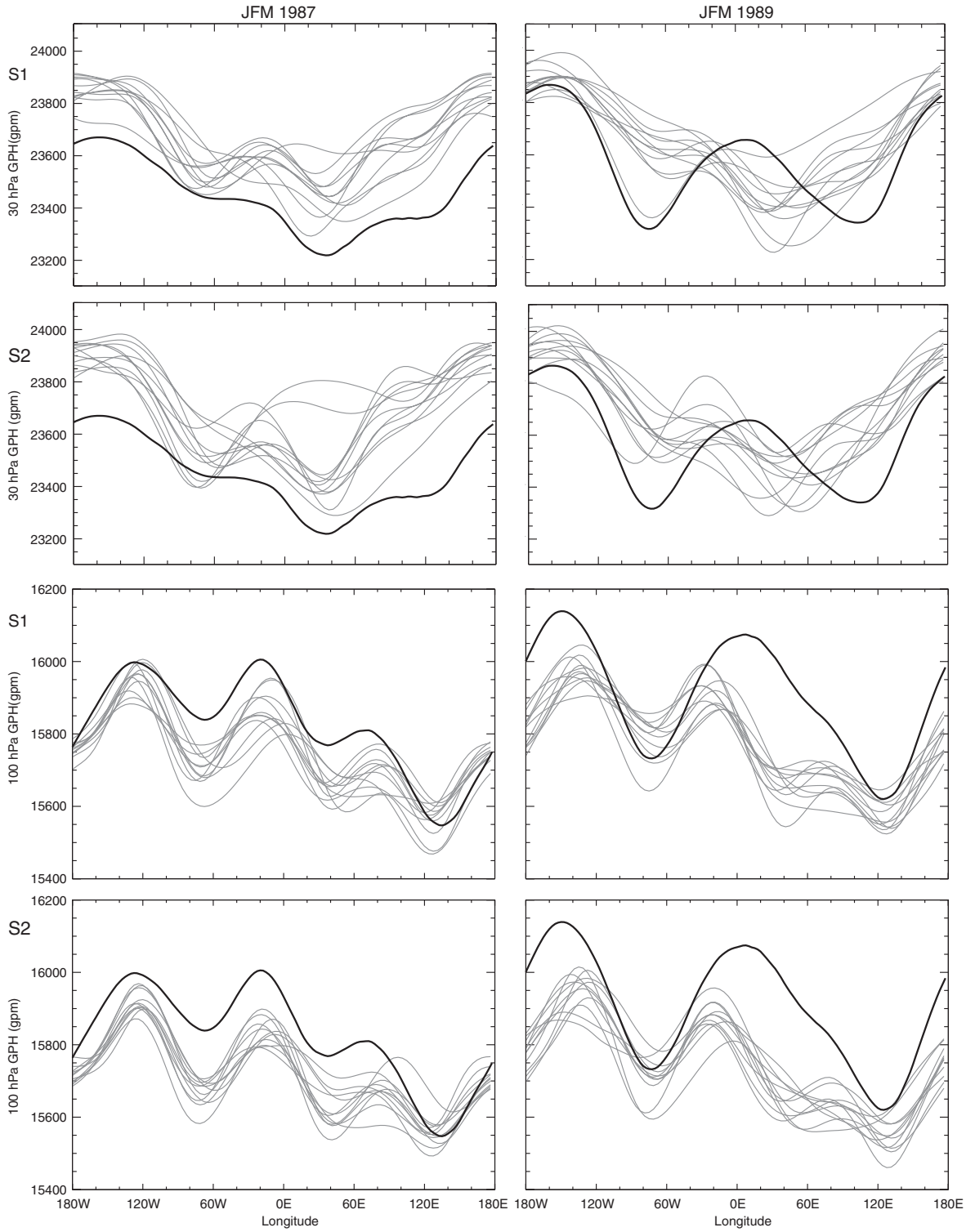


Figure A.5 Longitudinal variation of 30 hPa and 100 hPa GPH at 50° N in S1 and S2 averaged from January to March 1987 (left) and 1989 (right). The thick lines indicate ERA40 data.

Figure A.6 and Figure A.7 show zonal mean zonal wind and temperature as a function of latitude and altitude. In addition to the differences between 1987 and 1989, their mean value is also shown for S1 for the comparison of absolute values (S1 and S2 are almost

identical with respect to the mean value). SOCOL reproduces the structure as well as the magnitude of the zonal wind fairly well at all levels from the surface up to the middle stratosphere. The structure of the zonal mean temperature (Figure A.7) is also well reproduced, but absolute values are too low in the tropopause region and in the polar vortex. The differences between El Niño and La Niña agree well with the observations in a qualitative sense. In the zonal winds (Figure A.6) both simulations (S1 and S2) show a stronger subtropical jet and a weakened polar vortex (more so in S1 than S2), which is very similar to the ENSO signal found in statistical analyses of reanalysis data (e.g., *Chen, et al.*, 2003). Note that the subtropical jet is displaced southward in the models during El Niño compared with La Niña, but not in the observations. The magnitudes of the anomalies also agree well in the troposphere, but in the stratosphere they are clearly too small in both simulations, especially in the middle stratosphere. Significance is limited to the lowermost stratosphere and troposphere. Note that the tropical stratosphere is affected by the QBO nudging in S2. Clearly, easterly wind anomalies at the equator are stronger (more similar as in the observations) in S2 compared to S1. No obvious effects of the QBO nudging are seen in the subtropical jet and the polar vortex.

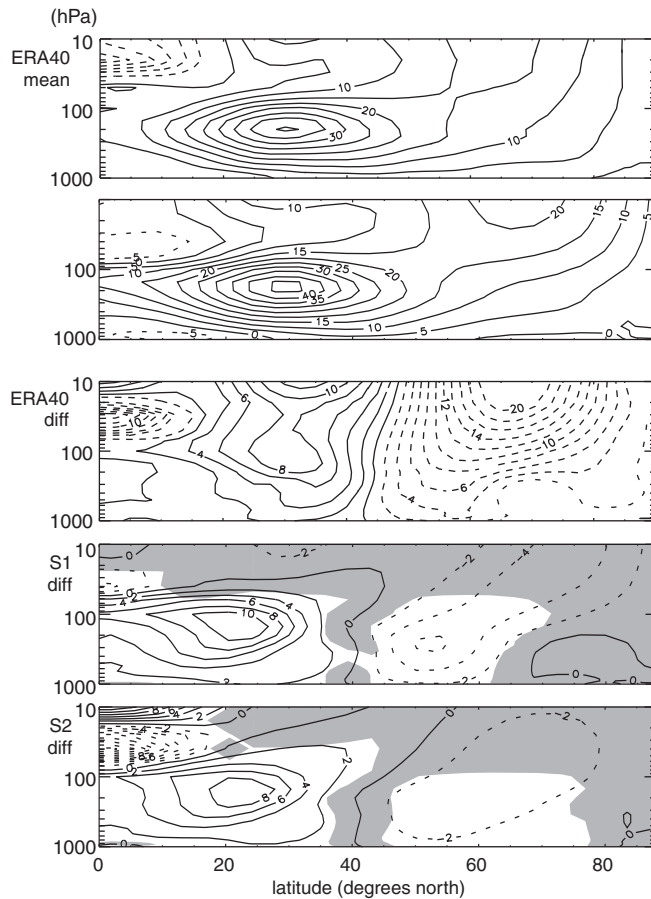


Figure A.6 Mean value and difference between 1987 and 1989 in zonal mean zonal wind (m/s), averaged from January to March, in ERA40, S1, and S2. Shaded areas are not significantly different from zero (t-test, $p < 0.05$).

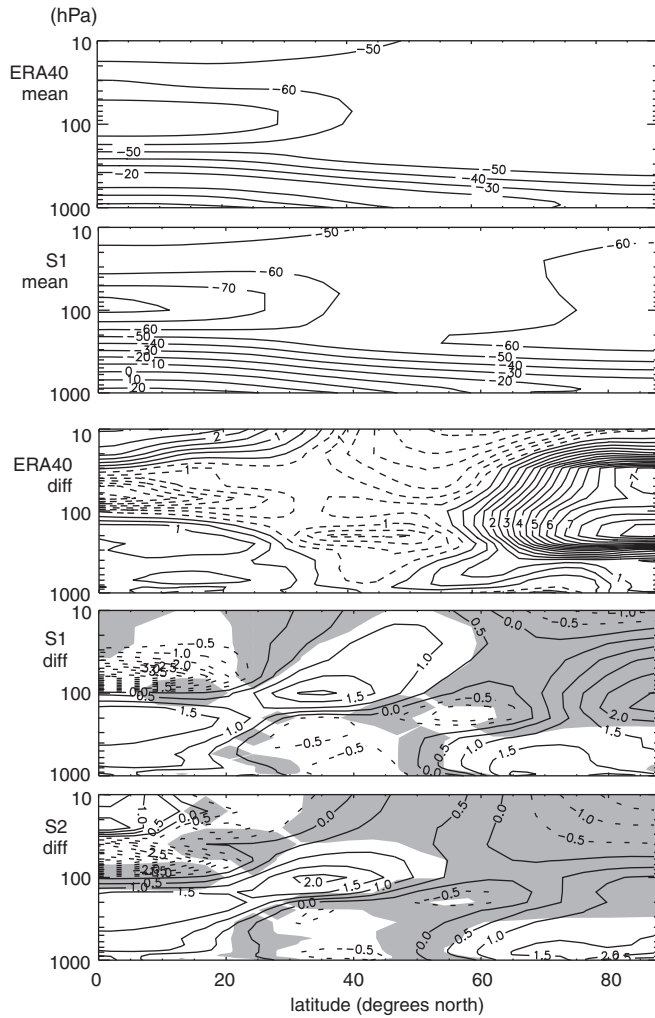


Figure A.7 Mean value and difference between 1987 and 1989 in zonal mean temperature ($^{\circ}\text{C}$), averaged from January to March, in ERA40, S1, and S2. Shaded areas are not significantly different from zero (t -test, $p < 0.05$).

Another factor that needs to be considered is solar irradiance, which was higher in 1989 than in 1987. According to observation-based studies (Labitzke, *et al.*, 2006) one would expect a stronger northern vortex in 1989 because both events occurred during the easterly QBO phase (however, the effect for the easterly QBO phase is smaller and less certain than for the westerly phase). Steady-state SOCOL simulations without QBO (and hence stratospheric easterlies) found a stronger northern stratospheric polar vortex for solar maximum conditions compared to solar minimum conditions (Egorova, *et al.*, 2004), but the signal is not statistically significant and clearly smaller (around 1 m/s) than that in our simulations. Hence, solar irradiance changes do not seem to be sufficient to explain the signal.

Zonal mean temperature differences between El Niño and La Niña are shown in Figure A.7. The observations show a pronounced signal in the Arctic lower stratosphere. In S1, the pattern is well reproduced, but not its strength, whereas in S2 the pattern is less well reproduced. The Arctic temperature response in the model is significant below 200 hPa. At

higher levels, within-ensemble variability is too large for obtaining significant results. Both S1 and S2 show a significant warming of the subtropical tropopause and lower stratosphere which is not seen in the observations. This is probably related to the southward displacement of the subtropical jet in the model (Figure A.6) that is not seen in the observations.

In order to understand the modelled Arctic temperature response in the stratosphere, we analyzed 12-hourly series of temperature at the North Pole (3.8° E, 87.2° N in SOCOL) at 10 hPa and 100 hPa in the individual ensemble members as well as in ERA40 (Figure A.8). The reanalysis data for 1986/87 show a strong disturbance (major midwinter warming) in January. While at 10 hPa, temperatures dropped again during February and reached very low values in March, the disturbance at 100 hPa persisted into spring. In 1988/89, in contrast, the polar stratosphere was undisturbed and cold well into February, but the final warming then was very pronounced. In the SOCOL experiments major warmings appear in most of the simulations in both winters, sometimes already in late November or December. The large day-to-day variability causes a large within-ensemble variability, which hampers the statistical analysis of ensemble means.

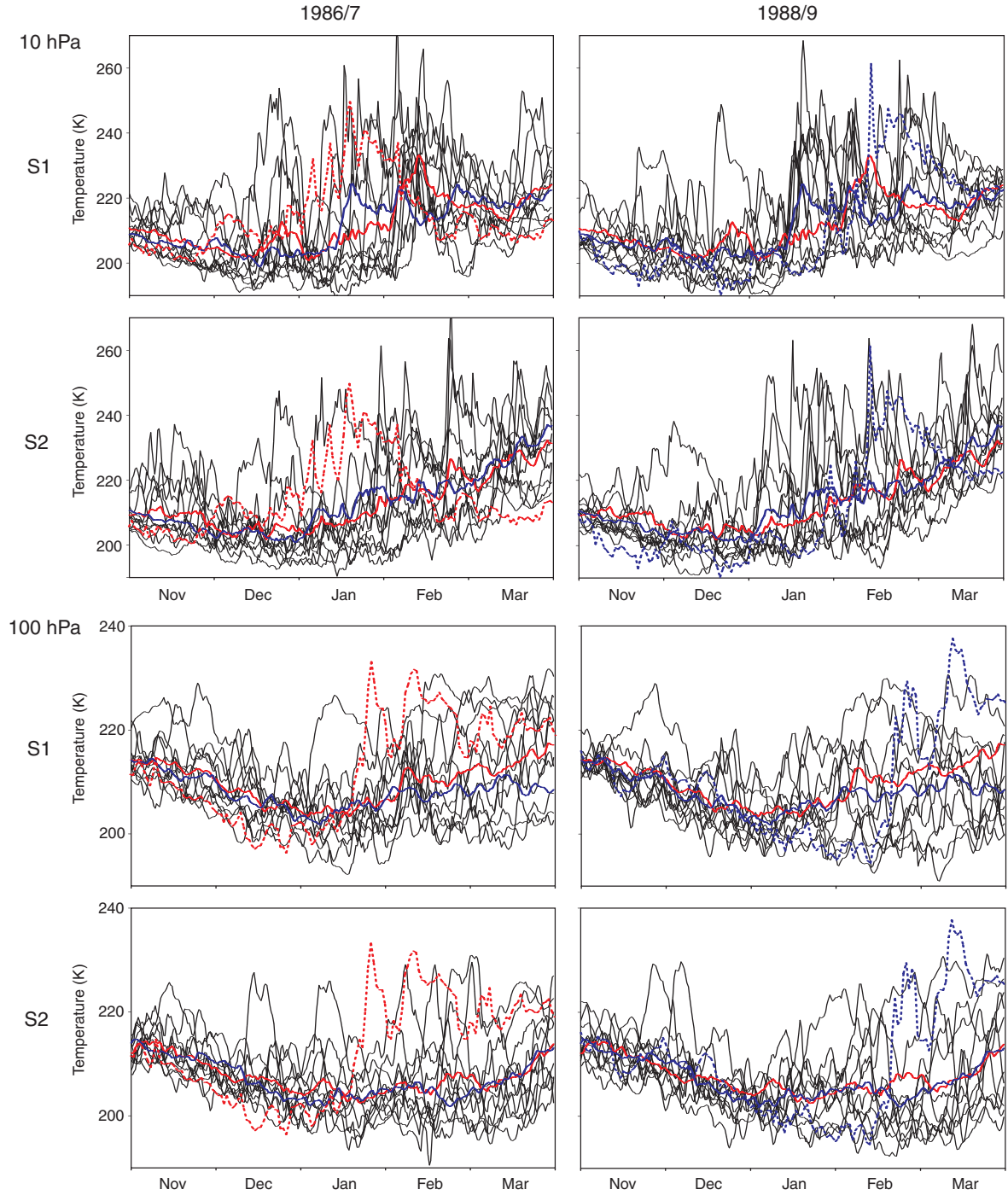


Figure A.8 12-hourly temperature at 10 hPa (top four panels) and 100 hPa (bottom four panels) at the North Pole from November to March in 1986/87 (left) and 1988/89 (right) for S1 and S2. The dotted lines indicate ERA40 data, the coloured lines give the ensemble means (red: 1986/87, blue: 1988/89).

In addition to zonal wind and temperature we also analyzed the EP flux as a measure of the planetary-wave driving of the stratospheric circulation. Figure A.9 shows zonal means of the upward and meridional components of the EP flux as well as its divergence, again for the mean of the two winters and their difference (note that we have averaged EP flux from

November to February, thus allowing a four-to-eight week lead with respect to the temperature, zonal wind, and ozone). For the mean values, the EP flux shows an excellent agreement with observations with respect to vertical and latitudinal structure as well as absolute values. This does not only hold for the divergence of the EP flux, but also for its vertical and meridional components. With respect to the differences between El Niño and La Niña, the observations show a negative anomaly in EP flux divergence in most of the extratropical stratosphere, which is also found in both sets of simulations. An analysis of the EP flux components implies two contributions: an increase in the vertical component as well as an increase (in the lower stratosphere) of the poleward component of the EP flux. The El Niño minus La Niña differences in the meridional component are again well reproduced by both sets of simulations (except for S1 in the upper stratosphere), while the agreement is worse for the vertical component. In all cases, however, significance is limited to the troposphere and lowermost stratosphere.

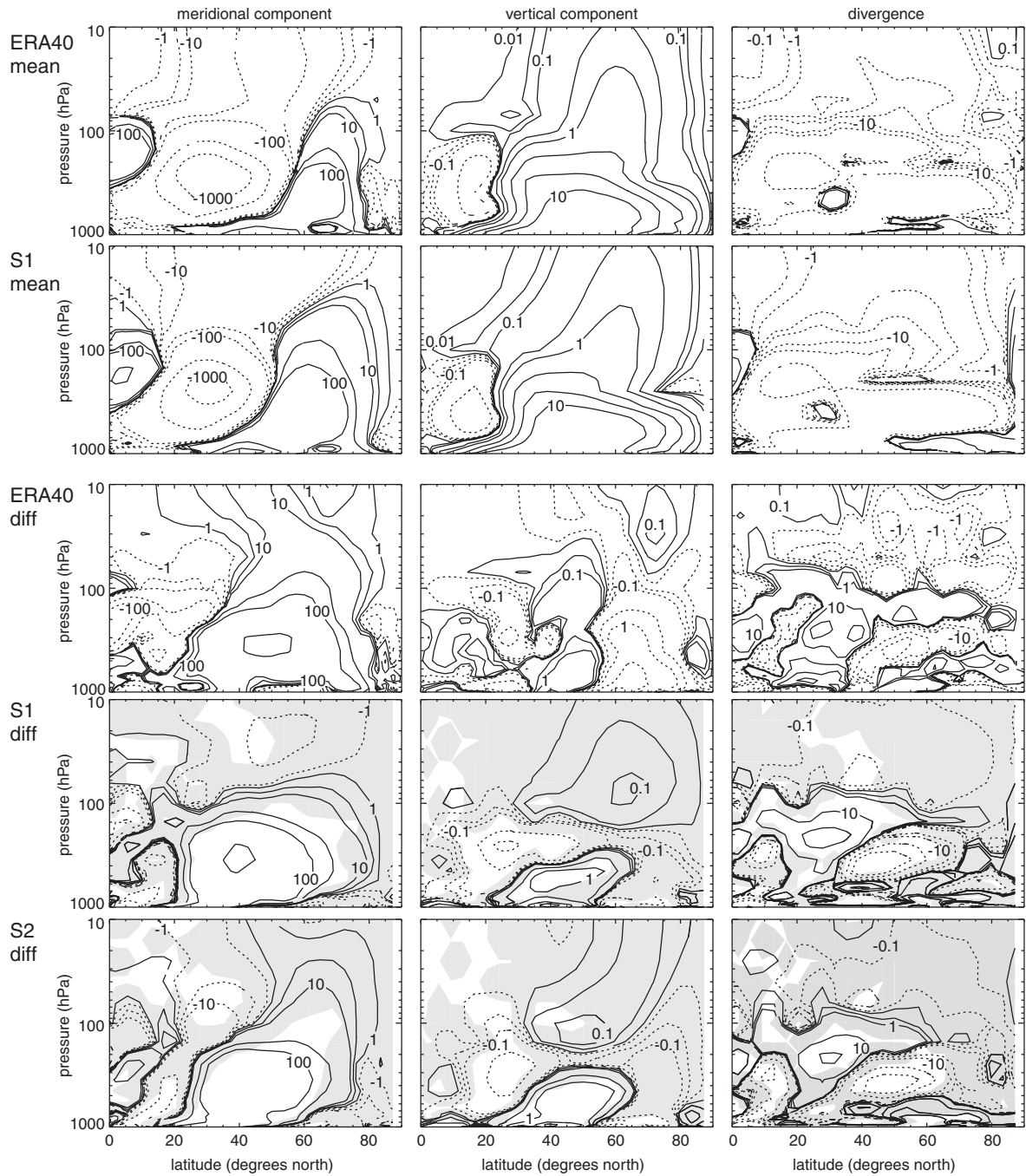


Figure A.9 Mean value and difference between El Niño and La Niña in zonal mean EP flux, averaged from November to February, in ERA40 reanalysis, S1, and S2. Left: poleward component, middle: upward component (both given as 10^5 kg s^{-2}). Right: divergence ($\text{kg m}^{-1} \text{ s}^{-2}$). Shaded areas are not significantly different from zero (t-test, $p < 0.05$).

In order to directly address the stratospheric meridional circulation, we calculated the meridional mass streamfunctions based on the Transformed Eulerian Mean residual velocities (see e.g., Butchart and Austin, 1998). The mean values and differences between El Niño and La Niña are shown in Figure A.10. The meridional mass streamfunction is very well reproduced in SOCOL on average both in terms of position and strength. The

only difference is that in SOCOL, the circulation cell reaches further southward in the middle and upper stratosphere. The differences in ERA40 show generally an enhancement and northward shift of the circulation. In the lower-to-middle stratosphere, this pattern is well reproduced by SOCOL, particularly in the S1 ensemble. Even though S2 also shows some signs of a strengthening circulation, the signal is only significant in the tropics. The signal in the middle-to-upper stratosphere is not reproduced (and is mostly insignificant in both S1 and S2).

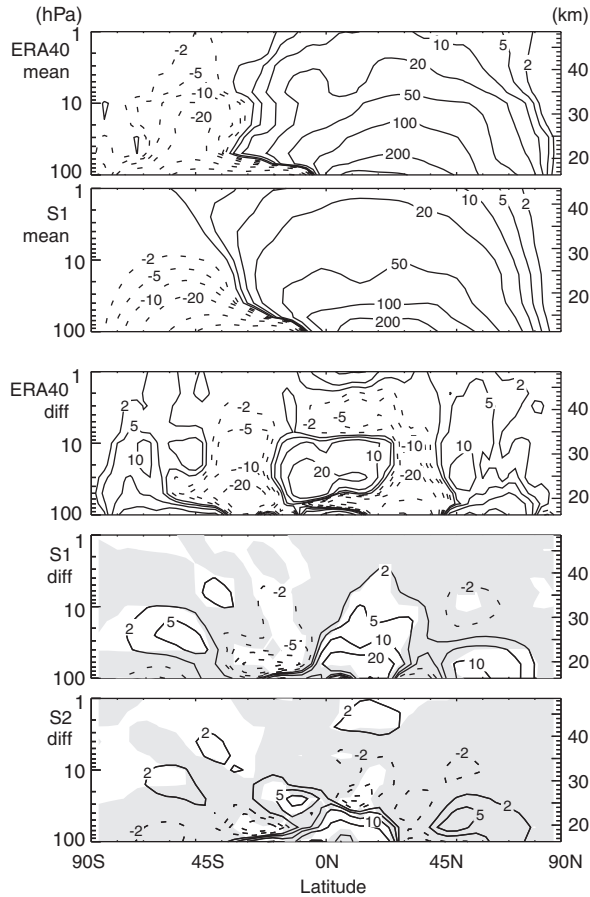


Figure A.10 Difference between El Niño and La Niña in the meridional mass streamfunction ($\text{kg s}^{-1} \text{m}^{-1}$, based on the Transformed Eulerian Mean residual velocities) averaged from November to February, in ERA40 reanalysis, S1, and S2. Shaded areas are not significantly different from zero (t -test, $p < 0.05$).

Further comparisons were performed with respect to ozone. Except for the subtropical middle stratosphere, ozone concentrations are higher in S1 than in S2 (not shown) because of the differences in the model set-up. No such difference, however, is apparent when analysing El Niño minus La Niña. For both S1 and S2 the simulated total ozone difference (January-to-March average, Figure A.11) shows a very good agreement with TOMS observations with respect to the main structure in the tropics and mid-latitudes. Total ozone was reduced over the tropics, especially the tropical Pacific, but enhanced over the mid-latitudes with a pronounced imprint of the planetary wave structure. These main features

are also significant in the model simulations, though underestimated in the ensemble mean. A similar tropical ENSO pattern was also found in other analyses of TOMS data and chemical climate models (e.g., *Steinbrecht, et al.*, 2006). Over the polar region (where no TOMS data are available) S1 shows an increase and S2 a decrease in total ozone, but neither is significant.

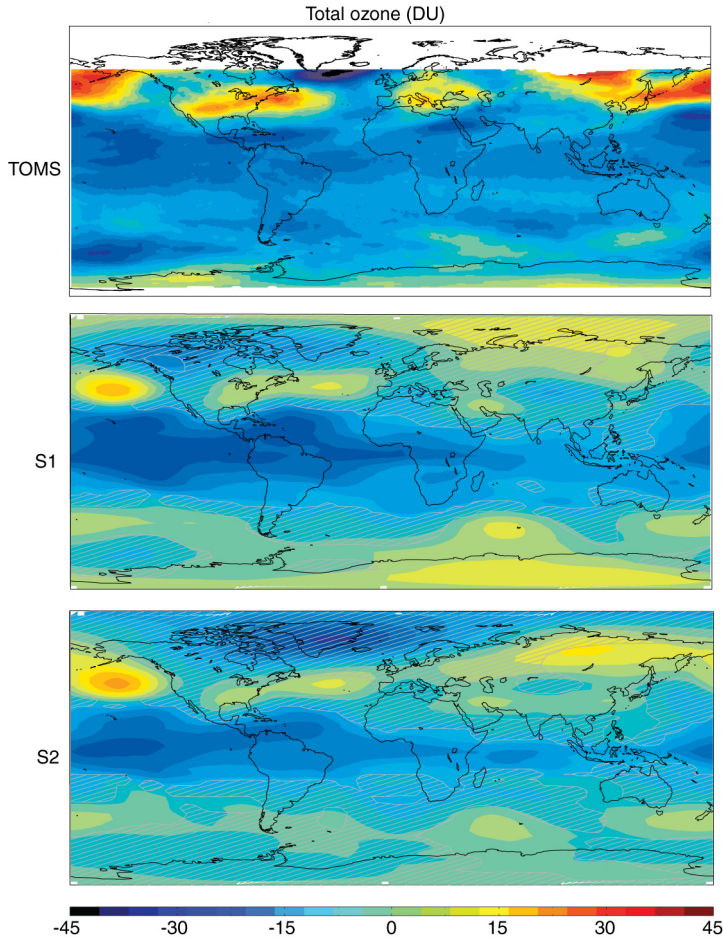


Figure A.11 Difference between 1987 and 1989 in total ozone, averaged from January to March, in TOMS Version 8 data, S1, and S2. Hatched areas are not significantly different from zero (*t*-test, $p < 0.05$).

We also analyzed the zonal mean vertical distribution of ozone in the SOCOL model and compared it to SAGE II data (Figure A.12, left). Prominent features in the observations are high concentrations in the midlatitude lower stratosphere and the subtropical upper stratosphere and low ozone concentrations in the tropical middle stratosphere. Both S1 and S2 also show an ozone decrease in the tropical stratosphere. The midlatitude signal is well reproduced both with respect to altitude and magnitude of the signal. These anomalies are all statistically significant in the ensemble means. However, the ozone increase in the subtropical upper stratosphere is not reproduced.

In order to obtain a better picture of the ozone anomalies at middle and high latitudes we plotted ozone differences as a function of equivalent latitudes (Figure A.12, right). This allows focusing on the effects of chemistry and of the meridional circulation by removing the planetary wave imprint. CATO was used as the corresponding observational data set. The transformation to the equivalent latitude coordinates was only possible for S2, which, as discussed above, fits worse with the observations in the stratosphere than S1. The most pronounced feature is the ozone increase poleward of 65° equivalent latitude (which is not reproduced by S2), providing clear evidence for a strong ozone increase in the Arctic lower stratosphere. Outside the Arctic the agreement between S2 and CATO is good. Interestingly, the positive ozone anomaly in the subtropical middle stratosphere found in SAGEII and CATO appears also in S2 after the transformation to equivalent latitude coordinates.

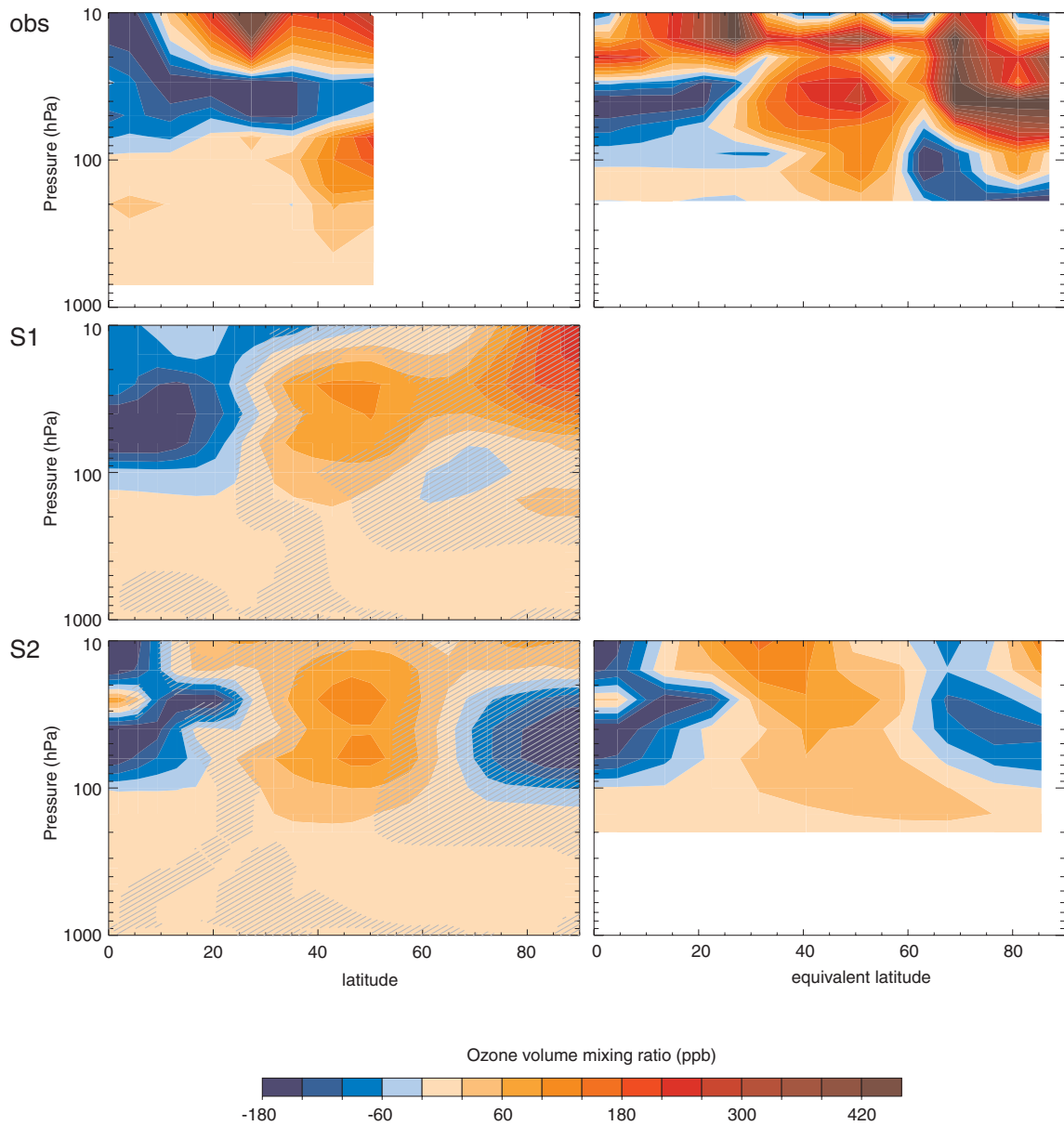


Figure A.12 Difference between 1987 and 1989 in zonal mean ozone mixing ratio as a function of latitude and altitude, averaged from January to March, in observations (SAGE II and CATO), S1, and S2. Left: geographical latitudes, right: equivalent latitudes. Hatched areas are not significantly different from zero (t -test, $p < 0.05$).

A.4 Discussion

At the Earth's surface, SOCOL reproduced the main anomalies of the two winters 1987 and 1989 relatively well with respect to most analyzed features, even though the magnitudes of the anomalies are underestimated. Most importantly, both analyzed models reproduced the changes in the circulation over the Pacific-North American and North Atlantic-European sectors, i.e., a strengthened Aleutian low and weakened Icelandic low, which is important with respect to the stratospheric signal (Brönnimann, *et al.*, 2004). The

model results are in good agreement with studies performed with other models (e.g., *Mathieu, et al.*, 2004). Note that the results do not imply a causal relationship between the extratropical anomalies and ENSO, as SST fields were prescribed globally. For the same reasons, care should be taken when drawing conclusions on predictability (see *van Oldenborgh*, 2005). What would be necessary to address these issues are sensitivity experiments prescribing only the tropical or only the Indo-Pacific SSTs and setting the remaining SSTs to climatology (or using a mixed-layer ocean), which is beyond the scope of this paper.

However, the model simulations and comparison with observations do allow conclusions with respect to the processes behind ENSO effects on the stratosphere and stratosphere-troposphere coupling, given the consistent tropospheric ENSO response. SOCOL reproduced the observed anomalies of lower stratospheric temperature, GPH as well as total ozone in the tropics. This is the typical ENSO pattern that is directly related to the longitudinal shift of the region of intense atmospheric convection (*Hatsushika and Yamazaki*, 2001). All sets of simulations also reproduced a planetary wave imprint in the midlatitude lower stratosphere that appears in the fields of GPH, total ozone (in SOCOL), and to some extent temperature. Deficiencies have been detected in S1 and S2 in the representation of the stratospheric wave-pattern during the La Niña case.

Of special interest with respect to the polar stratosphere are the features that are supposedly caused by wave-mean flow interaction. *Brönnimann et al.* (2004) suggested that El Niño (relative to La Niña) increases the planetary wave activity propagating from the troposphere to the stratosphere (see also *Garcia-Herrera, et al.*, 2006; *Manzini, et al.*, 2006; *Sassi, et al.*, 2004). Increased upward propagating planetary wave activity, which accompanies the negative NAO mode, is expected to lead to a weak polar vortex, higher temperature of the Arctic stratosphere in spring, and more major midwinter warmings (*Taguchi and Hartmann*, 2006). At the same time, the meridional circulation is expected to be strengthened, transporting more ozone from the tropical source regions to the extra tropics, which would lead to higher ozone column at mid latitudes and especially in the polar vortex, where the descent is enhanced (see *Randel, et al.*, 2002). In addition, reduced chemical ozone depletion (because of the warmer temperatures) would further increase the Arctic ozone column (*Sassi, et al.*, 2004).

The observations are in very good agreement with this hypothesis. They not only exhibit all of the features discussed above (for El Niño minus La Niña a weak and warm polar vortex, a major midwinter warming, more ozone at mid latitudes and in the polar vortex and less ozone, in the tropics, most pronounced in the CATO data), but also show anomalous EP flux convergence in the stratosphere, which indicates strengthened planetary-wave driving. The analysis of the meridional mass streamfunction provides clear evidence for a strengthening of the Brewer-Dobson circulation, especially in the lower-to-middle stratosphere. The SOCOL model reproduces most of the features up to around 30 hPa (S1 better than S2) and hence compares reasonably well, at least qualitatively, with the observations and with other modelling studies (see e.g., *Garcia-Herrera, et al.*, 2006;

Manzini, et al., 2006; *Sassi, et al.*, 2004). However, the signal in the stratosphere, especially in the middle stratosphere and in the polar vortex, is too weak when compared with observations and some of the prominent features in the observations that are supposedly caused by ENSO are not significant in the ensemble mean.

The agreement between S1, S2, and observations is very good for the meridional component and the divergence of the EP flux, somewhat less so for the vertical component. The results imply that the observed and modelled weakening of the polar vortex during El Niño is largely due to wave-mean flow interaction (see also *Manzini, et al.*, 2006). It is interesting to note that not only the vertical component of the EP flux (and thus the amount of wave energy that reaches the stratosphere) contributes, but also the meridional component (and thus the degree to which this wave energy is refracted poleward). This is in agreement with the results of *Chen et al.* (2003) who distinguish between two modes of interannual EP flux variability: a tropospheric mode that is strongly related to the Northern Annular Mode (or NAO) and controls upward propagation of planetary wave energy as well as a stratospheric mode which is strongly related to ENSO and the Pacific North American pattern and controls the poleward refraction of wave energy. The modes are defined as a tropospheric and stratospheric dipole in the anomaly field of EP flux divergence, respectively (see *Chen, et al.*, 2003). Both dipoles also appear in the difference field of EP flux divergence in the ERA40 reanalysis and, somewhat less clear, in S1 and S2 (Figure A.9). Thus, in the “canonical” ENSO case, both patterns contribute.

With respect to ozone, all of the above results suggest a strengthening of the Brewer-Dobson circulation, which is particularly evident in the meridional mass stream function (Figure A.10). This leads to a decrease of ozone concentrations in the tropical lower stratosphere and an increase at mid latitudes and in the polar lower stratosphere (see also *Garcia-Herrera, et al.*, 2006; *Pyle, et al.*, 2005; *Sassi, et al.*, 2004). The chemical contribution at high latitudes has the same sign as the dynamical contribution, but is dependent on temperature and might therefore be underestimated by SOCOL.

The comparison between S1 and S2 shows that both agree well with each other and with observations in the tropics. S1 fits better with the observations in the Arctic stratosphere (but S2 also reproduces some of the features such as the weak polar vortex during El Niño). The differences between S1 and S2 are consistent among EP flux, zonal wind, stream function, and ozone and seem to be related to a weaker wave-driving signal in S2. However, the differences are not statistically significant and can not be attributed to changes in the model set-up, which affect absolute values more than differences between El Niño and La Niña case. Generally, significant differences between El Niño and La Niña in one ensemble set are mostly also significant in the other one. In this sense, comparing S1 and S2 suggests that results are relatively robust with respect to changes in the model set-up.

A.5 Conclusions

The main anomalies in atmospheric circulation and ozone observed during the “canonical” ENSO cycle 1986-1989 were successfully reproduced with the chemical climate model SOCOL. While deficiencies could be identified with respect to the signal in the middle to upper stratosphere and with respect to vertical wave propagation in the La Niña case, the ENSO signal in surface climate, especially the circulation over the North Atlantic-European region, as well as the imprint in the lower stratosphere agree well with observations. Comparison with GCM runs confirmed that the tropospheric response is a robust response to the SST forcing and hence we interpret the stratospheric signal in terms of a coupling to this tropospheric response. As such, the results provide insight into the mechanisms relating ENSO to stratospheric circulation changes. They suggest that both the upward and poleward components of anomalous EP flux are important for obtaining the stratospheric ENSO signal and that an increase in strength of the Brewer-Dobson circulation during El Niño is part of that signal.

A.6 Acknowledgements

SB was funded by the Swiss National Science Foundation, AF is funded by ETH Zürich (TH project CASTRO). TE was supported by Swiss National Science Foundation and COST-724. GPCP data were obtained via NOAA/CIRES-CDC. We thank Gilbert Compo and Prashant Sardeshmukh for providing the MRF9 simulations, NASA for providing TOMS and SAGE II data, and Ingo Wohltmann for providing data and support for the calculation of EP fluxes. ECMWF ERA40 data used in this study have been provided by ECMWF.

References

- Adler, R. F., et al. (2003), The version-2 global precipitation climatology project (GPCP) monthly precipitation analysis (1979-present), *J. Hydrometeor.*, *4*, 1147-1167.
- Alexander, M. A., I. Blade, M. Newman, J. R. Lanzante, N. C. Lau, and J. D. Scott (2002), The atmospheric bridge: The influence of ENSO teleconnections on air-sea interaction over the global oceans, *J. Clim.*, *15*, 2205-2231.
- Allen, R. J., and S. C. Sherwood (2008), Warming maximum in the tropical upper troposphere deduced from thermal winds, *Nature Geoscience*, *1*, doi:10.1038/ngeo1208.
- Ambaum, M. H. P., and B. J. Hoskins (2002), The NAO troposphere-stratosphere connection, *J. Clim.*, *15*, 1969-1978.
- Andrews, D. G., J. R. Holton, and C. B. Leovy (1987), *Middle Atmosphere Dynamics*, Academic Press.
- Austin, J., L. L. Hood, and B. E. Soukharev (2007), Solar cycle variations of stratospheric ozone and temperature in simulations of a coupled chemistry-climate model, *Atmos. Chem. Phys.*, *7*, 1693-1706.
- Austin, J., et al. (2003), Uncertainties and assessments of chemistry-climate models of the stratosphere, *Atmos. Chem. Phys.*, *3*, 1-27.
- Austin, J., and R. J. Wilson (2006), Ensemble simulations of the decline and recovery of stratospheric ozone, *J. Geophys. Res.*, *111*, D16314, doi:10.1029/2005JD006907.
- Baldwin, M. P., and T. J. Dunkerton (2001), Stratospheric harbingers of anomalous weather regimes, *Science*, *294*, 581-584.
- Baldwin, M. P., et al. (2001), The quasi-biennial oscillation, *Rev. Geophys.*, *39*, 179-229.
- Baldwin, M. P., D. B. Stephenson, D. W. J. Thompson, T. J. Dunkerton, A. J. Charlton, and A. O'Neill (2003), Stratospheric memory and skill of extended-range weather forecasts, *Science*, *301*, 636-640.
- Bodeker, G. E., H. Shiona, and H. Eskes (2005), Indicators of Antarctic ozone depletion, *Atmos. Chem. Phys.*, *5*, 2603-2615.
- Bourqui, M. S., C. P. Taylor, and K. P. Shine (2005), A new fast stratospheric ozone chemistry scheme in an intermediate general-circulation model. II: Application to effects of future increases in greenhouse gases, *Q. J. R. Meteorol. Soc.*, *131*, 2243-2261.
- Brönnimann, S. (2007), Impact of El Niño-Southern Oscillation on European climate, *Rev. Geophys.*, *45*, RG3003, doi:10.1029/2006RG000199.

- Brönnimann, S., J. L. Annis, C. Vogler, and P. D. Jones (2007), Reconstructing the quasi-biennial oscillation back to the early 1900s, *Geophys. Res. Lett.*, *34*, L22805, doi:10.1029/2007GL031354.
- Brönnimann, S., T. Ewen, T. Griesser, and R. Jenne (2006a), Multidecadal signal of solar variability in the upper troposphere during the 20th century, *Space Sci. Rev.*, *125*, 305-317.
- Brönnimann, S., et al. (2008), Exceptional Atmospheric Circulation during the "Dust Bowl", *Nature Geoscience*, submitted.
- Brönnimann, S., and J. Luterbacher (2004), Reconstructing Northern Hemisphere upper-level fields during World War II, *Clim. Dyn.*, *22*, 499-510.
- Brönnimann, S., J. Luterbacher, J. Staehelin, T. M. Svendby, G. Hansen, and T. Svenoe (2004), Extreme climate of the global troposphere and stratosphere in 1940-42 related to El Niño, *Nature*, *431*, 971-974.
- Brönnimann, S., M. Schraner, B. Muller, A. Fischer, D. Brunner, E. Rozanov, and T. Egorova (2006b), The 1986-1989 ENSO cycle in a chemical climate model, *Atmos. Chem. Phys.*, *6*, 4669-4685.
- Brunner, D., J. Staehelin, H. R. Kunsch, and G. E. Bodeker (2006a), A Kalman filter reconstruction of the vertical ozone distribution in an equivalent latitude-potential temperature framework from TOMS/GOME/SBUV total ozone observations, *J. Geophys. Res.*, *111*, D12308, doi:10.1029/2005JD006279.
- Brunner, D., J. Staehelin, J. A. Maeder, I. Wohltmann, and G. E. Bodeker (2006b), Variability and trends in total and vertically resolved stratospheric ozone based on the CATO ozone data set, *Atmos. Chem. Phys.*, *6*, 4985-5008.
- Butchart, N., and J. Austin (1998), Middle atmosphere climatologies from the troposphere-stratosphere configuration of the UKMO's unified model, *J. Atmos. Sci.*, *55*, 2782-2809.
- Butchart, N., A. A. Scaife, J. Austin, S. H. E. Hare, and J. R. Knight (2003), Quasi-biennial oscillation in ozone in a coupled chemistry-climate model, *J. Geophys. Res.*, *108*, 4486, doi:10.1029/2002JD003004.
- Butchart, N., et al. (2006), Simulations of anthropogenic change in the strength of the Brewer-Dobson circulation, *Clim. Dyn.*, *27*, 727-741.
- Butler, J. H., M. Battle, M. L. Bender, S. A. Montzka, A. D. Clarke, E. S. Saltzman, C. M. Sucher, J. P. Severinghaus, and J. W. Elkins (1999), A record of atmospheric halocarbons during the twentieth century from polar firn air, *Nature*, *399*, 749-755.
- Camp, C. D., and K. K. Tung (2007), Stratospheric polar warming by ENSO in winter: A statistical study, *Geophys. Res. Lett.*, *34*, L04809, doi:10.1029/2006GL028521.
- Chaffey, J. D., and J. C. Fyfe (2001), Arctic polar vortex variability in the Canadian Middle Atmosphere Model, *Atmosphere-Ocean*, *39*, 457-469.
- Chen, W., M. Takahashi, and H. F. Graf (2003), Interannual variations of stationary planetary wave activity in the northern winter troposphere and stratosphere and their relations to NAM and SST, *J. Geophys. Res.*, *108*, 4797, doi:10.1029/2003JD003834.

- Chiang, J. C. H., and A. H. Sobel (2002), Tropical tropospheric temperature variations caused by ENSO and their influence on the remote tropical climate, *J. Clim.*, *15*, 2616-2631.
- Claud, C., N. A. Scott, and A. Chedin (1999), Seasonal, interannual, and zonal temperature variability of the tropical stratosphere based on TOVS satellite data: 1987-91, *J. Clim.*, *12*, 540-550.
- Claussen, M., U. Lohmann, E. Roeckner, and U. Schulzweida (1994), A global data set of land-surface parameters, *MPI Report 135, Hamburg, Germany*.
- Compo, G. P., and P. D. Sardeshmukh (2004), Storm track predictability on seasonal and decadal scales, *J. Clim.*, *17*, 3701-3720.
- Compo, G. P., P. D. Sardeshmukh, and C. Penland (2001), Changes of subseasonal variability associated with El Niño, *J. Clim.*, *14*, 3356-3374.
- Crooks, S. A., and L. J. Gray (2005), Characterization of the 11-year solar signal using a multiple regression analysis of the ERA-40 dataset, *J. Clim.*, *18*, 996-1015.
- Dameris, M., et al. (2005), Long-term changes and variability in a transient simulation with a chemistry-climate model employing realistic forcing, *Atmos. Chem. Phys.*, *5*, 2121-2145.
- Egorova, T., E. Rozanov, E. Manzini, M. Haberreiter, W. Schmutz, V. Zubov, and T. Peter (2004), Chemical and dynamical response to the 11-year variability of the solar irradiance simulated with a chemistry-climate model, *Geophys. Res. Lett.*, *31*, L06119, doi:10.1029/2003GL019294.
- Egorova, T., E. Rozanov, V. Zubov, E. Manzini, W. Schmutz, and T. Peter (2005a), Chemistry-climate model SOCOL: a validation of the present-day climatology, *Atmos. Chem. Phys.*, *5*, 1557-1576.
- Egorova, T., E. Rozanov, V. Zubov, W. Schmutz, and T. Peter (2005b), Influence of solar 11-year variability on chemical composition of the stratosphere and mesosphere simulated with a chemistry-climate model, *Adv. Space Res.*, *35*, 451-457.
- Egorova, T. A., E. V. Rozanov, M. E. Schlesinger, N. G. Andronova, S. L. Malyshev, I. L. Karol, and V. A. Zubov (2001), Assessment of the effect of the Montreal Protocol on atmospheric ozone, *Geophys. Res. Lett.*, *28*, 2389-2392.
- Egorova, T. A., E. V. Rozanov, V. A. Zubov, and I. L. Karol (2003), Model for investigating ozone trends (MEZON), *Atmos. Ocean. Phys.*, *39*, 277-292.
- Enfield, D. B., A. M. Mestas-Nunez, and P. J. Trimble (2001), The Atlantic multidecadal oscillation and its relation to rainfall and river flows in the continental US, *Geophys. Res. Lett.*, *28*, 2077-2080.
- Etheridge, D. M., L. P. Steele, R. J. Francey, and R. L. Langenfelds (1998), Atmospheric methane between 1000 AD and present: Evidence of anthropogenic emissions and climatic variability, *J. Geophys. Res.*, *103*, 15979-15993.

- Etheridge, D. M., L. P. Steele, R. L. Langenfelds, R. J. Francey, J. M. Barnola, and V. I. Morgan (1996), Natural and anthropogenic changes in atmospheric CO₂ over the last 1000 years from air in Antarctic ice and firn, *J. Geophys. Res.*, *101*, 4115-4128.
- Eyring, V., et al. (2006), Assessment of temperature, trace species, and ozone in chemistry-climate model simulations of the recent past, *J. Geophys. Res.*, *111*, D22308, doi:10.1029/2006JD007327.
- Eyring, V., D. E. Kinnison, and T. G. Shepherd (2005), Overview of planned coupled chemistry-climate simulations to support upcoming ozone and climate assessments, *SPARC Newsletter*, *25*, 11-17.
- Farman, J. C., B. G. Gardiner, and J. D. Shanklin (1985), Large Losses of Total Ozone in Antarctica Reveal Seasonal ClO_x/NO_x Interaction, *Nature*, *315*, 207-210.
- Fischer, A. M., et al. (2008a), Interannual-to-Decadal Variability of the Stratosphere during the 20th Century: Ensemble Simulations with a Chemistry-Climate Model, *Atmos. Chem. Phys. Disc.*, *8*, 14371-14418.
- Fischer, A. M., D. T. Shindell, B. Winter, M. S. Bourqui, G. Faluvegi, S. Brönnimann, M. Schraner, and E. Rozanov (2008b), Stratospheric Winter Climate Response to ENSO in three Chemistry-Climate Models, *Geophys. Res. Lett.*, *35*, L13819, doi:10.1029/2008GL034289.
- Folland, C. K., J. Shukla, J. Kinter, and M. Rodwell (2002), The Climate of the Twentieth Century Project, *CLIVAR Exchanges*, *7*(2), 37-39.
- Forster, P. M., M. Blackburn, R. Glover, and K. P. Shine (2000), An examination of climate sensitivity for idealised climate change experiments in an intermediate general circulation model, *Clim. Dyn.*, *16*, 833-849.
- Fouquart, Y., and B. Bonnel (1980), Computations of solar heating of the Earth's atmosphere: A new parameterization, *Beitr. Phys. Atmos.*, *53*, 35-62.
- Fraedrich, K. (1994), An ENSO Impact on Europe - a Review, *Tellus*, *46*, 541-552.
- Fraedrich, K., and K. Muller (1992), Climate Anomalies in Europe Associated with ENSO Extremes, *Int. J. Climatol.*, *12*, 25-31.
- Garcia-Herrera, R., N. Calvo, R. R. Garcia, and M. A. Giorgetta (2006), Propagation of ENSO temperature signals into the middle atmosphere: A comparison of two general circulation models and ERA-40 reanalysis data, *J. Geophys. Res.*, *111*, D06101, doi:10.1029/2005JD006061.
- Garcia, R. R., D. R. Marsh, D. E. Kinnison, B. A. Boville, and F. Sassi (2007), Simulation of secular trends in the middle atmosphere, 1950-2003, *J. Geophys. Res.*, *112*, D09301, doi:10.1029/2006JD007485.
- Gillett, N. P., and D. W. J. Thompson (2003), Simulation of recent Southern Hemisphere climate change, *Science*, *302*, 273-275.

- Giorgetta, M. A. (1996), Der Einfluss der quasi-zweijährigen Oszillation auf die allgemeine Zirkulation: Modellrechnungen mit ECHAM4, *Examensarbeit Nr. 40, University of Hamburg, Hamburg, Germany*.
- Goldewijk, K. K. (2001), Estimating global land use change over the past 300 years: The HYDE Database, *Global Biogeochem. Cy.*, 15, 417-433.
- Gouirand, I., and V. Moron (2003), Variability of the impact of El Niño-southern oscillation on sea-level pressure anomalies over the North Atlantic in January to March (1874-1996), *Int. J. Climatol.*, 23, 1549-1566.
- Graf, H. F., Q. Li, and M. A. Giorgetta (2007), Volcanic effects on climate: revisiting the mechanisms, *Atmos. Chem. Phys.*, 7, 4503-4511.
- Grant, A. N., S. Brönnimann, T. Griesser, T. Ewen, and A. Nagurny (2008), A closer look at the 20th century Arctic warm events, *J. Clim.*, in preparation.
- Griesser, T., S. Brönnimann, A. Grant, T. Ewen, A. Stickler, and J. Comeaux (2008), Reconstruction of global monthly upper-level temperature and geopotential height fields back to 1880, *J. Clim.*, in preparation.
- Hadjinicolaou, P., A. Jarrar, J. A. Pyle, and L. Bishop (2002), The dynamically driven long-term trend in stratospheric ozone over northern middle latitudes, *Q. J. R. Meteorol. Soc.*, 128, 1393-1412.
- Hagemann, S. (2002), An Improved Land Surface Parameter Dataset for Global and Regional Climate Models, *MPI Report 336, Hamburg, Germany*.
- Hagemann, S., M. Botzet, L. Dümenil, and B. Machenhauer (1999), Derivation of global GCM boundary conditions from 1 km land use satellite data, *MPI Report 289, Hamburg, Germany*.
- Haigh, J. D. (1996), The impact of solar variability on climate, *Science*, 272, 981-984.
- Hartmann, D. L., J. M. Wallace, V. Limpasuvan, D. W. J. Thompson, and J. R. Holton (2000), Can ozone depletion and global warming interact to produce rapid climate change?, *Proc. Nat. Acad. Sci.*, 97, 1412-1417.
- Hastenrath, S. (2007), Equatorial zonal circulations: Historical perspectives, *Dynam. Atmos. Oceans*, 43, 16-24.
- Hatsushika, H., and K. Yamazaki (2001), Interannual variations of temperature and vertical motion at the tropical tropopause associated with ENSO, *Geophys. Res. Lett.*, 28, 2891-2894.
- Hoerling, M. P., M. L. Blackmon, and M. F. Ting (1992), Simulating the Atmospheric Response to the 1985-87 El-Niño Cycle, *J. Clim.*, 5, 669-682.
- Hoerling, M. P., J. W. Hurrell, T. Xu, G. T. Bates, and A. S. Phillips (2004), Twentieth century North Atlantic climate change. Part II: Understanding the effect of Indian Ocean warming, *Clim. Dyn.*, 23, 391-405.

- Hoerling, M. P., and M. F. Ting (1994), Organization of Extratropical Transients during El-Nino, *J. Clim.*, 7, 745-766.
- Holton, J. R., P. H. Haynes, M. E. McIntyre, A. R. Douglass, R. B. Rood, and L. Pfister (1995), Stratosphere-Troposphere Exchange, *Rev. Geophys.*, 33, 403-439.
- Holton, J. R., and H. C. Tan (1980), The Influence of the Equatorial Quasi-Biennial Oscillation on the Global Circulation at 50 mb, *J. Atmos. Sci.*, 37, 2200-2208.
- Hood, L. L. (1999), Effects of short-term solar UV variability on the stratosphere, *J. Atmos. Solar-Terrestrial Phys.*, 61, 45-51.
- Horowitz, L. W., et al. (2003), A global simulation of tropospheric ozone and related tracers: Description and evaluation of MOZART, version 2, *J. Geophys. Res.*, 108, 4784, doi:10.1029/2002JD002853.
- Hoskins, B. J., and A. J. Simmons (1975), Multilayer Spectral Model and Semi-Implicit Method, *Q. J. R. Meteorol. Soc.*, 101, 637-655.
- Huebener, H., U. Cubasch, U. Langematz, T. Spanghel, F. Niehörster, I. Fast, and M. Kunze (2007), Ensemble climate simulations using a fully coupled ocean-troposphere-stratosphere general circulation model, *Phil. Trans. R. Soc. A*, 365, 2089-2101, doi:10.1098/rsta.2007.2078.
- Karpetchko, A., E. Kyro, and B. M. Knudsen (2005), Arctic and Antarctic polar vortices 1957-2002 as seen from the ERA-40 reanalyses, *J. Geophys. Res.*, 110, D21109, doi:10.1029/2005JD006113.
- Kerzenmacher, T. E., P. Keckhut, A. Hauchecorne, and M. L. Chanin (2006), Methodological uncertainties in multi-regression analyses of middle-atmospheric data series, *J. Environ. Monit.*, 8, 682-690.
- Kistler, R., et al. (2001), The NCEP-NCAR 50-year reanalysis: Monthly means CD-ROM and documentation, *Bull. Am. Meteorol. Soc.*, 82, 247-267.
- Knight, J. R., C. K. Folland, and A. A. Scaife (2006), Climate impacts of the Atlantic Multidecadal Oscillation, *Geophys. Res. Lett.*, 33, L17706, doi:10.1029/2006GL026242.
- Kodera, K. (1995), On the Origin and Nature of the Interannual Variability of the Winter Stratospheric Circulation in the Northern-Hemisphere, *J. Geophys. Res.*, 100, 14077-14087.
- Kodera, K., and H. Koide (1997), Spatial and seasonal characteristics of recent decadal trends in the northern hemispheric troposphere and stratosphere, *J. Geophys. Res.*, 102, 19433-19447.
- Kodera, K., and Y. Kuroda (2002), Dynamical response to the solar cycle, *J. Geophys. Res.*, 107, doi:10.1029/2002JD002224.
- Kousky, V. E., and A. Leetma (1989), The 1986-87 Pacific warm episode: Evolution of oceanic and atmospheric anomaly fields, *J. Clim.*, 2, 254-267.

- Kumar, A., M. Hoerling, M. Ji, A. Leetmaa, and P. Sardeshmukh (1996), Assessing a GCM's suitability for making seasonal predictions, *J. Clim.*, *9*, 115-129.
- Labitzke, K. (1987), Sunspots, the QBO, and the Stratospheric Temperature in the North Polar-Region, *Geophys. Res. Lett.*, *14*, 535-537.
- Labitzke, K., M. Kunze, and S. Brönnimann (2006), Sunspots, the QBO and the Stratosphere in the North Polar Region - 20 years later, *Meteorol. Z.*, *15*, 355-363.
- Langematz, U., M. Kunze, K. Kruger, K. Labitzke, and G. L. Roff (2003), Thermal and dynamical changes of the stratosphere since 1979 and their link to ozone and CO₂ changes, *J. Geophys. Res.*, *108*, 4027, doi:10.1029/2002JD002069.
- Latif, M., and T. P. Barnett (1994), Causes of Decadal Climate Variability over the North Pacific and North-America, *Science*, *266*, 634-637.
- Lean, J. (2000), Evolution of the sun's spectral irradiance since the Maunder Minimum, *Geophys. Res. Lett.*, *27*, 2425-2428.
- Limpasuvan, V., D. W. J. Thompson, and D. L. Hartmann (2004), The life cycle of the Northern Hemisphere sudden stratospheric warmings, *J. Clim.*, *17*, 2584-2596.
- Logan, J. A. (1994), Trends in the Vertical-Distribution of Ozone - an Analysis of Ozone-sonde Data, *J. Geophys. Res.*, *99*, 25553-25585.
- Lohmann, U., J. Feichter, C. C. Chuang, and J. E. Penner (1999), Prediction of the number of cloud droplets in the ECHAM GCM, *J. Geophys. Res.*, *104*, 9169-9198.
- Machida, T., T. Nakazawa, Y. Fujii, S. Aoki, and O. Watanabe (1995), Increase in the Atmospheric Nitrous-Oxide Concentration during the Last 250 Years, *Geophys. Res. Lett.*, *22*, 2921-2924.
- Maeder, J. A., J. Staehelin, D. Brunner, W. A. Stahel, I. Wohltmann, and T. Peter (2007), Statistical modeling of total ozone: Selection of appropriate explanatory variables, *J. Geophys. Res.*, *112*, D11108, doi:10.1029/2006JD007694.
- Mantua, N. J., S. R. Hare, Y. Zhang, J. M. Wallace, and R. C. Francis (1997), A Pacific interdecadal climate oscillation with impacts on salmon production, *Bull. Am. Meteorol. Soc.*, *78*, 1069-1079.
- Manzini, E., M. A. Giorgetta, M. Esch, L. Kornblueh, and E. Roeckner (2006), The influence of sea surface temperatures on the northern winter stratosphere: Ensemble simulations with the MAECHAM5 model, *J. Clim.*, *19*, 3863-3881.
- Manzini, E., and N. McFarlane (1998), The effect of varying the source spectrum of a gravity wave parameterization in a middle atmosphere general circulation model, *J. Geophys. Res.*, *103*, 31523-31539.
- Manzini, E., N. A. McFarlane, and C. McLandress (1997), Impact of the Doppler spread parameterization on the simulation of the middle atmosphere circulation using the MA/ECHAM4 general circulation model, *J. Geophys. Res.*, *102*, 25751-25762.

- Mariotti, A., N. Zeng, and K. M. Lau (2002), Euro-Mediterranean rainfall and ENSO - a seasonally varying relationship, *Geophys. Res. Lett.*, **29**, 1621, doi:10.1029/2001GL014248.
- Mathieu, P. P., R. T. Sutton, B. Dong, and M. Collins (2004), Predictability of winter climate over the North Atlantic European region during ENSO events, *J. Clim.*, **17**, 1953-1974.
- Matsuno, T. (1971), Dynamical Model of Stratospheric Sudden Warming, *J. Atmos. Sci.*, **28**, 1479-1494.
- Mc Phaden, M. J., S. P. Hayes, L. J. Mangum, and J. M. Toole (1990), Variability in the Western Equatorial Pacific-Ocean during the 1986-87 El-Nino Southern Oscillation Event, *J. Phys. Oceanogr.*, **20**, 190-208.
- Melo-Goncalves, P., A. C. Rocha, J. M. Castanheira, and J. A. Ferreira (2005), North Atlantic oscillation sensitivity to the El Nino/Southern Oscillation polarity in a large-ensemble simulation, *Clim. Dyn.*, **24**, 599-606.
- Merkel, U., and M. Latif (2002), A high resolution AGCM study of the El Nino impact on the North Atlantic/European sector, *Geophys. Res. Lett.*, **29**, 1291, doi:10.1029/2001GL013726.
- Miller, L., R. E. Cheney, and B. C. Douglas (1988), Geosat Altimeter Observations of Kelvin Waves and the 1986-87 El-Nino, *Science*, **239**, 52-54.
- Morcrette, J. J. (1991), Radiation and Cloud Radiative Properties in the European Center for Medium Range Weather Forecasts Forecasting System, *J. Geophys. Res.*, **96**, 9121-9132.
- Moron, V., and G. Plaut (2003), The impact of El Nino-southern oscillation upon weather regimes over Europe and the North Atlantic during boreal winter, *Int. J. Climatol.*, **23**, 363-379.
- Newman, P. A., E. R. Nash, and J. E. Rosenfield (2001), What controls the temperature of the Arctic stratosphere during the spring?, *J. Geophys. Res.*, **106**, 19999-20010.
- Olson, J. S. (1994), Global ecosystem framework-definitions, *USGS EROS Data Center Internal Report, Sioux Falls, SD*.
- Oltmans, S. J., et al. (2006), Long-term changes in tropospheric ozone, *Atmos. Env.*, **40**, 3156-3173.
- Oman, L., A. Robock, G. Stenchikov, G. A. Schmidt, and R. Ruedy (2005), Climatic response to high-latitude volcanic eruptions, *J. Geophys. Res.*, **110**, D13103, doi:10.1029/2004JD005487.
- Oman, L., A. Robock, G. L. Stenchikov, and T. Thordarson (2006), High-latitude eruptions cast shadow over the African monsoon and the flow of the Nile, *Geophys. Res. Lett.*, **33**, L18711, doi:10.1029/2006GL027665.
- Palmer, T. N., and D. L. T. Anderson (1993), Scientific assessment fo the prospect of seasonal forecasting: a European perspective, *ECMWF Technical report*, **70**.

- Patterson, K. A. (1990), Global distributions of total and total-available soil water-holding capacities, *Master thesis, University of Delaware, Newark, DE*.
- Pozo-Vazquez, D., S. R. Gamiz-Fortis, J. Tovar-Pescador, M. J. Esteban-Parra, and Y. Castro-Diez (2005), North Atlantic winter SLP anomalies based on the autumn ENSO state, *J. Clim.*, *18*, 97-103.
- Prather, M. J. (1986), Numerical Advection by Conservation of 2nd-Order Moments, *J. Geophys. Res.*, *91*, 6671-6681.
- Pyle, J. A., P. Braesicke, and G. Zeng (2005), Dynamical variability in the modelling of chemistry-climate interactions, *Faraday Discuss.*, *130*, 27-39.
- Randel, W. J., and J. B. Cobb (1994), Coherent variations of monthly mean total ozone and lower stratospheric temperature, *J. Geophys. Res.*, *99*, 5433-5447.
- Randel, W. J., and F. Wu (1996), Isolation of the ozone QBO in SAGE II data by singular-value decomposition, *J. Atmos. Sci.*, *53*, 2546-2559.
- Randel, W. J., and F. Wu (2007), A stratospheric ozone profile data set for 1979-2005: Variability, trends, and comparisons with column ozone data, *J. Geophys. Res.*, *112*, D06313, doi:10.1029/2006JD007339.
- Randel, W. J., F. Wu, and R. Stolarski (2002), Changes in column ozone correlated with the stratospheric EP flux, *J. Meteorol. Soc. Jpn.*, *80*, 849-862.
- Rayner, N. A., D. E. Parker, E. B. Horton, C. K. Folland, L. V. Alexander, D. P. Rowell, E. C. Kent, and A. Kaplan (2003), Global analyses of sea surface temperature, sea ice, and night marine air temperature since the late nineteenth century, *J. Geophys. Res.*, *108*, 4407, doi:10.1029/2002JD002670.
- Robock, A. (2000), Volcanic eruptions and climate, *Rev. Geophys.*, *38*, 191-219.
- Roeckner, E., et al. (1996), The atmospheric general circulation model ECHAM-4: model description and simulation of present-day climate, *MPI Report 218, Hamburg, Germany*.
- Rosenfield, J. E., S. M. Frith, and R. S. Stolarski (2005), Version 8 SBUV ozone profile trends compared with trends from a zonally averaged chemical model, *J. Geophys. Res.*, *110*, D12302, doi:10.1029/2004JD005466.
- Rozanov, E., M. Schraner, C. Schnadt, T. Egorova, M. Wild, A. Ohmura, V. Zubov, W. Schmutz, and T. Peter (2005), Assessment of the ozone and temperature variability during 1979-1993 with the chemistry-climate model SOCOL, *Adv. Space Res.*, *35*, 1375-1384.
- Rozanov, E. V., M. E. Schlesinger, N. G. Andronova, F. Yang, S. L. Malyshev, V. A. Zubov, T. A. Egorova, and B. Li (2002), Climate/chemistry effects of the Pinatubo volcanic eruption simulated by the UIUC stratosphere/troposphere GCM with interactive photochemistry, *J. Geophys. Res.*, *107*, 4594, doi:10.1029/2001JD000974.
- Rozanov, E. V., M. E. Schlesinger, and V. A. Zubov (2001), The University of Illinois, Urbana-Champaign three-dimensional stratosphere-troposphere general circulation model with interactive ozone photochemistry: Fifteen-year control run climatology, *J. Geophys. Res.*, *106*, 27233-27254.

- Rozanov, E. V., V. A. Zubov, M. E. Schlesinger, F. L. Yang, and N. G. Andronova (1999), The UIUC three-dimensional stratospheric chemical transport model: Description and evaluation of the simulated source gases and ozone, *J. Geophys. Res.*, *104*, 11755-11781.
- Sander, S. P., et al. (2000), Chemical kinetics and photochemical data for use in stratospheric data, supplemented to evaluation 12: Update of key reactions, *JPL Publication 00-3*.
- Sardeshmukh, P. D., G. P. Compo, and C. Penland (2000), Changes of probability associated with El Nino, *J. Clim.*, *13*, 4268-4286.
- Sassi, F., D. Kinnison, B. A. Boville, R. R. Garcia, and R. Roble (2004), Effect of El Nino-Southern Oscillation on the dynamical, thermal, and chemical structure of the middle atmosphere, *J. Geophys. Res.*, *109*, D17108, doi:10.1029/2003JD004434.
- Sato, M., J. E. Hansen, M. P. McCormick, and J. B. Pollack (1993), Stratospheric Aerosol Optical Depths, 1850-1990, *J. Geophys. Res.*, *98*, 22987-22994.
- Scaife, A. A., J. Austin, N. Butchart, S. Pawson, M. Keil, J. Nash, and I. N. James (2000), Seasonal and interannual variability of the stratosphere diagnosed from UKMO TOVS analyses, *Q. J. R. Meteorol. Soc.*, *126*, 2585-2604.
- Scaife, A. A., et al. (2008), The CLIVAR C20C project: selected twentieth century climate events, *Clim. Dyn.*, doi:10.1007/s00382-008-0451-1.
- Schaller, N., T. Griesser, A. M. Fischer, A. Stickler, and S. Brönnimann (2008), Climate effects of the 1883 Krakatoa eruption: Historical and present perspectives, *Vierteljahrsschrift der Naturforschenden Gesellschaft in Zürich*, submitted.
- Schmidt, G. A., et al. (2006), Present-day atmospheric simulations using GISS ModelE: Comparison to in situ, satellite, and reanalysis data, *J. Clim.*, *19*, 153-192.
- Schmitt, A., and B. Brunner (1997), Emissions from aviation and their development over time, in Pollutants from air traffic - results of atmospheric research 1992 - 1997, *DLR-Mitt. 97-04*, 37-52.
- Schnadt, C., M. Dameris, M. Ponater, R. Hein, V. Grewe, and B. Steil (2002), Interaction of atmospheric chemistry and climate and its impact on stratospheric ozone, *Clim. Dyn.*, *18*, 501-517.
- Schraner, M. (2008), Systematische Untersuchung der Abhängigkeiten eines Klima-Chemie-Modells von Randbedingungen und Parametrisierungen, *Dissertation No. 17824*, *ETH Zurich*, Switzerland.
- Schraner, M., et al. (2008), Technical Note: Chemistry-climate model SOCOL: version 2.0 with improved transport and chemistry/microphysics schemes, *Atmos. Chem. Phys. Disc.*, *8*, 11103-11147.
- Sexton, D. M. H., D. P. Rowell, C. K. Folland, and D. J. Karoly (2001), Detection of anthropogenic climate change using an atmospheric GCM, *Clim. Dyn.*, *17*, 669-685.

- Shindell, D. T., G. Faluvegi, and N. Bell (2003), Preindustrial-to-present-day radiative forcing by tropospheric ozone from improved simulations with the GISS chemistry-climate GCM, *Atmos. Chem. Phys.*, *3*, 1675-1702.
- Shindell, D. T., G. Faluvegi, N. Unger, E. Aguilar, G. A. Schmidt, D. M. Koch, S. E. Bauer, and R. L. Miller (2006), Simulations of preindustrial, present-day, and 2100 conditions in the NASA GISS composition and climate model G-PUCCINI, *Atmos. Chem. Phys.*, *6*, 4427-4459.
- Shindell, D. T., D. Rind, and P. Lonergan (1998), Increased polar stratospheric ozone losses and delayed eventual recovery owing to increasing greenhouse-gas concentrations, *Nature*, *392*, 589-592.
- Shindell, D. T., G. A. Schmidt, R. L. Miller, and D. Rind (2001), Northern Hemisphere winter climate response to greenhouse gas, ozone, solar, and volcanic forcing, *J. Geophys. Res.*, *106*, 7193-7210.
- Shine, K. P., et al. (2003), A comparison of model-simulated trends in stratospheric temperatures, *Q. J. R. Meteorol. Soc.*, *129*, 1565-1588.
- Smith, A. K., and K. Matthes (2008), Decadal-scale periodicities in the stratosphere associated with the solar cycle and the QBO, *J. Geophys. Res.*, *113*, D05311, doi:10.1029/2007JD009051.
- Smith, T. M., and R. W. Reynolds (2004), Improved extended reconstruction of SST (1854-1997), *J. Clim.*, *17*, 2466-2477.
- Solomon, S. (1999), Stratospheric ozone depletion: A review of concepts and history, *Rev. Geophys.*, *37*, 275-316.
- Soukharev, B. E., and L. L. Hood (2006), Solar cycle variation of stratospheric ozone: Multiple regression analysis of long-term satellite data sets and comparisons with models, *J. Geophys. Res.*, *111*, doi:10.1029/2006JD007107.
- Staehelin, J., A. Renaud, J. Bader, R. McPeters, P. Viatte, B. Hoegger, V. Bugnion, M. Giroud, and H. Schill (1998), Total ozone series at Arosa (Switzerland): Homogenization and data comparison, *J. Geophys. Res.*, *103*, 5827-5841.
- Steil, B., C. Bruhl, E. Manzini, P. J. Crutzen, J. Lelieveld, P. J. Rasch, E. Roeckner, and K. Kruger (2003), A new interactive chemistry-climate model: 1. Present-day climatology and interannual variability of the middle atmosphere using the model and 9 years of HALOE/UARS data, *J. Geophys. Res.*, *108*, 4290, doi:10.1029/2002JD002971.
- Steinbrecht, W., et al. (2006), Interannual variation patterns of total ozone and lower stratospheric temperature in observations and model simulations, *Atmos. Chem. Phys.*, *6*, 349-374.
- Stenchikov, G., K. Hamilton, A. Robock, V. Ramaswamy, and M. D. Schwarzkopf (2004), Arctic oscillation response to the 1991 Pinatubo eruption in the SKYHI general circulation model with a realistic quasi-biennial oscillation, *J. Geophys. Res.*, *109*, D03112, doi:10.1029/2003JD003699.

- Stenchikov, G., A. Robock, V. Ramaswamy, M. D. Schwarzkopf, K. Hamilton, and S. Ramachandran (2002), Arctic Oscillation response to the 1991 Mount Pinatubo eruption: Effects of volcanic aerosols and ozone depletion, *J. Geophys. Res.*, *107*, 4803, doi:10.1029/2002JD002090.
- Stolarski, R. S., G. J. Labow, and R. D. McPeters (1997), Springtime Antarctic total ozone measurements in the early-1970s from the BUUV instrument on Nimbus 4, *Geophys. Res. Lett.*, *24*, 591-594.
- Sturges, W. T., H. P. McIntyre, S. A. Penkett, J. Chappellaz, J. M. Barnola, R. Mulvaney, E. Atlas, and V. Stroud (2001), Methyl bromide, other brominated methanes, and methyl iodide in polar firn air, *J. Geophys. Res.*, *106*, 1595-1606.
- Sutton, R. T., and D. L. R. Hodson (2005), Atlantic Ocean forcing of North American and European summer climate, *Science*, *309*, 115-118.
- Symons, G. J. (1888), The eruption of Krakatoa and subsequent phenomena, Trübner, London, 494pp.
- Taguchi, M., and D. L. Hartmann (2006), Increased occurrence of stratospheric sudden warmings during El Niño as simulated by WACCM, *J. Clim.*, *19*, 324-332.
- Taylor, C. P., and M. S. Bourqui (2005), A new fast stratospheric ozone chemistry scheme in an intermediate general-circulation model. I: Description and evaluation, *Q. J. R. Meteorol. Soc.*, *131*, 2225-2242.
- Tegtmeier, S., and T. G. Shepherd (2007), Persistence and photochemical decay of springtime total ozone anomalies in the Canadian Middle Atmosphere Model, *Atmos. Chem. Phys.*, *7*, 485-493.
- Thomason, L., and T. Peter (2006), Assessment of Stratospheric Aerosol Properties (ASAP), *SPARC Report No. 4*, WCRP-124.
- Tie, X. X., and G. Brasseur (1995), The Response of Stratospheric Ozone to Volcanic-Eruptions - Sensitivity to Atmospheric Chlorine Loading, *Geophys. Res. Lett.*, *22*, 3035-3038.
- Uppala, S. M., et al. (2005), The ERA-40 re-analysis, *Q. J. R. Meteorol. Soc.*, *131*, 2961-3012.
- van Aardenne, J. A., F. J. Dentener, J. G. J. Olivier, C. G. M. K. Goldewijk, and J. Lelieveld (2001), A 1 degrees x 1 degrees resolution data set of historical anthropogenic trace gas emissions for the period 1890-1990, *Global Biogeochem. Cy.*, *15*, 909-928.
- Van Loon, H., and K. Labitzke (1987), The Southern Oscillation .5. The Anomalies in the Lower Stratosphere of the Northern-Hemisphere in Winter and a Comparison with the Quasi-Biennial Oscillation, *Mon. Wea. Rev.*, *115*, 357-369.
- van Oldenborgh, G. J. (2005), Comment on 'Predictability of winter climate over the North Atlantic European region during ENSO events' by P.-P. Mathieu, R. T. Sutton, B. Dong, and M. Collins, *J. Clim.*, *18*, 2770-2772.
- Verbeek, R. D. M. (1884), The Krakatoa eruption, *Nature*, *30*, 10-15.

- Vogler, C., S. Brönnimann, and G. Hansen (2006), Re-evaluation of the 1950-1962 total ozone record from Longyearbyen, Svalbard, *Atmos. Chem. Phys.*, *6*, 4763-4773.
- Vogler, C., S. Brönnimann, J. Staehelin, and R. E. M. Griffin (2007), Dobson total ozone series of Oxford: Reevaluation and applications, *J. Geophys. Res.*, *112*, D20116, doi:10.1029/2007JD008894.
- Wallace, J. M., R. L. Panetta, and J. Estberg (1993), Representation of the Equatorial Stratospheric Quasi-Biennial Oscillation in Eof Phase-Space, *J. Atmos. Sci.*, *50*, 1751-1762.
- Warwick, N. J., J. A. Pyle, G. D. Carver, X. Yang, N. H. Savage, F. M. O'Connor, and R. A. Cox (2006), Global modeling of biogenic bromocarbons, *J. Geophys. Res.*, *111*, D24305, doi:10.1029/2006JD007264.
- Williamson, D. L., and P. J. Rasch (1989), Two-dimensional semi-lagrangian transport with shape-preserving interpolation, *Mon. Wea. Rev.*, *117*, 102-129.
- WMO (2003), Scientific assessment of ozone depletion: 2002, *No. 47*, World Meteorological Organization, Geneva.
- WMO (2006), Scientific assessment of ozone depletion: 2006, *No. 50*, World Meteorological Organization, Geneva.
- Wu, A. M., and W. W. Hsieh (2004), The nonlinear association between ENSO and the Euro-Atlantic winter sea level pressure, *Clim. Dyn.*, *23*, 859-868.
- Zerefos, C. S., V. T. Gerogiannis, D. Balis, S. C. Zerefos, and A. Kazantzidis (2007), Atmospheric effects of volcanic eruptions as seen by famous artists and depicted in their paintings, *Atmospheric Chemistry and Physics*, *7*, 4027-4042.
- Zubov, V. A., E. V. Rozanov, and M. E. Schlesinger (1999), Hybrid scheme for three-dimensional advective transport, *Mon. Wea. Rev.*, *127*, 1335-1346.

Acknowledgments

I sincerely would like to thank all the people who provided guidance, encouragement and friendship during my thesis.

First and foremost, a special thank goes to my doctoral supervisor Stefan Brönnimann for accepting me as a PhD student and for his continuous support and guidance throughout the last three years. His professional expertise and encouragement helped me a lot to move forward and finally succeed whenever problems surfaced. I also want to thank him for giving me the opportunity to present my work at various conferences, workshops and summer schools.

I would like to thank Eugene Rozanov who immensely helped in all aspects of programming and model development. I am most grateful for his patience during these years and his extremely fast e-mail support. I also appreciated his sense of pragmatism which helped to realistically set milestones during all these years.

Further thanks go to Martin Schraner for introducing me to the model at the beginning of my PhD and for his enormous work concerning model development. I also enjoyed the working environment in our office together with him and David Volken. I am thankful to Patricia Kenzelmann for assistance in various programming aspects as well as for reading part of the thesis. A warm thank goes to my current and former group members Thomas Griesser, Andrea Grant, Alex Stickler, Reto Spadin, and Tracy Ewen for support and encouragement during this time. I always enjoyed the inspiring discussions during coffee breaks and at lunch time. I am also grateful to all people at the institute who helped in computational (Daniel Lüthi, Marc Wüest) and administrative (Rahel Buri) issues.

Outside of ETH, a special thank goes to the wonderful people of the Verein waldstock. I always enjoyed the few drinks with you at weekends which brought a refreshing diversion to my daily work.

I would also like to sincerely thank my family, my parents and my brother, for their support and encouragement throughout my studies.

Curriculum Vitae

Andreas Marc Fischer, Hallwylstrasse 80, 8004 Zürich, fisch@gmx.net

born on 22 October 1979 in Winterthur (ZH)

citizen of Steinhausen (ZG) and Menznau (LU)

Education

Since 2008	PostDoc at ETH Zurich, Institute for Atmospheric and Climate Science
2005 - 2008	PhD student at ETH Zurich, Institute for Atmospheric and Climate Science (supervisor: Prof. S. Brönnimann)
2005 – 2007	Diploma of Advanced Studies ETH in Applied Statistics
1999 – 2005	Study of Environmental Sciences ETH Zurich <i>Master Thesis: Sensitivity of the ozone production in the UT/LS region based on box-modeling</i>
1994 – 1999	Maturity, Type B (Latin), Kantonsschule Zug

Work Experience

2005 (4 months)	Internship at Environment Division Canton Appenzell Innerrhoden <i>Project Development on noise abatement of road traffic: consideration of financial costs and environmental issues</i>
2002/2003 (5 months)	Internship at the UN-specialized agency World Meteorological Organization, Geneva <i>Survey on the state of the ozone hole intended for general public and made available on WMO-website.</i>

Teaching

Supervision of Bachelor Thesis:

- Christoph Keller, *Validierung der Troposphärenchemie im chemischen Klimamodell SOCOL anhand von Ozon und OH*, 2006.
- Nico Zeltner, *Analyse des Klimamodells SOCOL anfangs des 20. Jahrhunderts - basierend auf dem Vulkanausbruch St. Maria*, 2007.
- Andreas Lustenberger, *Häufigkeit und Stärke von Major Warmings im Chemie-Klimamodell SOCOL*, 2007.
- Nathalie Schaller, *Klimaauswirkungen des Krakatau-Ausbruchs*, 2007.

Supervision of Master Thesis:

- Stefan Krähenmann, *Klimaauswirkung nach dem Ausbruch des Katmai 1912*, 2007.

Supervision of Internship:

- Veruska Muccione, Oct. 2006 – Feb. 2007

Teaching Assistant:

- Numerical Methods in Environmental Physics, Fall 2005 and 2007
- Atmospheric Chemistry, Fall 2006
- Bachelor Student Seminar, Fall 2007

Publications

Fischer, A. M., et al. (2008), Interannual-to-Decadal Variability of the Stratosphere during the 20th Century: Ensemble Simulations with a Chemistry-Climate Model, *Atmos. Chem. Phys. Disc.*, 8, 14371-14418.

Fischer, A. M., D. T. Shindell, B. Winter, M. S. Bourqui, G. Faluvegi, S. Brönnimann, M. Schraner, and E. Rozanov (2008), Stratospheric Winter Climate Response to ENSO in three Chemistry-Climate Models, *Geophys. Res. Lett.*, 35, L13819, doi:10.1029/2008GL034289.

Brönnimann, S., et al. (2008), Exceptional Atmospheric Circulation during the "Dust Bowl", *Nature Geoscience*, submitted.

Scaife, A. A., et al. (2008), The CLIVAR C2oC project: selected twentieth century climate events, *Clim. Dyn.*, doi:10.1007/s00382-008-0451-1.

Kucharski, F., et al. (2008), The CLIVAR C2oC Project. Skill of simulating Indian monsoon rainfall on interannual to decadal timescales. Does GHG forcing play a role?, *Clim. Dyn.*, accepted.

Zhou, T., et al. (2008), The CLIVAR C2oC Project: Which components of the Asian-Australian Monsoon circulation variations are forced and reproducible?, *Clim. Dyn.*, submitted.

Schraner, M., et al. (2008), Technical Note: Chemistry-climate model SOCOL: version 2.0 with improved transport and chemistry/microphysics schemes, *Atmos. Chem. Phys. Disc.*, 8, 11103-11147.

Schaller, N., T. Griesser, A. M. Fischer, A. Stickler, and S. Brönnimann (2008), Climate effects of the 1883 Krakatoa eruption: Historical and present perspectives, *Vierteljahrsschrift der Naturforschenden Gesellschaft in Zürich*, submitted.

Fischer, A. M., R. Sausen, D. Brunner, J. Staehelin, and U. Schumann (2008), Flugverkehr und Klimaschutz, *GAIA*, submitted.

Brönnimann, S., M. Schraner, B. Muller, A. Fischer, D. Brunner, E. Rozanov, and T. Egorova (2006), The 1986-1989 ENSO cycle in a chemical climate model, *Atmos. Chem. Phys.*, 6, 4669-4685.

Fischer, A., and J. Staehelin (2003), The Antarctic Ozone hole: 1996-2002, *WMO Bull.*, 52, 264 - 269.

Oral Presentations

Fischer, A., S. Brönnimann, E. Rozanov, and M. Schraner 2008: Climate Variability in the Stratosphere during the 20th Century, *Workshop on Variability on the Global Atmospheric Circulation during the past 100 years*, June 15 – 20 2008, Monte Verita, CH.

Fischer, A., S. Brönnimann, and E. Rozanov 2008: Interannual-to-decadal variability of stratospheric chemistry and climate during the 20th century, *EGU General Assembly*, April 15, 2008, Vienna, Austria.

Fischer, A., S. Brönnimann, and E. Rozanov 2007: Interannual-to-decadal variability of stratospheric chemistry and climate during the 20th century, *Swiss Geoscience Meeting*, November 16, 2007, Geneva, CH.

Fischer, A., S. Brönnimann, and E. Rozanov 2007: Interannual-to-decadal variability of stratospheric chemistry and climate during the 20th century, *AMS 14th Conference on Middle Atmosphere*, August 20 – 24, 2007, Portland OR, USA.

Fischer, A., S. Brönnimann, E. Rozanov, D. Shindell, G. Faluvegi, M. Bourqui, B. Winter, and C. Bell 2007: Winter Climate Response to ENSO in three Chemical-Climate Models, *SPARC CCMVal Workshop*, June 26 – 28, 2007, Leeds, UK.

Fischer, A., S. Brönnimann, E. Rozanov, N. Zeltner, and S. Krähenmann 2007: Stratospheric Chemical-Climate Variability during the 20th century, *4th International CLIVAR Climate of the 20th Century Workshop*, March 13 – 15, 2007, Exeter, UK.

Poster Presentations

SPARC 4th General Assembly, Bologna, Italy, September 2008

9th Swiss Global Change Day, Berne, Switzerland, April 2008

ETH Latsis Symposium, Zurich, Switzerland, September 2007

AGU Chapman Conference, Santorini, Greece, September 2007

6th NCCR Climate Summer School, Grindelwald, Switzerland, August 2007

8th Swiss Global Change Day, Berne, Switzerland, April 2007

EGU General Assembly, Vienna Austria, April 2007

CSCS User Day, Manno, Switzerland, September 2006

Workshop Climate Variability and Extremes during the past 100 years, Gwatt, Switzerland, July 2006

7th Swiss Global Change Day, Berne, Switzerland, April 2006

EGU General Assembly, Vienna, Austria, April 2006

4th NCCR Climate Summer School, Grindelwald, Switzerland, August 2005